UiT
THE ARCTIC UNIVERSITY OF NORWAY

Faculty of Science and Technology

Department of Geology

# Reconstruction of Holocene Paleoenvironment in Smeerenburgfjorden, northwest Svalbard

*based on benthic foraminifera and sedimentological investigations*

—

**Erna Ósk Arnardóttir**

*Master thesis in Marine Geology and Geophysics (GEO 3900)*
*May 2015*

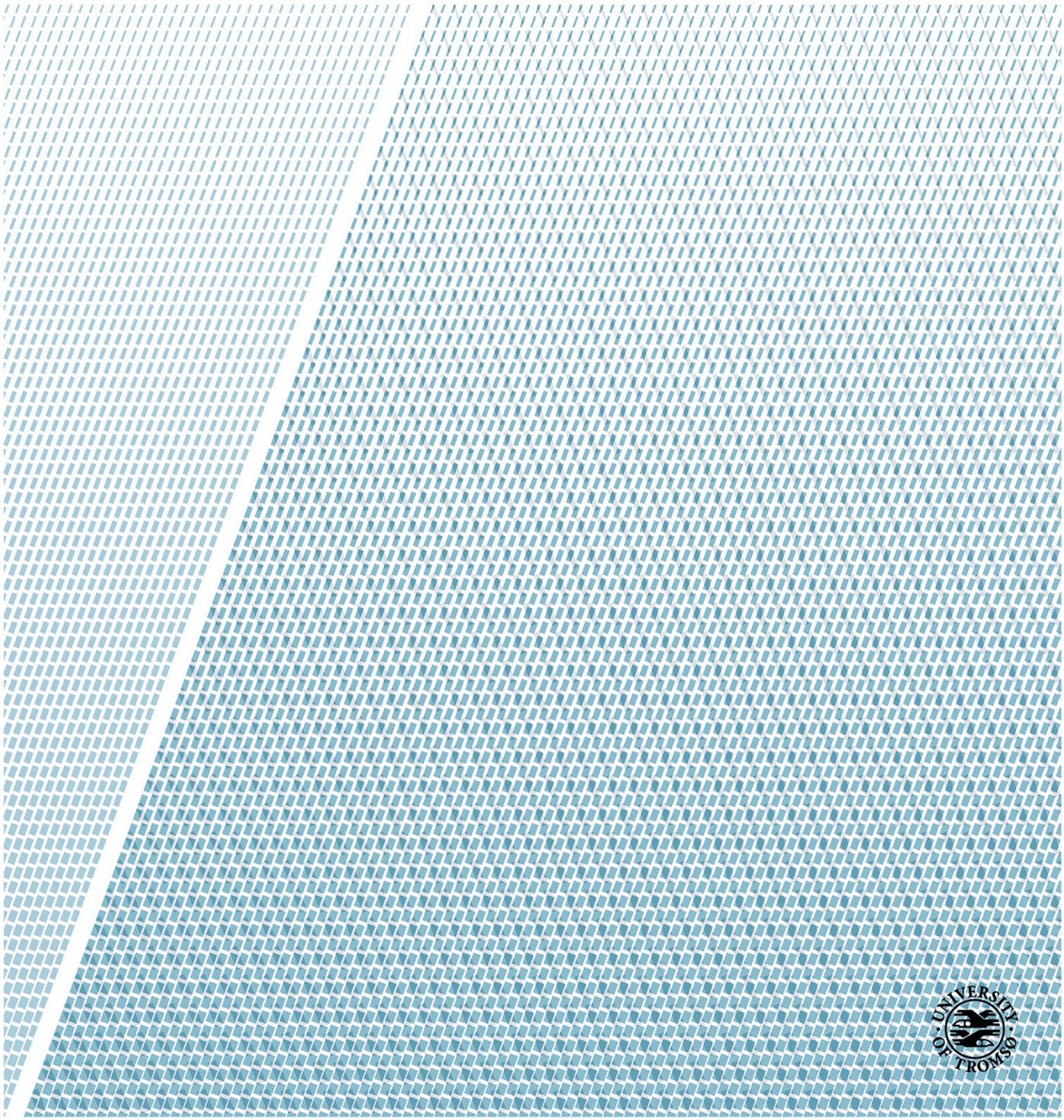

# Abstract

Two gravity cores JM06-024-GC3 and JM07-049-GC1 from Smeerenburgfjorden at the northwestern corner of Svalbard have been investigated for the distribution pattern of the benthic foraminiferal faunas. The oxygen and carbon isotope values in benthic foraminifera were analysed and together with other proxy data such as ice rafted debris (IRD), were used in order to reconstruct the paleoceanography and the paleoenvironment. The data are compared to several other records from the western and northern Svalbard margin. The results indicate high degree of variability between inflow of the warmer and saline Atlantic Water to the cold and fresh Arctic and the Polar Water in the area during the Holocene. The distribution patterns of the stable isotopies, the IRD and the benthic foraminifera indicate a concomitant temperature change around 5000 cal yr. BP. This temperature change is a result of a general cooling of the bottom water during the early Holocene. Conditions during the last 2000 years have been unstable, indicating an episodic inflow of Atlantic Water. The concentrations of calcareous and agglutinated benthic foraminifera vary in the late early Holocene, indicating bottom water oscillations between warmer and colder water masses. These oscillations indicate the repeated intrusion of the warmer Atlantic Water to the cold Arctic Water during the last 2000 years BP. The data indicates an interaction between the flow of the Atlantic Water and the amount of polar melt water and sea-ice.

# Table of content

**Acknowledgements** ..... **viii**

1 **Introduction** ..... **1**
1.1 Figures ..... 1
1.2 Background ..... 1
1.2.1 The Svalbard archipelago ..... 1
1.3 Oceanography ..... 2
1.4 Last glacial maximum (LGM) in Svalbard ..... 4
1.5 Holocene climate ..... 5

2 **Study area** ..... **9**
2.1 The modern Smeerenburgfjorden environment ..... 9
2.2 Water masses and the bathymetry in Smeerenburgfjorden. ..... 10

3 **Material and methods** ..... **13**
3.1 Fieldwork ..... 13
3.2 Coring ..... 13
3.3 Chirp sonar ..... 14
3.4 CTD (Conductivity, Temperature, Depth) ..... 14
3.5 Laboratory work ..... 14
3.6 Previous laboratory work ..... 15
3.6.1 Physical properties ..... 15
3.6.2 X-ray photography ..... 15
3.6.3 Radiocarbon dating ..... 16
3.7 Current lab work ..... 16
3.7.1 Description of the cores ..... 16
3.7.2 Magnetic susceptibility ..... 17
3.7.3 Sediment sampling ..... 17
3.7.4 Foraminiferal analysis ..... 17
3.7.5 Ice Rafted Debris (IRD) analysis ..... 18
3.7.6 Isotope analysis of benthic foraminifera ..... 19
3.8 Radiocarbon dating ..... 20
3.8.1 Accelerator Mass Spectrometry (AMS) ..... 20
3.8.2 Marine reservoir effects ..... 20
3.8.3 The sampling ..... 20

4 **Benthic foraminifera** ..... **23**
4.1 Ecology ..... 23
4.2 Ecological preferences of dominating species ..... 24
4.2.1 *Cassidulina reniforme* (Nørvang, 1945) ..... 24
4.2.2 *Cibicides lobatulus* (Walker & Jacob, 1798) ..... 24
4.2.3 *Elphidium excavatum* forma *clavata* (Cushman, 1944) ..... 25
4.2.4 *Nonionellina labradorica* (Dawson, 1860) ..... 25
4.2.5 *Astrononion gallowayi* (Loebilch & Tappan, 1953) ..... 26
4.2.6 *Buccella frigida* (Cushman, 1922) ..... 26
4.3 Ecological preferences of the secondary species ..... 27
4.3.1 *Cassidulina neoteretis* (Seidenkrantz, 1995) ..... 27

4.3.2 *Elphidium subarcticum/albiumblicatum* (Cushman, 1944) ..... 27
4.3.3 *Glabratella wrightii* (Brady 1881) ..... 27
4.3.4 *Triloculina trihedra* (Loeblich & Tappan, 1953) ..... 27
4.3.5 *Stainforthia feylingi / Stainforthia schreibersiana* (Knudsen & Seidenkrantz, 1944) ..... 27
4.4 Agglutinated species ..... 28
4.4.1 *Verneuilinulla advena* (Cushman, 1922) ..... 28
4.4.2 *Spiroplectammina biformis* (Parker & Jones, 1865) ..... 28
4.4.3 *Lepidodeuterammina ochracea* (Williamson, 1858) ..... 28
4.4.4 *Quinqueloculina stalkeri* (Loeblich & Tappan, 1953) ..... 28
4.4.5 *Labrospira crassimargo* (Norman 1892) ..... 28

**5 Results ..... 29**
5.1 Sedimentological description ..... 29
5.2 Description of biozones ..... 29
5.3 CTD (Conductivity, Temperature, Depth) description ..... 29
5.4 JM06-024-GC3 ..... 32
5.4.1 Unit 1 (410 – 303.5 cm) ..... 32
5.4.2 Unit 2 (303.5 – 203 cm) ..... 32
5.4.3 Unit 3 (203 – 101 cm) ..... 32
5.4.4 Unit 4 (101 – 0 cm) ..... 33
5.5 Biozones in core JM06-024-GC3 ..... 37
5.5.1 Assemblage zone 1: *Cassidulina reniforme* (253 – 183 cm) ..... 37
5.5.2 Assemblage zone 2: *Cassidulina reniforme & Elphidium excavatum* f. *clavata* (183 – 97 cm) ..... 38
5.5.3 Assemblage zone 3: *Elphidium excavatum* f *clavata* (97 – 0 cm) ..... 39
5.6 JM07-049-GC1 ..... 43
5.6.1 Unit 1 (304.5 – 202.5 cm) ..... 43
5.6.2 Unit 2 (202.5 – 102 cm) ..... 43
5.6.3 Unit 3 (102 – 0 cm) ..... 43
5.7 Biozones in core JM07-049-GC1 ..... 47
5.7.1 Assemblage zone A: *Nonionellina labradorica* (298 – 255 cm) ..... 47
5.7.2 Assemblage zone B: *Cibicides lobatulus* (255 – 219 cm) ..... 48
5.7.3 Assemblage zone C: *Elphidium excavatum* f. *clavata, Astrononion gallowayi & Cibicides lobatulus* (219 – 0 cm) ..... 49
5.8 CTD desctiption ..... 51
5.8.1 JM06-024-GC3 ..... 51
5.8.2 JM07-049-GC1 ..... 51

**6 Chronology ..... 53**
6.1 Radiocarbon dates ..... 53
6.2 Age model ..... 54
6.2.1 Sedimentation rate ..... 55

**7 Interpretation ..... 59**
7.1 JM06-024-GC3 ..... 62
7.1.1 Time interval 10,000 – 6800 $^{14}$C yr BP (early Holocene). ..... 62
7.1.2 Time interval 6800 – 4500 $^{14}$C yr BP (mid - Holocene). ..... 64
7.1.3 Time interval 4500 $^{14}$C yr BP – present (late Holocene) ..... 65
7.2 JM07-049-GC1 ..... 70

7.2.1 Time interval 10,000 – 6800 $^{14}$C yr BP (early Holocene). ..... 70
7.2.2 Time interval 6800 – 4500 $^{14}$C yr BP (mid - Holocene)..... 72
7.2.3 Time interval 4500 $^{14}$C yr BP – present (late Holocene)..... 72

8 **Discussion and correlation.....75**
8.1 Environment and climate.....75
8.2 Paleoceanographic implications: development during the Holocene and comparison to west and north Svalbard .....78
8.2.1 Early Holocene ..... 78
8.2.2 Middle Holocene ..... 79
8.2.3 Late Holocene..... 80
8.2.4 CTD ..... 81
8.3 Application of benthic foraminifera stable isotopes.....82
8.3.1 Oxygen Isotopes ..... 82
8.3.2 Carbon isotopes ..... 86
8.4 IRD from Smeerenburgfjorden compared to Sea Surface Temperature in Svalbard and in the Barents Sea.....87
8.5 Paleoenvironmental reconstruction in Smeerenburgfjorden using proxy records in cores JM06-024-GC3 and JM07-049-GC1 .....89
8.5.1 Proxy variations..... 89
8.5.2 Data from JM06-024-GC3..... 90
8.5.3 Data from JM07-049-GC1..... 92

9 **Conclusions and summary.....95**

10 **References.....97**

## Acknowledgements

First, I want to thank my supervisor Professor Tine L. Rasmussen for great supervision and guidance while writing this thesis. Because of you, I was able to experience sailing adventures by participating in scientific cruises and get a taste of what the future might hold for a young geologist. You have increased my interests in marine geology and been very patient and supportive during the last stages of writing.

I would like to thank CAGE (Centre for Arctic Gas Hydrate, Environment and Climate, the Norwegian Research Council Centres of Excellence grant no. 223259) for providing financial support of my thesis.

My great office-foraminifera-gym buddy, Björg Jónsdóttir receives big hugs for being there for me from the beginning. You have been my rock!

Andri Hrafn Ingvason, my fiancé has been the most patient and the most understanding man on earth. You have supported me and encouraged me to follow my dream and I am forever grateful. Without you in my life, it would have been a lot more difficult. Thank you.

Special thanks goes to Professor Tove Nielsen at the Geological Survey of Denmark and Greenland, Denmark, and Dr. Matthias Forwick at the University in Tromsø, for providing me the two cores to investigate. Additionally I would like to thank Julie Heggdal Velle for data.

The microscopic room in the laboratory of the University in Tromsø was my second home for a year, while picking foraminifera. Big thanks go to the staff, Trine Dahl for helping with the identification of mollusc shells and learning to handle the lab equipment, and Ingvild Hald for teaching and trusting me with the lab equipment. You have been very helpful.

I want to thank the captain and the crew on board the research vessel, R/V Helmer Hanssen in April 2015 for receiving CTD, multi-beam and chirp data and Bjørn Runar Olsen for processing and helping me with these data. I also want to thank Torger Grytå for scanning of the X-ray images.

Big thanks goes out to my friends and fellow students, Liz for a great help with my foraminifera graphs, Karoline for a great company in the microscopy lab and interesting conversations about foraminifera and polar bears, and Ingrid for a great company during lunch breaks. You girls are wonderful!

Finally, I would like to thank my wonderful family in Iceland, especially my mom for pushing me forward and believing in me, and my dad for always being there for me. Stuðningur ykkar hefur verið ómetanlegur! You are the best!

Thank you.

Erna Ósk Arnardóttir

Tromsø, May 2015

# 1 Introduction

## 1.1 Figures

The main objective of this master thesis is to reconstruct the paleoenvironment and paleoceanography in Smeerenburgfjorden, Svalbard. The reconstruction is based on two gravity cores from Smeerenburgfjorden. The benthic foraminiferal faunas and the lithology is described. Detailed AMS $^{14}C$ datings show that both records date from the Holocene.

## 1.2 Background

### 1.2.1 The Svalbard archipelago

The northernmost landmass along the Euro-Arctic continental margin is the Svalbard Archipelago (Fig. 1.1). It stretches between 76° - 81°N and 10° - 35°E. The archipelago comprises two larger islands, Spitsbergen and Nordaustlandet, and several smaller islands. Spitsbergen is the largest island covering more than half of the archipelago. Glacially eroded fjords and high mountains characterize it. The site investigated in this study is the shelf area of Smeerenburgfjorden, a fjord located in Albert I Land of the northwestern corner of Spitsbergen (Fig. 1.1).

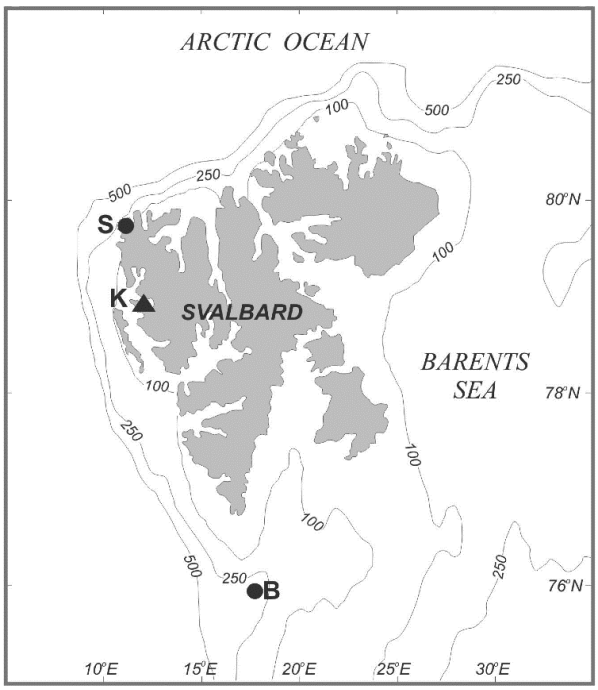


***Figure 1-1 Overview of the Svalbard archipelago. S stands for Smeerenburgfjorden, K for Kongsfjorden and B for Storfjorden Trench, southern Barents Sea. Image from Sun et al., 2007.***

## 1.3 Oceanography

The oceanography of western Spitsbergen is highly influenced by the currents flowing around the Svalbard archipelago. It is dominated mainly by three water masses, the Atlantic Water, the Arctic Water and the Polar Water (Loeng, 1991).

The West Spitsbergen Current (WSC) is the northernmost branch of the Norwegian Atlantic Current (NAC). The WSC transports large amounts of heat and salt into the Arctic Ocean. It is derived from the warm (T > 3°C) and saline (S > 34.9‰) Atlantic Water (AW) (Gammelsrød and Rudels, 1983; Saloranta et al., 2001). The AW layer of the WSC occupies the upper 600 m, resulting in ice-free areas west of Spitsbergen (Svendsen et al., 2002). As the water masses travel further north, they lose more heat. The heat loss causes the water density to increase, and at 78°N, they flow under fresher and colder water masses and follow the continental margin of Spitsbergen (Aagaard et al., 1975). Water masses tend to follow the bathymetry of the ocean bottom (Rudels, 1987) and at 79.5° N, the WSC splits into three branches (Manley, 1995) (Fig. 1.2).

Arctic type water (ArW) has lower salinity (34.4 – 34.7‰) and is easily recognized by its low temperature (core temperature < -1.5°C) (Loeng. 1991). ArW originates from the East Spitsbergen Current (ESC) and travels as an anticyclonal coastal current (Cottier et al., 2005; Nilsen et al., 2008). It is colder and fresher and flows onshore the continental shelf from Storfjorden, rounds the southern tip of Spitsbergen and flows along the Spitsbergen shelf, where a northward flow prevails (Fig. 1.2). On the coast, additional freshwater influx comes from the fjord glaciers on Spitsbergen (Hopkins, 1991; Saloranta and Svendsen, 2001; Svendsen et al., 2002; Cottier et al., 2005).

The upper Arctic Intermediate Water (AIW), a cold and oxygenated water, originates in the Icelandic and Greenland Sea gyres. AIW is carried northwards via the eastern Fram Strait, where it mixes with the West Spitsbergen Current (WSC), lowering the temperature of the warm AW inflow into the Arctic Ocean (Aagaard et al., 1985).

Polar Front Water (PFW) is a mixture of AW and ArW (Loeng, 1991), and marks the boundary (Polar Front) between two major water masses, the WSC and ArW. Water exchange between PFW and WSC cause dramatic heat loss from the WSC, both in the subsurface water column (50 – 100 m) and from the warm core. The polar front can be

divided into two layers; a surface layer (0 – 50 m) and a subsurface layer (> 50 m) which can be characterized as salinity-temperature front (Saloranta and Svendsen, 2001). Arctic sea-ice extent has diminished in recent years, resulting in increased temperature of the AW in the WSC (Svendsen et al., 2002).

A process in the North Atlantic Ocean where temperate saline water gradually cools until it sinks to the bottom (Broecker 1991, 1997) and flows southwards again into the Atlantic Ocean, is termed the North Atlantic Deep Water formation (NAWD). This process is an important driving force in the thermohaline circulation (Broecker, 1991).

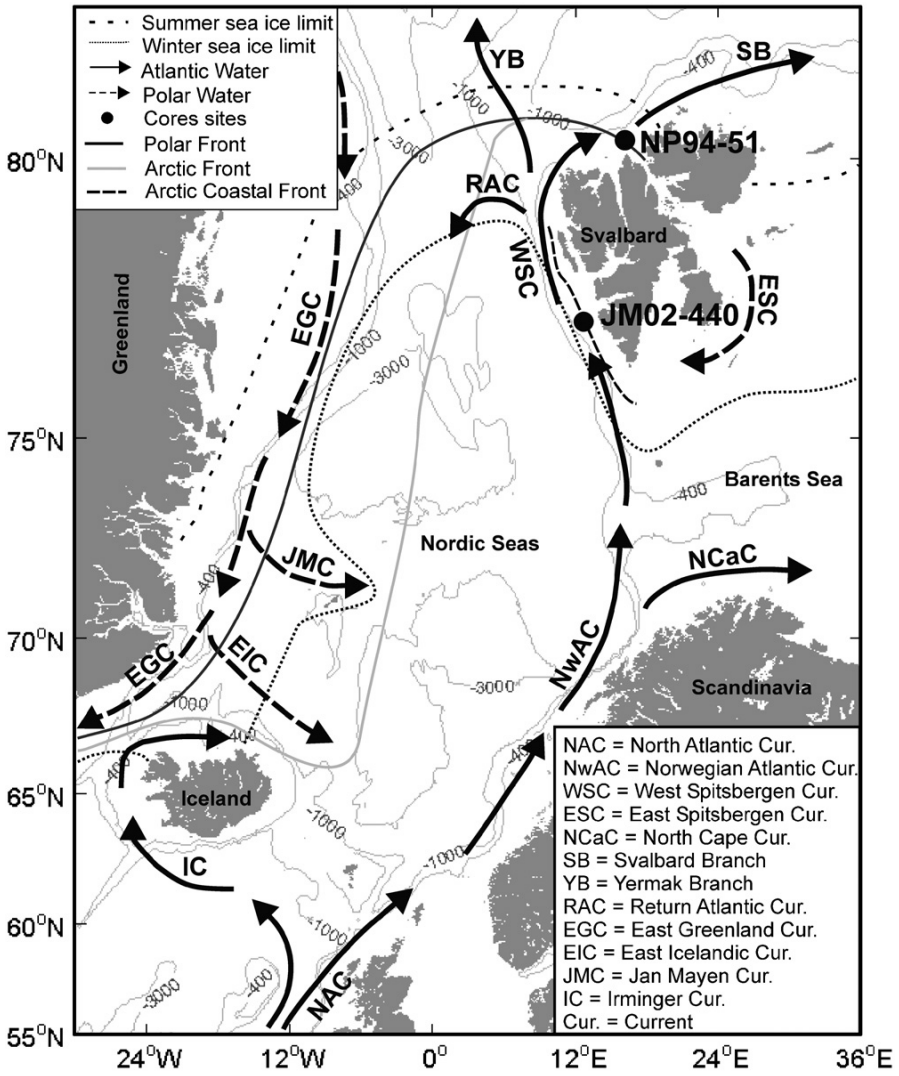


***Figure 1-2 Overview of the major ocean currents in the North Atlantic Ocean and in Svalbard. Image from Ślubowska-Woldengen, 2007.***

## 1.4 Last glacial maximum (LGM) in Svalbard

During the late Quaternary, ice sheets have grown and advanced at high latitudes, covering the continents and reaching out to the shelf edge several times (Mangerud et al., 1998). The timing and extent of the Late Weichselian ice sheet is controversial and has been the subject of several studies. Some studies indicate that the ice sheet did not reach far out on the shelf and that the shelf might even have remained ice-free during the Late Weichselian (Boulton, 1979; Forman, 1989, 1990; Miller., 1989). Other studies show the reconstruction of the Barents Sea ice sheet covering the entire archipelago of Svalbard (Grosswald, 1980; Denton and Hughes, 1981).

Ottesen and Dowdeswell (2009) conducted an investigation on the northwestern corner of Svalbard, studying the three main fjords that link the continental shelf to the ice covered mountain interior. The fjords are Magdalenafjorden, Smeerenburgfjorden and Raudfjorden. Modern glaciers in Smeerenburgfjorden flow from Vasahalvøya and Albert I Land into the catchment area of 420 $km^2$. Today the catchment area is 40 % - 60 % covered with ice. Ottesen and Dowdeswell (2007) have also reconstructed the ice-flow directions and locations of ice streams, where the ice streams seem to restrict the size of the glacial ice sheet flowing into Smeerenburgfjorden (Fig. 1.3).

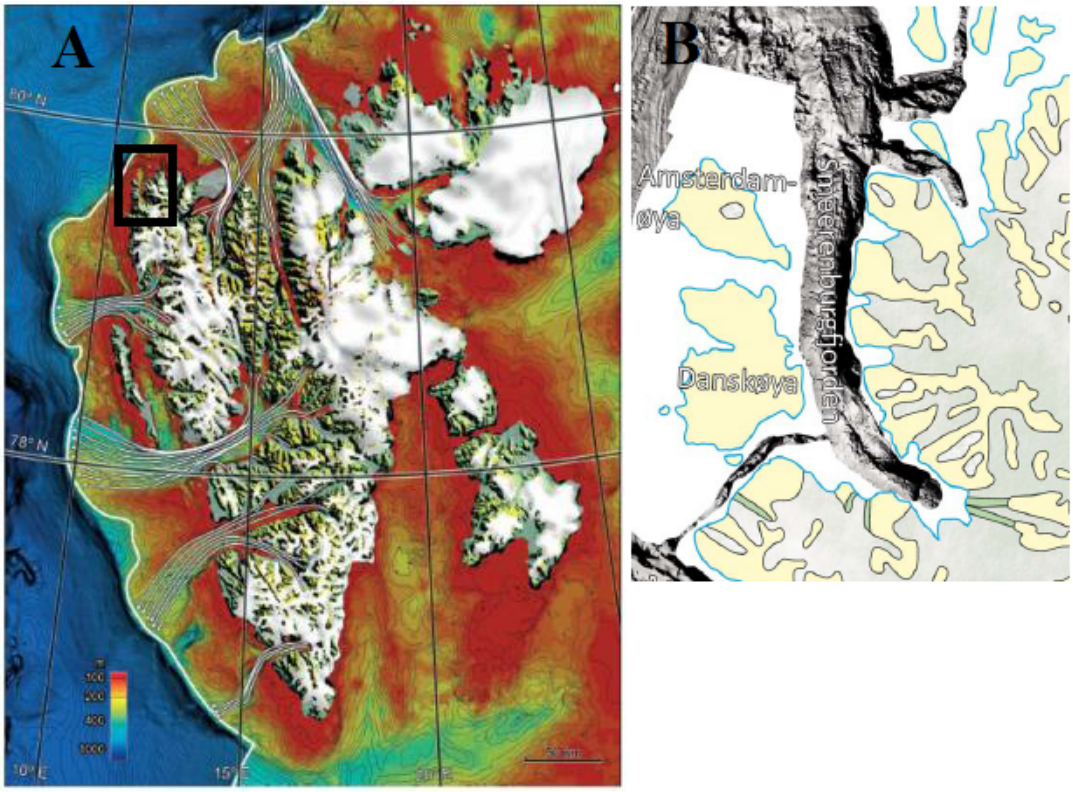


***Figure 1-3 A: Reconstruction of paleoicestreams in Svalbard during the Late Weichselian. Image from Ottesen and Dowdeswell, 2007. B: Swath bathymetry of the sea floor area in Smeerenburgfjorden. Image from Ottesen and Dowdeswell, 2009.***

## 1.5 Holocene climate

The Holocene has been divided into early, mid- and late Holocene intervals depending on oceanographic and climatic conditions (Ślubowska et al., 2005; Slubowska-Woldengen et al., 2007; Kubischta et al., 2011; Rasmussen et al., 2012, 2014). Though the climate is cold and dry today, it is warmer and more humid on the western side of Svalbard. This mild climate is due to the influx of the temperate water in the WSC. The coastal areas of Spitsbergen record a mean annual air temperature of -5°C (Svendsen and Mangerud, 1992; Humlum et al., 2003). The climate on Svalbard depends on the water masses surrounding the archipelago, especially the flow of the warm Atlantic Water reaching the western margin via the Western Spitsbergen Current (see 1.3 Oceanography).

Ice core $\delta^{18}O$ records from Austfonna (Nordaustlandet) and Lomonosovfonna (east Spitsbergen) in the study of Isaksson et al. (2003), show a warming from 1920 to the mid-1950s, and from the 1970s to present (Fig. 1.4). The periods were interrupted by colder temperatures in the 1940s and from the mid-1950s to the mid-1970s. Isaksson et al. (2003)

mentions that the $\delta^{18}O$ data from both ice cores suggest that the 20th century was the warmest during the last 600 years. The borehole temperature record from Lomonosovfonna further supports the general warming trend, with an increase of 2°C from the end of the 1800s. A sediment core from a proglacial lake called Linnévatnet, shows that a major ice advance started in the 14th and the 15th centuries and culminated in the 19th century (Svendsen and Mangerud, 1997).

Influences of cold polar air and drift ice strongly affect the climate in the northern and eastern Svalbard. The temperature difference between the north and south can vary up to 2.5°C during the wintertime, but the difference is not as high during the summer time (Hisdal, 1998; Isaksson et al., 2005).

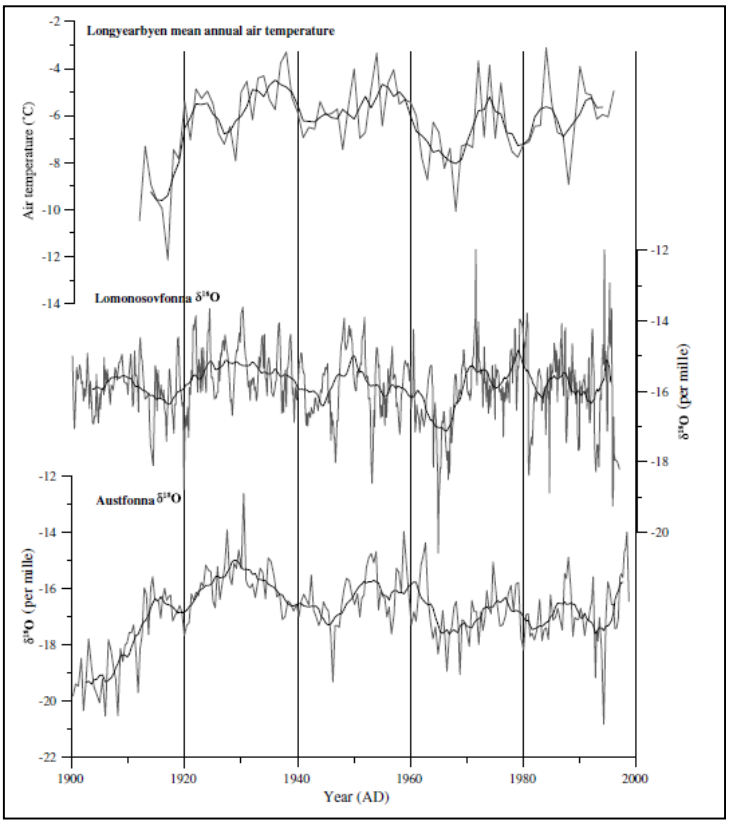


***Figure 1-4 Ice core oxygen isotope record from Lomonosovfonna and Austfonna along with the mean annual temperature in Longyearbyen, Svalbard.***

# 2 Study area

## 2.1 The modern Smeerenburgfjorden environment

Smeerenburgfjorden is located on the northwestern corner of Spitsbergen in the region of Albert I Land (Fig. 1.1 & 1.3), between 79°37'N – 79°51'N and 11°00'E – 11°30'E. The outer fjord has a north-south orientation, is approximately 20 km long and 2 – 5 km wide. The innermost part of the fjord named Bjørnfjorden, has a north-northwest – south-southeast orientation. To the west of Smeerenburgfjorden are two islands, Amsterdamøya and Danskøya, and Vasahalvøya peninsula is to the east. The sounds between Amsterdamøya-Danskøya and Danskøya-Spitsbergen are called Danskegattet and Sørgattet respectively. The mouth of the fjord is called Nordgattet (Fig. 2.1).

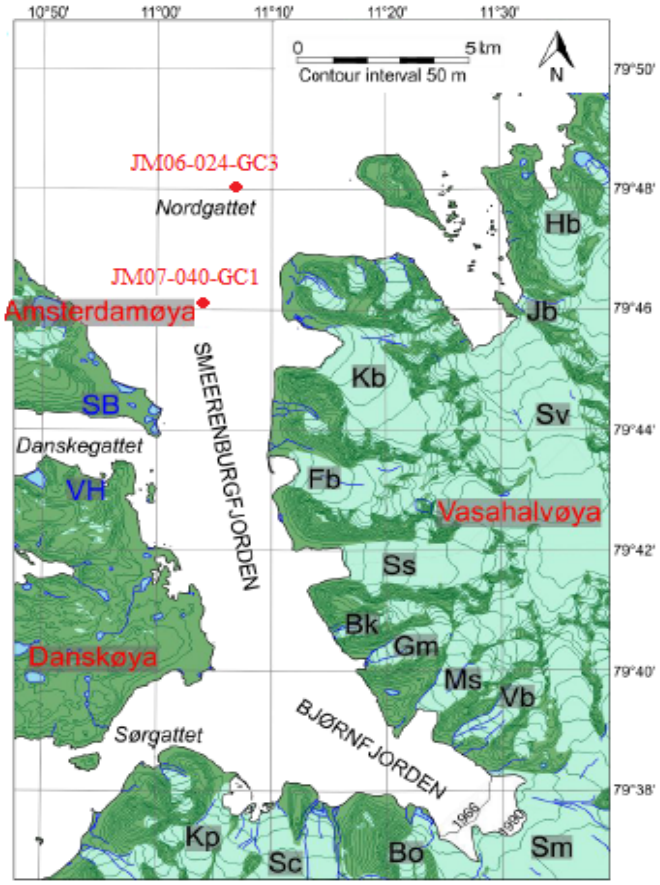


***Figure 2-1 Land image showing the location of cores JM06-024-GC3 and JM07-049-GC1. Abbreviations of glaciers in the fjord are marked (figure modified from Velle, 2012).***

A total of 11 glaciers terminate in the fjord, from Sørgattet to the northern part of Vasahalvøya: Kvasspiggbreen (Kp), Scheibreen (Sc), Borgbreen (Bo), Smeerenburgbreen (Sm), Viksbreen (Vb), Marstrandbreen (Ms), Gullmarbreen (Gm), Brattkleivbreen (Bk), Sellströmbreen (Ss), Frambreen (Fb), Kennedybreen (Kb) and Svitjodbreen (Sv) (Fig. 1.2).

## 2.2 Water masses and the bathymetry in Smeerenburgfjorden.

There are several factors to consider regarding the water masses in a fjord. Still fjords have a distinct vertical stratification with approximately three-layer structure: a surface layer with low salinity, an intermediate layer, which is more saline and a high salinity deeper basin (Skarðhamar and Svendsen, 2010). Arctic fjords generally show this stratification during the summer season (Svendsen et al., 2002) while winter masses are overturned due to cooling (Skarðhamar and Svendsen, 2010). The bathymetry in Smeerenburgfjorden shows a distinct sill close to the fjord mouth (Fig. 2.2) which plays an important role in the water mass distribution over the two core locations, JM06-024-GC3 and JM07-049-GC1. The outer part of the fjord is connected to the open ocean and the inner part is behind the sill (Fig. 2.1 and 2.2).

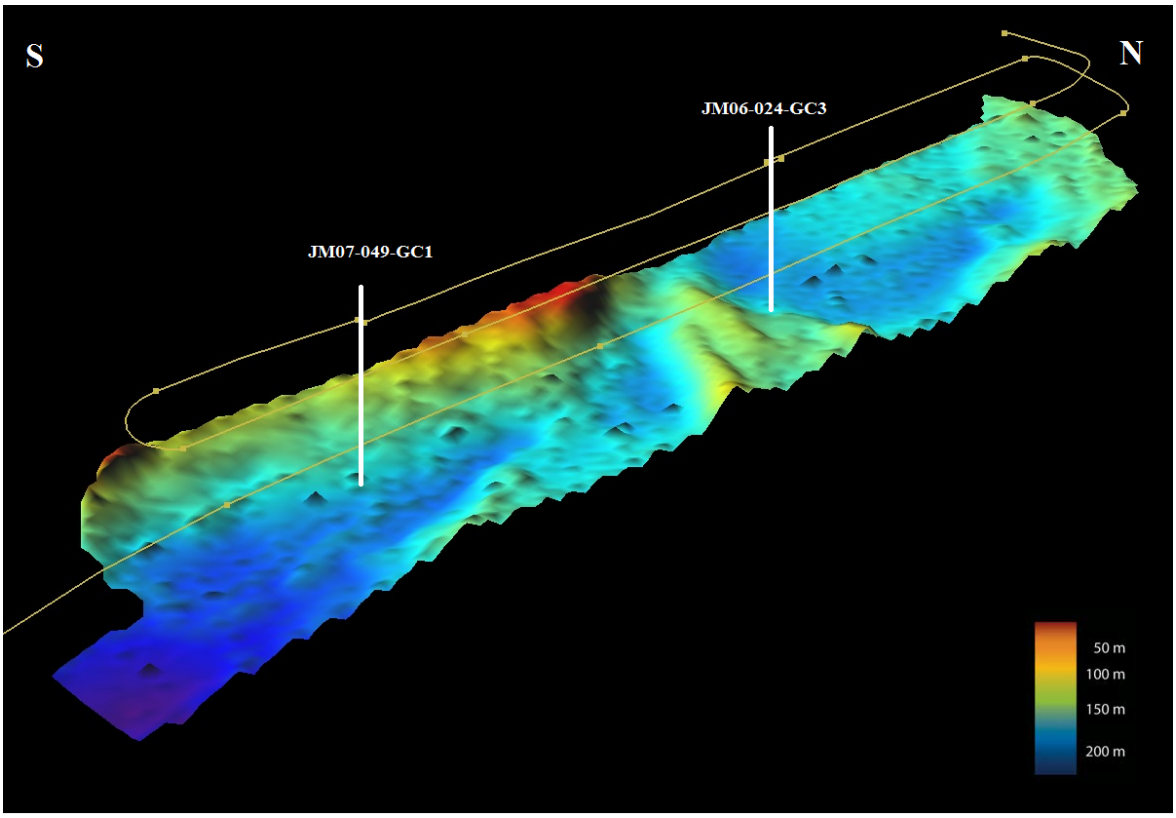


***Figure 2-2 Shaded relief swath bathymetry over the coring location showing the distinct sill, separating the core locations of JM06-024-GC3, to the right and JM07-049-GC1 to the left. The yellow line indicates the transect line sailed to collect the swath bathymetry, and the CTD data in April 2015. Image made by Bjørn Runar Olsen, and modified by the author.***

In the study of Ottesen and Dowdeswell (2009), this distinct sill is an arched ridge that cuts across the fjord adjacent to Svitjodbreen (Fig. 1.3B and 2.1), which drains into the fjord from Vasahalvøya. They interpret this ridge to have formed during still-stands in ice retreat, allowing the sediments to accumulate for a significant amount of time. These kind of ridges can act as pinning points for still-stands of the ice front during retreat.

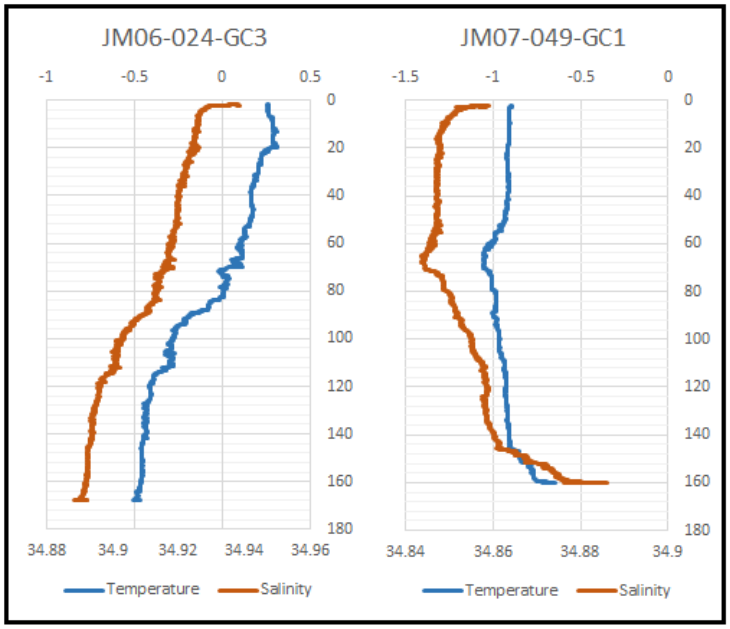


***Figure 2-3 CTD data collected over JM06-024-GC3 and JM07-049-GC1 core locations in April 2015. Orange line indicates salinity and blue line indicates temperature.***

In the study of Ślubowska-Woldengen et al. (2007) water mass distribution with maximum temperature and salinity were collected outside Smeerenburgfjorden in August 2004. The CTD profile indicates that the shelf has a mixture of two water masses, Arctic Surface Water and Polar water. The warmer Atlantic Water is confined to the continental margin. The CTD measurements collected over the coring sites in April 2015 for this study, show different temperature and salinity trends (Fig. 2.3). Waters from the outer part of the sill influence the fjord mouth (core location JM06-024-GC3) while the inner part of the fjord (core location JM07-049-GC1) shows a still fjord characterization, described by Skarðhamar and Svendsen (2010). The early summer temperatures in Smeerenburgfjorden varies between the core locations. The salinity over JM06-024-GC3 is decreasing along with the temperature while JM07-049-GC1 shows the salinity has an increasing trend towards the bottom. The temperature is more stable, although there is a small change

towards the bottom. At the bottom, both salinity and temperature increase rapidly, showing the characterization of a still fjord.

# 3 Material and methods

## 3.1 Fieldwork

The material provided for this master thesis, cores JM06-024-GC3 and JM07-049-GC1 were collected during two educational cruises in Smeerenburgfjorden in May 2006 and 2007, respectively (Table 3.1). The cores were retrieved with a gravity corer on board the research vessel of the University of Tromsø, R/V Jan Mayen, (today R/V Helmer Hanssen) during the courses AG-202 and AG-211, Arctic Marine Geology at the University Centre in Svalbard.

*The two cores chosen for this thesis, JM06-024-GC3 and JM07-024-GC1 (hereafter referred to as core JM24 and core JM49, respectively), were retrieved from each side of a sill at the mouth of the fjord. Core JM24 was taken outside the sill and core JM49 from inside the fjord, behind the sill (Fig. 3.1)*

***Table 3.1 Position of coring site, length of the cores and the water depth at the coring site.***

| Core | Position | Water depth (m) | Core length (m) |
|---|---|---|---|
| JM06-024-GC3 | 79°48,26' N, 11°06,87' E | 181 | 4.10 |
| JM07-049-GC1 | 79°46,28' N, 11°04,75' E | 174.4 | 3.04 |

## 3.2 Coring

The gravity corer consists of a 6-meter long steel tube with a 1.6-ton weight at the top. Inside the tube is put a plastic core liner and at the bottom, the steel tube is fitted with a core cutter and a core catcher. During the core retrieval, the core cutter slices through the sediment, allowing the steel tube to penetrate. The core catcher holds the sediment inside the plastic liner, preventing the sediment escaping as the corer is being raised. When the gravity corer is pulled back on board, the plastic liner is pulled out from the steel tube and cut into 1-meter sections. Each section is closed with plastic caps, labelled accordingly with the section number, depth of the core and the core name. The core sections were stored in a cooling room in + 4°C, until they were opened in 2011.

## 3.3 Chirp sonar

Sub-bottom chirp profilers are high-resolution frequency-modulated marine sources showing vertical resolution of the top 30 m of unconsolidated sediments. The vertical resolution is dependent on the bandwidth of the source, and the horizontal resolution is dependent on the source characteristics (Quinn et al., 1998).

For this study, the chirp profile was collected during a cruise with R/V Helmer Hanssen April 5th, using EdgeTech 3300-HM hull-mounted sub-bottom profiler of the University in Tromsø (Fig. 3.1). The pulse frequency was 2 – 10 kHz and a 20 $ms^{-1}$ pulse length was used. The ship travelled at a speed between 5.8 and 6.0 knots and the ping rate was 2 Hz.

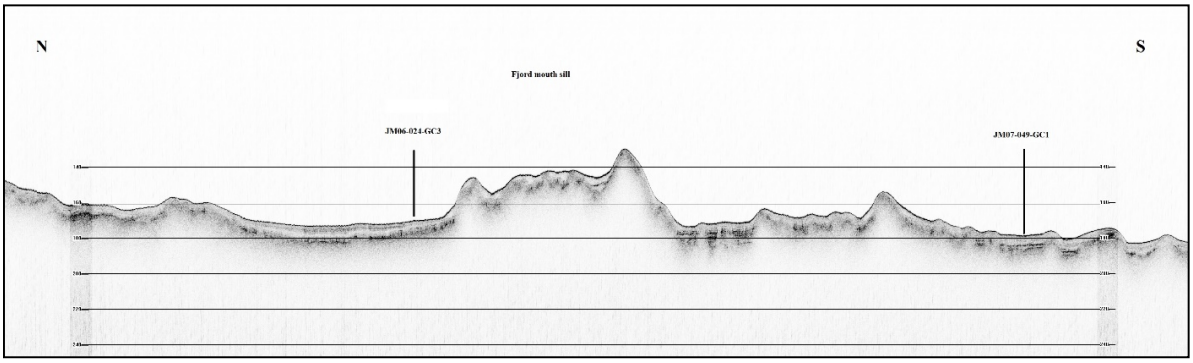


***Figure 3-1 Seismic profile showing the locations for cores JM24 and JM79. The fjord mouth is to the north, and the inner part is to the south.***

## 3.4 CTD (Conductivity, Temperature, Depth)

During the scientific cruise in April 2015, CTD measurements over the core positions were collected (Fig. 2.3). CTD gives information about oceanographic parameters. An instrument (Seabird 911 Plus) was lowered from the sea surface to the bottom of the fjord, measuring continuously and receiving information about the whole water mass. Conductivity and temperature are measured against the depth and the conductivity is then calculated to salinity. Temperature and is lower over the location behind the sill (JM49) and values show an opposite trend in front of the sill (Fig. 3.2).

## 3.5 Laboratory work

The laboratory work took place between January 2014 and February 2015 and was carried out in the laboratory of the Department of Geology, University of Tromsø, Norway. Samples for isotope analyses were measured at the Department of Earth Science and

Bjerknes Centre for Climate Research at the University of Bergen, Norway and samples for Accelerator Mass Spectrometry (AMS) were measured at the $^{14}$CHRONO Centre at Queen´s University in Belfast, Northern Ireland. Below is described previous laboratory work that has been done on the cores prior to the author's work (see also Velle, 2012).

## 3.6 Previous laboratory work

### 3.6.1 Physical properties

The physical properties of the cores were measured using a GEOTEK Multi Sensor Core logger (MSCL) before they were opened to determine the physical properties of the sediment (Fig.3.2). The core logger measures the wet bulk density, P-wave velocity, the magnetic susceptibility, core length, width and temperature of the cores.

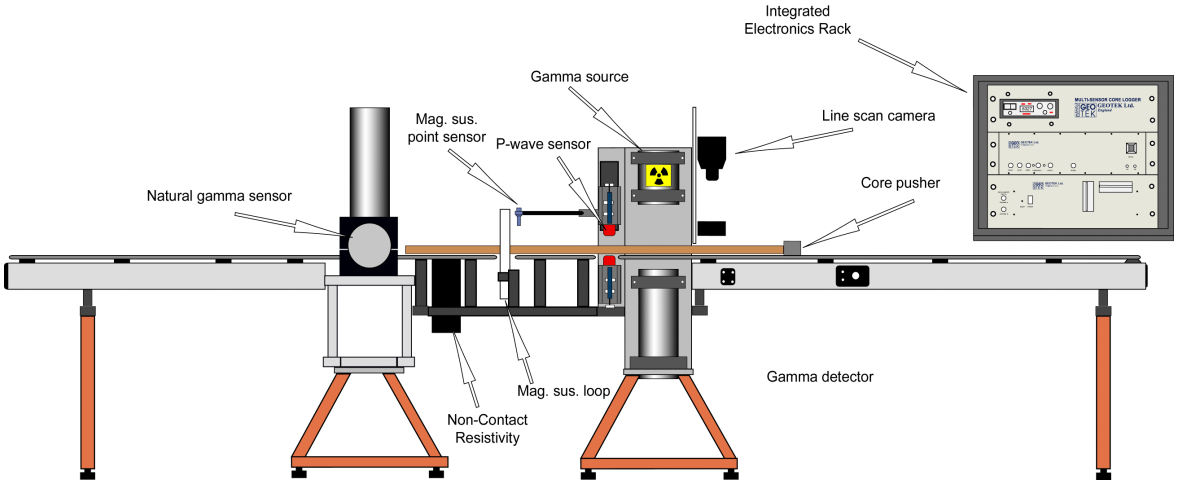


***Figure 3-2 Figure 3.2 Image form GEOTEK showing Multi Sensor Core Logger and its main features (GEOTEK, 2000)***

In July 2011, a circular saw and an osmotic knife were used to open the cores. One-half of the core was wrapped in plastic for archiving and stored in a cooling room at +4°C, while the work part was kept for further lab work.

### 3.6.2 X-ray photography

X-ray photographs were taken of half core sections using Philips Macrotank. The photographs show shadow images of different density, lighter objects are high density and darker objects are lower density. The photographs help with identifying objects in the core, when it is being described for features such as molluscs, clasts or sedimentary structures. The photographs were used in March 2015.

### 3.6.3 Radiocarbon dating

From Velle´s study (2012), JM24 records the oldest age and there are five datings that exist from approximately every 100 cm of the core. JM49 records the second oldest age, from the bottom of the core. Previous ages are shown in the table below (Table 3.2).

Velle (2012) used the CALIB 6.1.0 software and Marine09 calibration curve to calibrate the radiocarbon ages (Table 3.2). The ages were re-calibrated using the latest version CALIB7.0.4 (see Chronology).

***Table 3.2 Results from radiocarbon dating and the calibration from Velle (2012).***

| Core | Sampling depth (cm) | $^{14}$C age | Cal.yr BP Calib 6.1.0 1σ range | Cal.yr BP Calib 6.1.0 1 σ mean | Species |
|---|---|---|---|---|---|
| JM07-049-GC1 | 288 | 8441 ± 40 | 8843 – 8995 | 8919 | *Macoma calcarea* |
| JM06-024-GC3 | 402.5 | 10044 ± 46 | 10779 – 11031 | 10905 | *Nuculana sp.* |
| JM06-024-GC3 | 305 | 8311 ± 41 | 8602 – 8789 | 8695 | *Yoldiella lenticula* |
| JM06-024-GC3 | 205 | 6916 ± 44 | 7290 – 7394 | 7342 | *Nuculana pernula* |
| JM06-024-GC3 | 101 | 4654 ± 31 | 4708 – 4829 | 4764 | *Macoma calcarea* |
| JM06-024-GC3 | 2.5-3 | Modern | - | - | *Cardium sp.* |

After the previous lab work, the working half was wrapped in plastic and stored in a cooling room at +4°C.

## 3.7 Current lab work

### 3.7.1 Description of the cores

In January 2014 the working half was re-opened, the sediments visually described and logged. Colour of the cores was described using a Munsell´s soil colour chart (Munsell 1973). Later the X-ray images were used alongside the drawing of the cores, using the program CorelDraw. Based on these data, the characteristic elements of the core and their boundaries were identified.

### 3.7.2 Magnetic susceptibility

In April 2015, the Bartington point sensor (MS2E) for split cores only, was used to measure the magnetic susceptibility for both cores. The sensor is placed on the core surface for each measurement. It uses the same electronics as the loop sensor, however this sensor can only be used at a sampling rate of 1.0 Hz (equivalent to 1 second). The point sensor gives much higher spatial resolution but is less sensitive. It is more sensitive to temperature fluctuations so the temperature of the cores must reach room temperature before measurement. The sensor measures the frequency change of the magnetic field when it detects magnetic material in the sediment. The recorded change is then converted to magnetic susceptibility values in the unit of mass or volume specific (GEOTEK, 2000).

### 3.7.3 Sediment sampling

Sampling intervals of the two cores varied depending on lithology. In Velle´s study (2012), core JM24 was interpreted to be disturbed below 260 cm. Using that information, JM24 was sampled approximately every 5 cm down to 200 cm, and every 10 cm down to 250 cm.

Core JM49 was sampled approximately every 5 cm down to 300 cm.

Each sample was cut with an osmotic knife and a spatula into 1 cm slices. The samples were put into labelled plastic bags and weighed. The wet samples weighed from 15.14g to 52.77g and were stored in a freezer, until they were dried in a freeze-dryer. The type of the freeze dryer used, was Christ: Alpha 1 – 4 from the Geology Department Laboratory, University of Tromsø.

The samples were weighed again after the freeze-drying, the plastic bag was weighed and the dry weight of each sample calculated. The samples were wet sieved, using mesh sizes of 63 μm, 100 μm, 500 μm and 1 mm. After every sieving process, the residues were removed from the sieves, using distilled water, into wet strengthened filter paper, and dried in an oven for at least 48 hours at a temperature of 40°C. Finally, the residues were weighed, put into small sample glasses and labelled.

### 3.7.4 Foraminiferal analysis

The size-fraction of > 100 μm was used for foraminifera picking and counting. The residue, or a fraction of a residue, was evenly distributed over a picking tray with 45 squares with a collecting tray placed underneath. If the residue was very large, a splitter was used, to split the sample 50/50. Benthic foraminifera were counted and identified to

species level. Later the percentage of each species was calculated. Planktonic foraminifera were counted, but not identified. If the foraminifera were worn or broken, they were not counted or identified to species. Phleger (1960) suggested that 300 specimens provided sufficient accuracy for most quantitative examinations. Therefore, for this thesis, approximately 300 foraminifera were counted from 82 samples. The microscope used for picking and identifying species was Leica CLS 150X – MZ12.5.

The benthic foraminifera were subdivided into agglutinated and calcareous forms, and the concentration of each group was calculated as the number of specimens per gram dry weight sediment. The percentages of agglutinated and calcareous specimens were calculated relative to the total sum of calcareous and agglutinated specimens.

*3.3.4.1 Faunal modification*

Disturbances of the sediments can result in difficulties in interpretation of the faunal data. Common processes are re-sedimentation, bioturbation or diagenesis. According to Velle (2012), the section 253 – 400 cm in core JM24, is re-sedimented. Therefore, samples were not collected from that part.

*3.3.4.2 Major faunal parameters*

The relative abundance of each species is calculated relative to the total number of benthic specimens, to get the percentage of each species:

*Percentage = (number of specimens of species A)/(number of total specimens)*100*

The relative amount of foraminifera per dry weight sediment is calculated relative to the total number of benthic foraminifera:

*Concentration = (((amount foraminifera/squares counted)*45)*number of splits)/dry weight sediment*

### 3.7.5 Ice Rafted Debris (IRD) analysis

The content of IRD was calculated as the number of mineral grains in the > 500 μm grain size fraction per gram dry weight sediment. The samples were evenly distributed on the picking tray and all mineral grains were counted. The concentration of IRD in the two size fractions were calculated as number of grains per gram dry weight sediment.

*3.3.5.1 Processing of data and statistics*

All foraminiferal and IRD data were plotted using Excel for Windows along with all calculations. Later, all the graphs were plotted in Plot 2 for Apple for composite figures and fine-tuned in CorelDRAW for Windows.

### 3.7.6 Isotope analysis of benthic foraminifera

According to Shackleton (1974), "the oxygen isotope method of determining palaeotemperatures is widely regarded as a tool of unique potential in the investigation if past changes in the temperature of the earth". In this study, oxygen and carbon isotopes were used and compared with other proxies from both cores (see Discussion).

*3.7.6.1 The sampling*

Oxygen and carbon isotopes were measured in both cores. For JM24, well-preserved specimens without signs of dissolution of the benthic foraminiferal species *Cibicides lobatulus* and *Cassidulina reniforme* were measured and for JM49, the benthic foraminiferal species *Nonionellina labradorica* was measured. The samples were labelled, weighed and sent to the Bjerknes Centre for Climate Change, University of Bergen.

*3.7.6.1 The method*

The oxygen isotope measurements were performed at the Geological Mass Spectrometer (GMS) laboratory at the University in Bergen, Norway. The Finnigan MAT 253 mass spectrometer was used. The benthic foraminifera *Cibicides lobatulus* and *Cassidulina reniforme* were analysed for core JM24 at 5 cm intervals (0 – 198 cm) and 10 cm intervals (198 – 253 cm). For core JM49 the benthic foraminifera *Nonionellina labradorica* was analysed at 5 cm intervals (0 – 60 cm) and 10 cm intervals (60 – 298 cm). The external error based on the reproducibility of internal carbonate standards at the GMS laboratory is ± 0.06 for $\delta^{18}O$ and ± 0.03 for $\delta^{13}C$ versus PeeDee Belemnite (PDB) established on replicate measurements of 10 carbonate standards NBS19 (Coplen, 1996; Osterman and Curry, 2000). The oxygen isotope records were corrected for isotopic disequilibrium; +0.64‰ for *C. lobatulus* (Shackleton, 1974) and – 0.2‰ for *N. labradorica* (Duplessy et al., 2005; Ivanova et al., 2008; Rasmussen and Thomsen, 2009) to adjust for offsets between the various species (Rasmussen and Thomsen, 2009; Rasmussen and Thomsen, 2014). The values for *Cassidulina reniforme* were not corrected since there is no offset (Hald et al., 2004). To correct for the ice volume changes in oxygen isotopes, the sea-level

curve of Fairbanks (1989) was used. Global ice volume causes 0.11‰ change in the $\delta^{18}O$ every 10 meters of sea level change.

## 3.8 Radiocarbon dating

### 3.8.1 Accelerator Mass Spectrometry (AMS)

Five AMS $^{14}C$ dates were performed at the Chrono Centre, Queen´s University, Belfast, UK. All the dates were measured on bivalve shells (Table 3.2). In the accelerator, sample particles are accelerated to high speed towards a magnetic field. A mass spectrometer detects atoms of specific weights based on their angle. The heaviest particle will deflect the least towards the magnetic field. The particles are identified and the number of $^{14}C$ present in the sample is measured (Bowman, 1990).

### 3.8.2 Marine reservoir effects

The concentration of $^{14}C$ in the atmosphere and in the living organism is not constant. Therefore, the radiocarbon ages need to be calibrated to calendar years. Another factor to consider is the marine reservoir effect. The atmosphere-ocean boundary mixes fresh $^{14}C$ from the atmosphere to the $^{14}C$ of the oceans. The concentration of the $^{14}C$ at the ocean-atmosphere interface is constant. As the water sinks, the $^{14}C$ starts to decay. The age of the water mass increases, resulting in an apparent age. In addition is the local regional difference ($\Delta R$), which varies over short distances. Marine organisms take up the old $^{14}C$ from the surrounding water mass into their shells, obtaining an apparent age, which is older than their true age (Bowman, 1990; Mangerud et al., 2006).

The received radiocarbon dates were calibrated to calendar years Before Present (cal yr. BP) using Calib 7.0.4 and Marine 13 (Stuvier and Reimer, 1993; Reimer et al., 2013). The program automatically withdraws an average marine reservoir age of 405 years (Mangerud and Gulliksen, 1975), and the additional regional difference ($\Delta R$) was accounted for. In the study of Velle (2012), $\Delta R$ of 105 ± 24 was applied (Mangerud et al., 2006; Reimer et al., 2009) and in this study, the same regional difference was applied.

### 3.8.3 The sampling

After the sieving of the samples, the amount of shells and shell fragments in the size fraction >500 μm and 1 mm from both cores were sufficient to be used for radiocarbon dating at any depth of choice. Of all the cores taken in Smeerenburgfjorden in 2006 and 2007, JM24 is the longest. For this thesis, only one depth was chosen for dating in core JM24, where it has not been dated yet (Table 6.1). JM49 is the second oldest and four

depths were chosen at approximately every 50 cm down core. All shells were well preserved and unbroken (Table 6.1).

The shells and shell fragments for radiocarbon dating were carefully chosen with the naked eye and the state of the shells was investigated through a microscope. Whole shells were chosen for all depths except one. A total of five shells and shell fragments were sent for radiocarbon dating (see Table 6.1).

# 4 Benthic foraminifera

Benthic foraminifera are single celled organisms that mainly live in marine environments. Their tests are calcareous, agglutinated or organic. Their shells are divided into chambers where new chambers are added as the organism grows. Benthic foraminifera live on or in the sediment. The study of fossil foraminifera is useful in biostratigraphy, paleoecology, paleobiography and oil exploration.

Benthic foraminifera are sensitive to environmental changes and can be used to reconstruct modern and ancient marine environments. The calcareous species can be used for radiocarbon dating and isotope analysis and whole assemblages can provide insight into paleoceanographic changes through time. They also give information about previous glacial histories and the sedimentary environment. Studies on the foraminifera stratigraphy has proven to be an important tool in reconstructing the marine paleoenvironment (Hald & Vorren, 1987; Hald & Steinsund, 1996; Korsun & Hald, 2000; Jennings et al., 2004). A voluminous database exists of the distribution patterns of benthic foraminifera in the Kara Sea and Barents Sea (Steinsund et al., 1994; Hald & Steinsund, 1996) where the data from the 1960's is combined with monitoring programs today to enhance our knowledge of the response of benthic foraminifera to past changes. Through such investigations, it is possible to distinguish the controlling factors for long-term environmental changes in the Arctic (Saher et al., 2009).

Several studies from fjords of Svalbard have recorded the distribution patters of benthic foraminiferal fauna, such as Kiær (1899), Feyling-Hansen (1964), Nagy (1965), Elverhøi and others (1980), Hansen and Knudsen (1995) and Hald and Korsun (1997).

## 4.1 Ecology

The study of the relationship between the environment and the living organism is termed ecology. The foraminifera is dependent on the chemical, physical and biological parameters of the environment. The most important physical parameter is the temperature, but currents, turbidity and pressure also play an important role. The chemical parameters are salinity, alkalinity, oxygen, organic and inorganic substances. Salinity can be a limiting factor for some species; planktonic foraminifera prefer to live in normal saline waters, while some benthic foraminiferal species can live in brackish and/or hypersaline waters. The most important biological parameter is migration due to food distribution (Murray, 2001).

## 4.2 Ecological preferences of dominating species

In the following section, the ecological preferences and importance for the interpretation of the environment of the most common benthic foraminiferal species in cores JM24 and JM49 are described. In the investigated samples in both cores, six calcareous species constitute more than 87% of the total benthic foraminiferal fauna. In addition, selected secondary calcareous species are shortly presented, together with the most common agglutinated species.

### 4.2.1 *Cassidulina reniforme* (Nørvang, 1945)

This Arctic benthic species is typical in glaciomarine environments with very little influx of temperate water (Elverhøi and Bomstad, 1980; Holtedahl and Bjerkeli, 1982; Hald and Vorren, 1987; Hald and Korsun, 1997). In the Nordic Seas, it prefers cold and relatively saline Local and Intermediate Waters (Hald and Korsun 1997) such as the homohaline Norwegian Sea Bottom Water (Hald and Vorren, 1987). It is infaunal and prefers temperatures below c. 2°C, seasonal ice cover and muddy sediments, and can tolerate relatively low salinity (> 30‰) (Holtedahl and Bjerkeli, 1982; Steinsund et al., 1994; Polyak et al., 2002). In Svalbard today it occupies areas at fjord mouths and is associated with local water (Hald and Korsun, 1997).

### 4.2.2 *Cibicides lobatulus* (Walker & Jacob, 1798)

The species is well known as an epifaunal suspension feeder, clinging onto coarser particles in areas of high current activity (Elverhøi and Bomstad, 1980; Vorren et al., 1984; Hald and Vorren, 1987; Hald and Steinsund, 1992; Hald and Korsun, 1997; Polyak et al., 2002; Ivanova et al., 2008). *Cibicides lobatulus* relates to low total organic carbon (TOC), and thrives well in river-distal areas (Hald and Steinsund, 1992; Polyak et al., 2002). In the study of Zajączkowski et al. (2010), *Cibicides lobatulus* appears to be more infaunal than epifaunal, supported by abundant living *Cibicides lobatulus* at the depth of 3 – 6 cm below the sediment surface. Ivanova et al., (2008) followed previous studies of the species being infaunal and considered it to be an epifaunal species that can penetrate deep into the sediment. If attached to coarse substrate, it can be transported downwards in the sediments by bioturbation. The species prefers salinities higher than 32‰ but can tolerate wide range of temperature (Steinsund et al., 1994). Today in Svalbard it occurs in high-energy environment at the outer part of the fjords (Hald and Korsun, 1997).

### 4.2.3 *Elphidium excavatum* forma *clavata* (Cushman, 1944)

*Elphidium excavatum* forma *clavata* (Elverhøi et al., 1980) is the Arctic form of *Elphidium excavatum* and is an opportunistic species well adapted to unstable environments and high sedimentation rates (Hald and Korsun, 1997; Ivanova et al., 2008). The species is the most frequent shallow marine benthic species in late Quaternary glaciomarine sediments in the north, and is widely distributed in shallow polar seas (Hald and Vorren, 1987; Hald and Korsun, 1997). It is an indicator of low salinity, occurring close to the fronts of tidewater glaciers (Vorren et al., 1984; Polyak et al., 2002; Hald et al., 2004) and is frequent in near glacial environments (Hald and Korsun, 1997). Hald and others (1994) showed that the species is common in Arctic Bottom Water, sea ice covered areas and in water of high turbidity. Areas strongly dominated by *Elphidium excavatum* forma *clavata*, give evidence of restricted living conditions for the foraminifera (Elverhøi and Bomstad, 1980). The species is opportunistic with high ability to adapt to harsh environments and capable of colonizing areas that are otherwise unsuitable for life. The reason for this may be due to its high nutritional and habitat versatility (Polyak et al., 2002).

### 4.2.4 *Nonionellina labradorica* (Dawson, 1860)

*Nonionellina labradorica* is an infaunal species common in glaciomarine environments, with its main distribution in the shallow marine environment. Its preferred environment is characterized by rapid changes in salinity and temperature (Vorren et al., 1984). It prefers water masses with salinities of 33 – 34‰ and temperatures lower than 1°C (Steinsund et al., 1994). The species is connected to the influx of fresh organic rich phyto-detritus, and when it is found in glacial-distal environments it is assumed to characterize the enhanced primary production (Korsun and Hald, 2000; Polyak et al., 2002; Zajączkowski et al., 2010). It correlates positively to the environment of the Polar Front, with rapid changes and high organic content of the sediment (Jennings et al., 2004). *Nonionellina labradorica* is also found abundantly in deep basins, where it can tolerate bottom waters of low oxygen content (Aksu and Mudie, 1985) and it is capable of surviving prolonged starvation (Polyak et al., 2002) and is therefore indicative of oceanic fronts, such as the Polar Front (Steinsund et al., 1994). Low abundance of *N. labradorica* may indicate low supply of phyto-detritus at the sediment surface (Zajączkowski et al., 2010). Today in the fjords of Svalbard, the species occupies outer and deeper parts and is associated with transformed Atlantic water (Hald and Korsun., 1997).

### 4.2.5 *Astrononion gallowayi* (Loebilch & Tappan, 1953)

*Astrononion gallowayi* is considered an epifaunal species preferring river-distal, shallow areas and coarse sediments (Steinsund et al., 1994; Polyak et al., 2002; Jennings et al., 2004). It prefers low temperatures of < 1°C and high salinity from >30‰ and >33‰ (Steinsund et al., 1994). The species can also live as an infaunal species according to Wollenburg and Mackensen, (1998). If the species is found in muddy sediments together with *C. lobatulus*, it may indicate post-mortem transport (Jennings et al., 2004). Husum and Hald (2004) also suggested this, where the two species *C. lobatulus* and *A. gallowayi* were found dead, while other species show good accordance between living and dead assemblages in Malangen, north Norway. A study in Kongsfjorden recorded *A. gallowayi* predominantly in temperatures below 1°C and in high salinities, over 30‰ (Skirbekk, 2007).

### 4.2.6 *Buccella frigida* (Cushman, 1922)

This Arctic species (Jennings et al., 2004) is related to seasonal sea-ice cover and indicates high seasonal productivity. It prefers temperatures between 0° and 1°C, and salinity around 33-34‰ (Steinsund et al., 1994; Ślubowska et al., 2005). *Buccella* species are mainly epifaunal based on their test shape, which is plano-convex trochospiral (Rosoff and Corliss, 1992). The highest abundance of *Buccella* spp. is within areas influenced by seasonal sea-ice, where it can feed on algal blooms. It is commonly feeding close to the sediment surface (Steinsund et al., 1994). *Buccella tenerrima* and *Buccella frigida* are common accessory species to the epifaunal species *Cibicides lobatulus* and *Astrononion gallowayi* (Jennings et al., 2004).

## 4.3 Ecological preferences of the secondary species

### 4.3.1 *Cassidulina neoteretis* (Seidenkrantz, 1995)

*Cassidulina neoteretis* is an epifaunal species or shallow infaunal dweller feeding on organic material (Rosoff and Corliss, 1992; Steinsund et al., 1994). It follows the chilled Atlantic Water since the species prefers low temperatures. It is often found in stratified waters (Jennings and Helgadóttir, 1994)

### 4.3.2 *Elphidium subarcticum/albiumblicatum* (Cushman, 1944)

This species is commonly found on the shelf of Spitsbergen and in areas influenced by river discharge. *E. subarcticum* is an epifaunal species preferring coarse sediment, low temperatures of <1°C and salinity of 33-34‰. Similar to *Elphidium excavatum* forma *clavata* it is an opportunistic species, preferring sea ice cover and glacier-proximal environments (Steinsund et al., 1994). Miller (1991) suggests that *Elphidium subarcticum* and *Elphidium albiumbilicatum* are the same species, but with variant forms; *Elphidium subarcticum* being the Arctic type and *Elphidium albiumbilicatum* being the Boreo-arctic and Boreal form.

### 4.3.3 *Glabratella wrightii* (Brady 1881)

*Glabratella wrightii* is typically found in high-energy environments, and is a common additional species to *Elphidium excavatum* forma *clavata*. It is an epifaunal species, preferring hard substrate and temperate to warm waters. It is commonly found in marine inner shelf environments (Murray, 1991).

### 4.3.4 *Triloculina trihedra* (Loeblich & Tappan, 1953)

The species ranges into the northern temperate waters. It is widely distributed in shallow waters with salinity greater than 32‰ (Huddart & Peacock, 1990) and is considered an Arctic cold-water fauna (McCabe et al., 1986).

### 4.3.5 *Stainforthia feylingi / Stainforthia schreibersiana* (Knudsen & Seidenkrantz, 1944)

The species is commonly found at bank slopes where it is subjected to cold waters in arctic to subarctic environments. It prefers cold water with temperatures of 0°C and seasonal sea-ice cover. It is characterized by patchy distribution (Steinsund et al., 1994). In the study of Blais-Stevens and Patterson (1998), the species indicates deep water and, likely, low oxygen concentrations.

## 4.4 Agglutinated species

### 4.4.1 *Verneuilinulla advena* (Cushman, 1922)

The species indicates contamination and brackish water conditions in the study of Blais-Stevens and Patterson (1998), and is found to occupy regions, where the surface water mass is situated at a depth of less than 50 m (Saidova, 2009). The species is also known as *Eggerella advena* and according to Murray (1991), is found together with other agglutinated foraminifera in salinities of 31.5‰ and temperatures of -1.5°C. It prefers a muddy sand substrate.

### 4.4.2 *Spiroplectammina biformis* (Parker & Jones, 1865)

This is a cold-water species found abundantly in Arctic waters with temperatures below -1°C (Schafer and Cole, 1986; Schafer and Cole, 1988). May indicate low oxygen levels in deeper water (Blais-Stevens and Patterson, 1998) and can tolerate wide range of marine conditions (Murray, 1991).

### 4.4.3 *Lepidodeuterammina ochracea* (Williamson, 1858)

The species is also known as *Trochammina ochracea*, and is found attached to sand grains within the sediment down to at least 7 cm (Murray, 1991)

### 4.4.4 *Quinqueloculina stalkeri* (Loeblich & Tappan, 1953)

This is mainly an Arctic species occurring in shallow waters around Svalbard, Greenland and Alaska. The species is found to be restricted in distribution to ice proximal environments (Korsun and Hald, 1998) and has been found in similar settings in Svalbard fjords (Elverhøi et al., 1980). According to Korsun and Hald (1998), *Quinqueloculina stalkeri* appears to be an indicator of glacier-proximal shallow marine habitats.

### 4.4.5 *Labrospira crassimargo* (Norman 1892)

The species is a shallow water species, indicative of middle shelf environment (Schröder-Adams and McNeil, 1990). During a study in St. Anna Trough, the species is only found on the slopes of the through (Korsun et al., 1998; Stein et al., 1999). In Adventfjorden, west Spitsbergen, the species is dominating an assemblage zone, from the water depth of 100 m (Setoyama et al., 2011).

# 5 Results

In this chapter, the results of lithology and micro paleontological data from cores JM06-024-GC3 and JM07-049-GC1 are described.

## 5.1 Sedimentological description

The cores are described in stratigraphic order, from the oldest to the youngest. The sedimentological description of the cores is based on visual description, X-ray image analysis, magnetic susceptibility and IRD analysis (Fig. 5.2 and 5.7). The sediments in both cores are mainly clay/silt with number of shells and shell-beds distributed throughout the core (Fig. 5.1 and 5.6). Both cores are divided into units, where each unit is approximately 100 cm.

## 5.2 Description of biozones

Cores JM06-024-GC3 and JM07-049-GC1 have been analysed for down-core distribution of benthic foraminifera (Fig. 5.3; 5.4; 5.5 for JM24; Fig. 5.8; 5.9; 5.10 for core JM49). Records have been divided into three assemblage zones (abbreviated AZ or simply zone) based on early, middle and late Holocene boundaries. Assemblage zones are described in stratigraphic order, from the oldest to the youngest. Below is a general description of the AZ in in both cores. Zones for core JM06-024-GC3 are labelled by numbers (Fig. 5.3; 5.4; 5.5) and zones for JM07-049-GC1 are labelled by letters (Fig. 5.8; 5.9; 5.10).

## 5.3 CTD (Conductivity, Temperature, Depth) description

CTD measurements over the core locations of JM06-024-GC3 and JM07-049-GC1 are described below. The values represent water masses located in the study area at the present time.

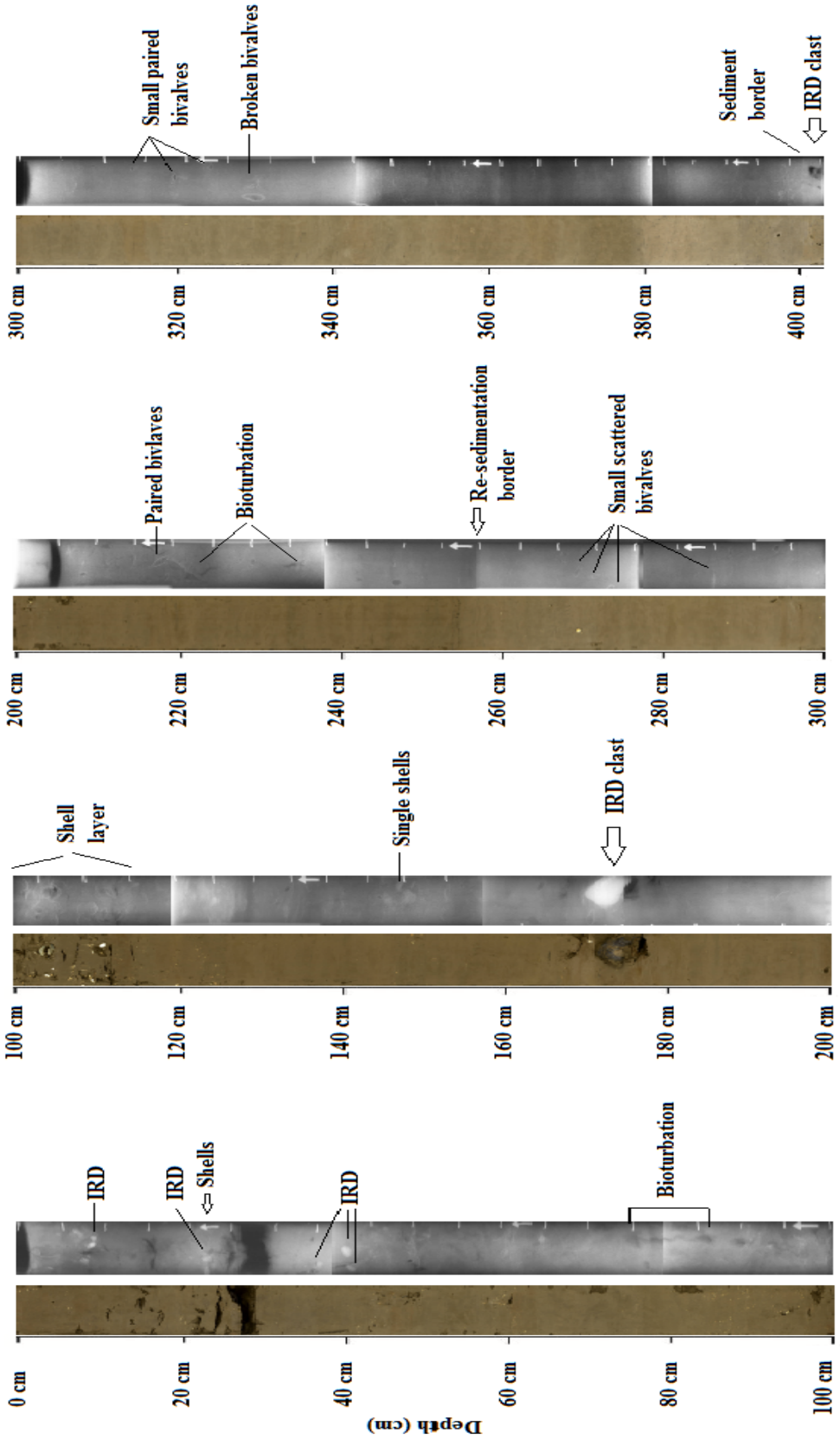


*Figure 5-1 Gravity core JM24 shown by photographs and X-ray images. Major features have been desribed in the core. Images are plotted against depth.*

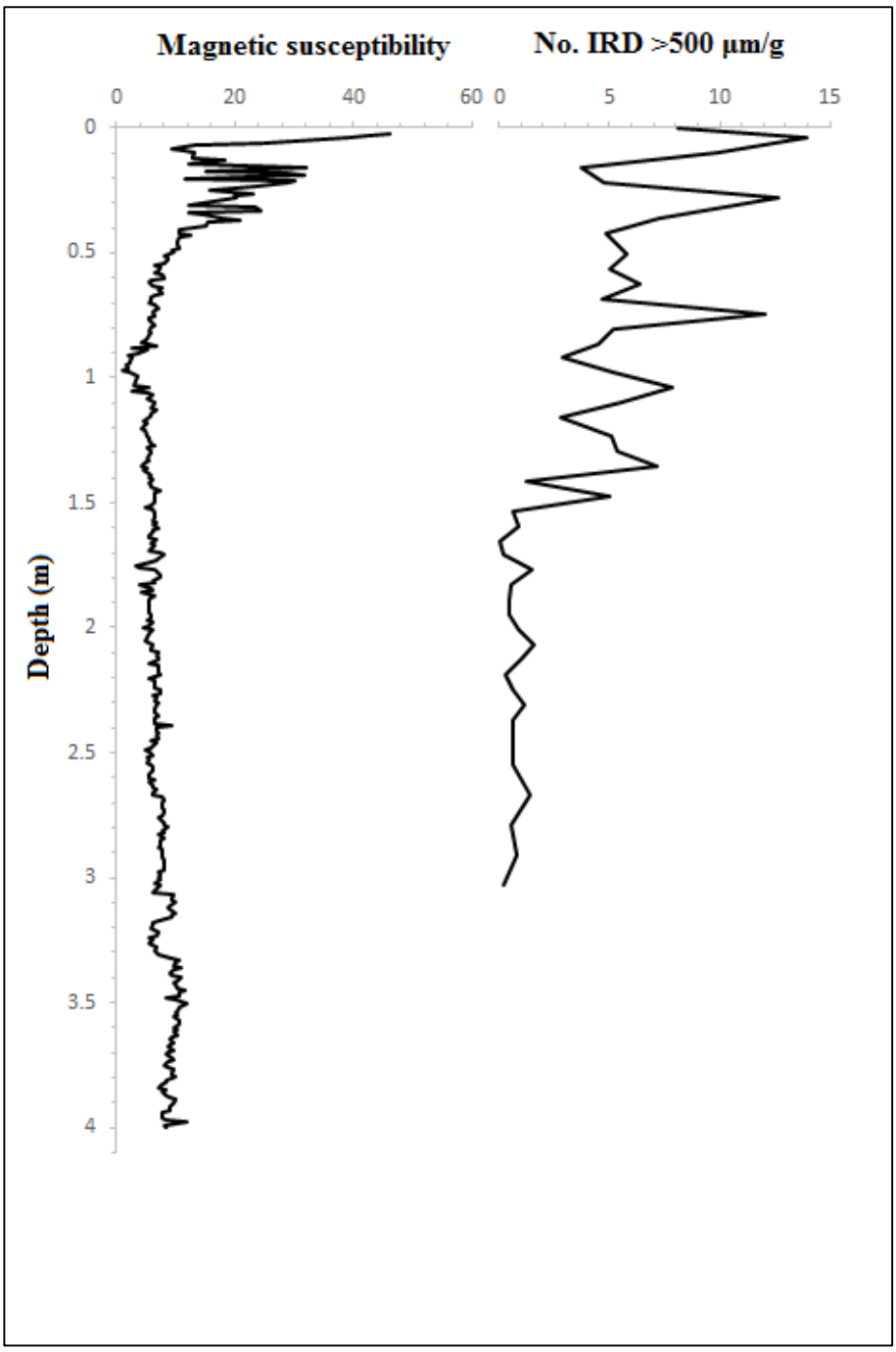


*Figure 5-2 Magnetic susceptibility and IRD concentration plotted against depth for core JM24.*

## 5.4 JM06-024-GC3

Core 24 was retrieved from the outer fjord basin, on the outer side of the sill (see Fig. 2.1 in Chapter 2.1). The total length of the core is 410 cm.

### 5.4.1 Unit 1 (410 – 303.5 cm)

Unit 1 consist of homogenous clay and silt sediment. From visual observation the unit is greyish brown (2.5Y 5/2) from 410 – 387 cm. An obvious boundary is observed at 387 cm, where the colour changes to dark greyish brown (2.5Y 4/2), and stays dark greyish brown throughout the unit. From X-ray analysis, the core shows a distinct boundary at ~ 405 cm. From 410 cm, a big clast and smaller pebbles are observed. Moving up-core the X-ray images show another distinct boundary is observed, at ~ 360 cm. Paired bivalve shells and shell fragments are distributed in the unit (Fig. 5.1). The magnetic susceptibility is generally low in the unit, with a relatively decreasing trend (Fig. 5.2). No IRD samples were taken from this unit (Fig 5.2).

### 5.4.2 Unit 2 (303.5 – 203 cm)

Unit 2 consists of homogenous clay and silt sediment. From the bottom of the unit the colour is dark greyish brown (2.5Y 4/2) until 262 cm, where the colour changes into olive-grey colour (5Y 4/2). Four distinct shell-beds are visible in the interval from 237 to 210 cm. Analysis of the X-ray images show a sedimentary interval characterized by a change in sediment density at the bottom of the unit (~ 290 cm). Paired bivalve shells are observed from ~ 290 to ~ 250 cm, followed by increased amount of shells up to 210 cm (Fig. 5.1). The magnetic susceptibility is generally decreasing and stable throughout the unit (Fig. 5.2). The IRD concentration is very low with an average of 0.72 grains per dry weight sediment (Fig. 5.2).

### 5.4.3 Unit 3 (203 – 101 cm)

For Unit 3 consist of homogenous clay and silt sediment. The colour is homogenous olive-grey (5Y 4/2) with shell-beds at various depths. A large clast is observed at 175 cm and the frequency of the shell layers increase up core. X-ray images show disturbed sediments probably from presence of tubeworms from ~ 175 cm to 160 cm. Bivalve shells and paired shells in this unit are considerably larger than in Unit 1 and Unit 2. From 140 – 120 cm several sedimentary layers consisting of coarser material are observed. From 120 cm up to ~ 100 cm very rich shell-bed layer is observed, with gastropods, bivalve shells and paired shells (Fig. 5.1). Magnetic susceptibility is decreasing and stable (Fig. 5.2). The IRD

concentration is still low, with an average of 1.73 grains per dry weight sediment, but after 128 cm, the amount of grains per gram starts to increase. The highest amount of IRD in the unit is at 113 cm, with about 7 grains per dry weight sediment (Fig. 5.2).

### 5.4.4 Unit 4 (101 – 0 cm)

Unit 4 consists of bioturbated olive-grey (5Y 4/2) silty-sand with bivalve shells and shell fragments. Paired shells are observed in X-ray images at the bottom of the unit. A shell bed occurs at 50 cm with IRD grains and pebbles increasing to the top of the unit (Fig. 5.1). The bivalve shells are well preserved and are also found in pairs. The magnetic susceptibility starts to increase considerably in the beginning of the unit (101 cm) with values of 2.1(SI x $10^{-5}$) towards 46(SI x $10^{-5}$) at the top of the core (Fig. 5.2). The IRD concentration is high and oscillating, with average of ~ 7 grains per gram (Fig5.2).

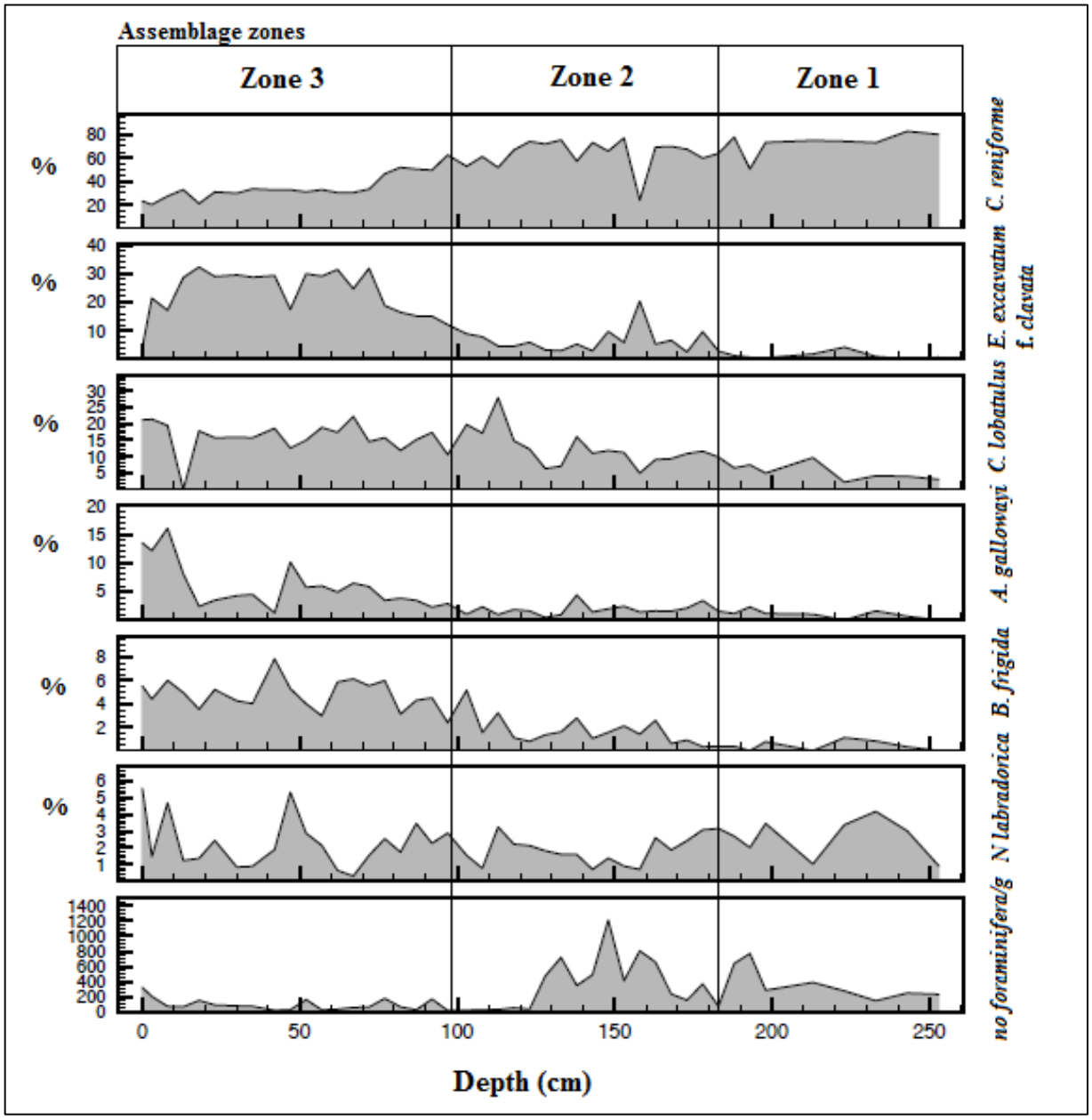


*Figure 5-3 The main calcareous benthic foraminifera calculated as percentages against depth in core JM24. All the benthic foraminifera are compared to the total benthic foraminifera concentration.*

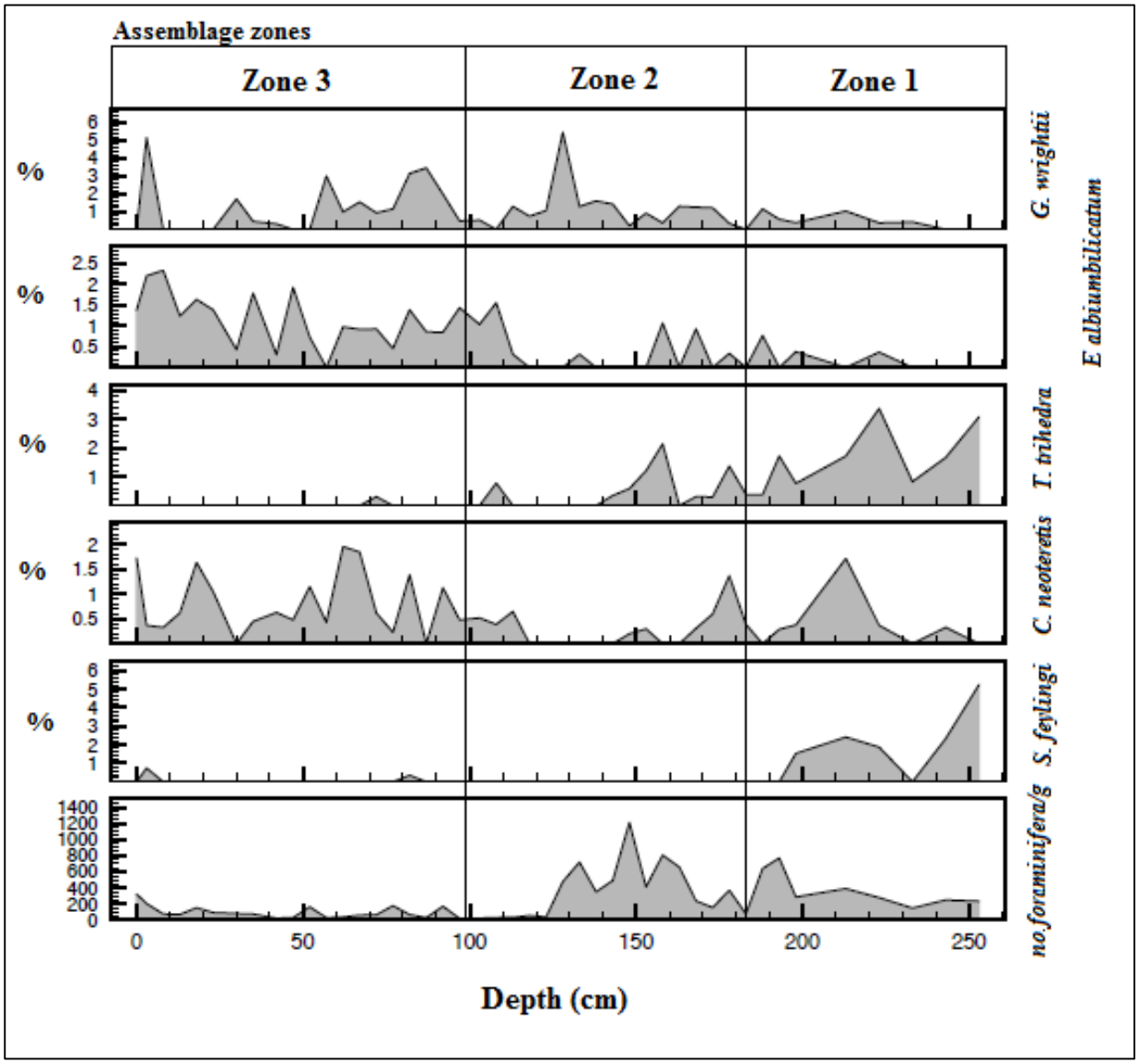


*Figure 5-4 The most common sub species of the benthic foraminifera fauna plotted against depth in core JM24. All the graphs are compared to the total benthic foraminifera concentration.*

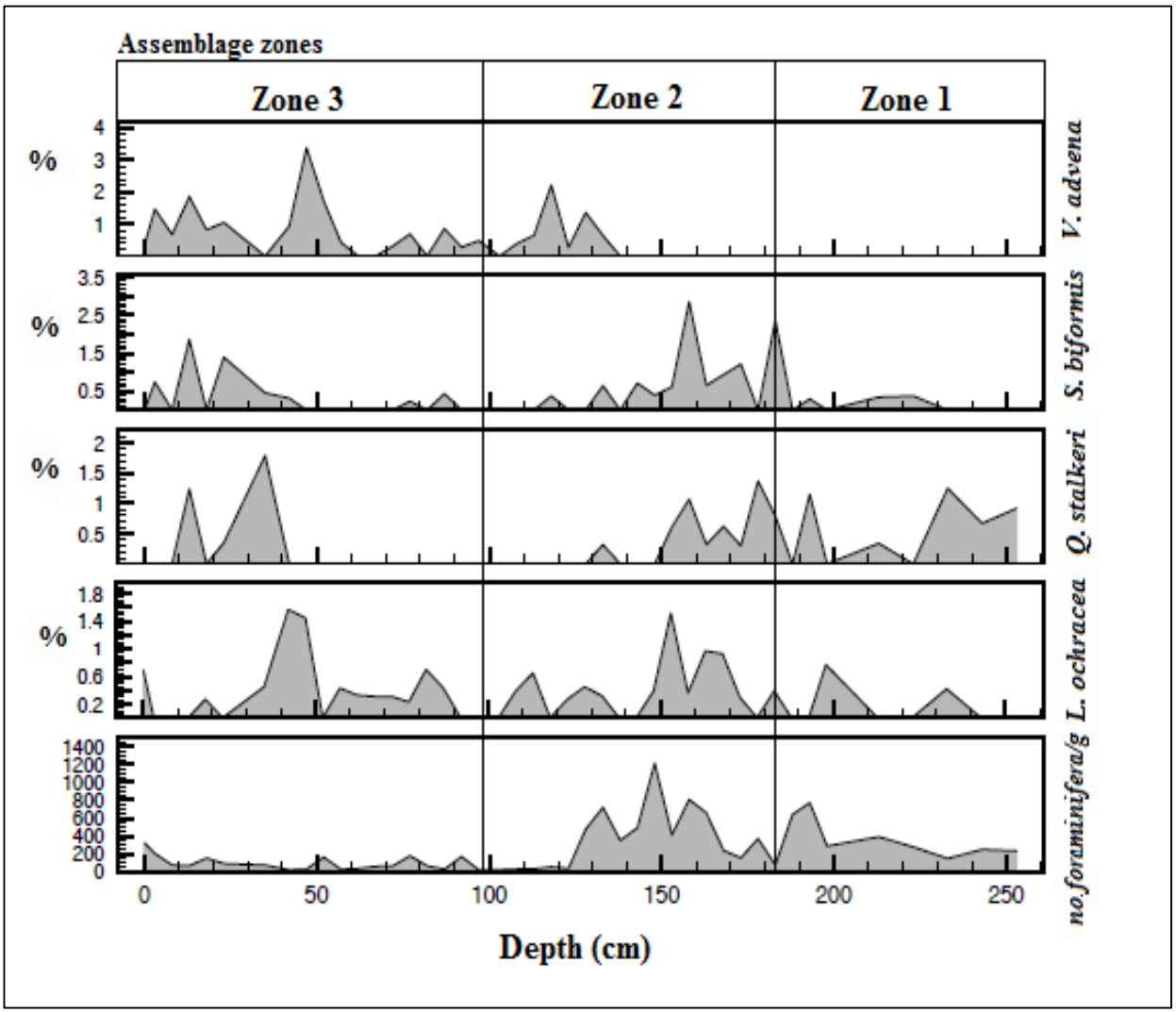


***Figure 5-5 The most common agglutinated species of the benthic foraminifera fauna plottet against depth in core JM24. All the graphs are compared to the total benthic foraminifera concentration.***

## 5.5 Biozones in core JM06-024-GC3

Only the upper 253 cm of the core is used in this study (Fig. 5.3; 5.4; 5.5). The abundance of foraminifera in the lower re-sedimented part of the core is very low and their test is poorly preserved. Based on that information, only the upper 253 cm was used for further investigation.

### 5.5.1 Assemblage zone 1: *Cassidulina reniforme* (253 – 183 cm)

*Cassidulina reniforme* is the dominant species in this assemblage zone with an average of 72 %. It reaches its maximum value of ~ 82 % at 243 cm and gradually decreases towards the upper part of the zone. The opportunistic species, *Elphidium excavatum* f. *clavata*, is low throughout the zone, with an average of 7 %. *Cibicides lobatulus* increases towards the upper part of the zone and *Astrononion gallowayi* is relatively low in the zone. The average for *C. lobatulus* is ~ 6 % and 1 % for *A.gallowayi. Nonionellina labradorica* has relatively high percentages in this zone, with a decrease in relative abundance in the middle part. Its average is 2.6 %. The seasonal sea-ice indicator (Chapter 4.2.6), *Buccella frigida* is relatively low in the zone. Its general average is 0.5 % (Fig. 5.3).

*Triloculina trihedra* and *Stainforthia feylingi* are the most common subspecies in this AZ. At the lowest part of the zone *S. feylingi* has a maximum of 5.2 % and shows a general decrease to 0 %. Its average is 1.3%. The Arctic cold-water (Chapter 4.3.4) foraminifera *Triloculina trihedra* is more abundant than *S. feylingi* throughout the zone. At 223 cm *T. trihedra* reaches its maximum of 3.4 % and its average is 1.5 %. *Cassidulina neoteretis, Elphidium albiumbilicatum* and *Glabratella wrightii* are present in the zone but with low values. They have the average of 0.4 %, 0.2 % and 0.4 %, respectively (Fig. 5.4).

Three agglutinated species are present in the zone. The most common one in the lower part of the zone is *Quinqueloculina stalkeri*. Its average is 0.6 %. *Lepidodeuterammina ochracea* and *Spiroplectammina biformis* are present in the core with an average of 0.2 % and 0.6 %, respectively. (Fig. 5.5).

The number of foraminiferal tests per gram sediment, from now on termed abundance, is relatively high in this zone, with an average of 340 foraminifera per dry weight sediment.

### 5.5.2 Assemblage zone 2: *Cassidulina reniforme & Elphidium excavatum* f. *clavata* (183 – 97 cm)

This zone is characterized by the rapid increase in relative abundance of *Elphidium excavatum* f. *clavata* and concomitant decrease of *Cassidulina reniforme*. As observed in the assemblage zone below, these two species show opposite distribution patterns. It is clear, when the whole core is taken into consideration that when there is a general decrease of *C. reniforme*, there is a general increase of *E. excavatum* f. *clavata.* The most distinct peak of *E. excavatum* f. *clavata* at 158 cm correlates with a drop of *C. reniforme*. At 158 cm, the values of the *C. reniforme* decrease considerably from 69 % to 24 %, while the values of *E. excavatum* f. *clavata* increase from 5.2 % to 20 %. The high bottom current indicator (Chapter 4.2.2) *Cibicides lobatulus* has increased from the beginning of the zone to values of 27.8 % at 113 cm. Together with this rapid increase, *Cassidulina reniforme* decreases from 67 % of the total fauna at 118 cm to 52 %. *Nonionellina labradorica*, a primary production indicator (Chapter 4.2.4) follows the same trend as *C. lobatulus* by increasing in relative abundance from the middle part of the zone and peak at 118 cm. Its average is 1.9 %. *Buccella frigida* also increases in relative abundance and has the average of 1.7 % (Fig. 5.3)

The high-energy indicator (Chapter 4.3.3), *Glabratella wrightii,* increases to its maximum value of 5.5 % in the middle of the zone. It decreases from its maximum value at 128 cm and is absent at 108 cm. *G. wrightii* has an average of 1.1% in this zone. At 118 cm *Elphidium albiumbilicatum* increases in relative abundance. Its average of 0.4 % is higher than in the previous zone. *Cassidulina neoteretis* and *Triloculina trihedra* are present in the zone (Fig. 5.4).

All of the most important agglutinated foraminifera are present in the zone. The ice proximal species (Chapter 4.4.4) *Quinqueloculina stalkeri* is relatively abundant in the beginning of the zone, and *Spiroplectammina biformis* has its maximum value in lower part, and decreases towards the upper part. *Verneuilinulla advena* is introduced in this zone with an average of 0.3 %. *Lepidodeuterammina ochracea* is high in the lower part of the zone with an average of 0.4 % (Fig. 5.5).

The abundance has its maximum value of 1212 foraminifera/g is recorded at 148 cm. The general trend in the lower part of the core is increasing and after 148 cm the values

decrease rapidly. at 123 cm the values are considerably lower compared to the previous zone. Its average is 341 foraminifera/g.

### 5.5.3 Assemblage zone 3: *Elphidium excavatum* f *clavata* (97 – 0 cm)

The name of the zone is given due to the relatively stable and high abundance of *Elphidium excavatum* f *clavata*. The abundance increase that initiated in zone 2 reaches its maximum in this zone. Apart from the distinct decreases in *E. excavatum* f.*clavata,* recorded at 47 cm and from 13 cm – 0 cm, it has its highest average of 25 % and a maximum value of 32 % at 18 cm in this zone. The sea-ice indicator (Chapter 4.2.6) *Buccella frigida*, reaches its highest value of 7.2 % at 42 cm depth and *Nonionellina labradorica* the primary production indicator (Chapter 4.2.4) gradually increases to a peak at 42 cm. The third species to increase at this depth is *Astrononion gallowayi*. It has been gradually increasing throughout the zone, until it peaks at 42 cm, reaching 10.1 % of the total fauna. In the upper half of the zone, *A. gallowayi* increases fast to reach its maximum value of 16 % at 8 cm depth. *Cassidulina reniforme* is decreasing in this zone, but has a peak at 18 cm. Its average of 32 % is the lowest of all the zones. On the opposite, *Cibicides lobatulus* has its highest average of 16 % in this zone. It has a distinct drop at 18 cm where it is absent from the record (Fig. 5.3).

The subspecies *Cassidulina neoteretis* has its highest average of 0.9 % in this zone, compared to the previous ones. *C. neoteretis* has its highest value of 2 % at 62 cm depth. *Elphidium albiumbilicatum* shows the same pattern as the majority of the species, by a peak of 1.9 % at 47 cm. Its abundance is similar to the main species, the highest in this zone. *E. albiumbilicatum* has the average of 1.2%. The values for *Glabratella wrightii* are fluctuating and the species is absent several times in the zone. Its average is 1.3 % (Fig. 5.4).

Four of the most common agglutinated species are present in the zone. *Spiroplectammina biformis* and *Quinqueloculina stalkeri* are absent in the lower part and present in the upper part. *Lepidodeuterammina ochracea* and *Verneuilinulla advena* are the most abundant agglutinated species and record their maximum abundance in this zone. *L. ochracea* has the average of 0.7 % and *V. advena* has the average of 0.8 % (Fig. 5.5).

The abundance is still low, compared to AZ1 and is decreasing in the lower part of the zone. It has peaks at 77 cm and at 52 cm with the value of 177 and 163 foraminifera/g,

respectively. At 42 cm, the values are low, but they have an increasing trend towards the end of the zone. The average abundance is 95 foraminifera/g.

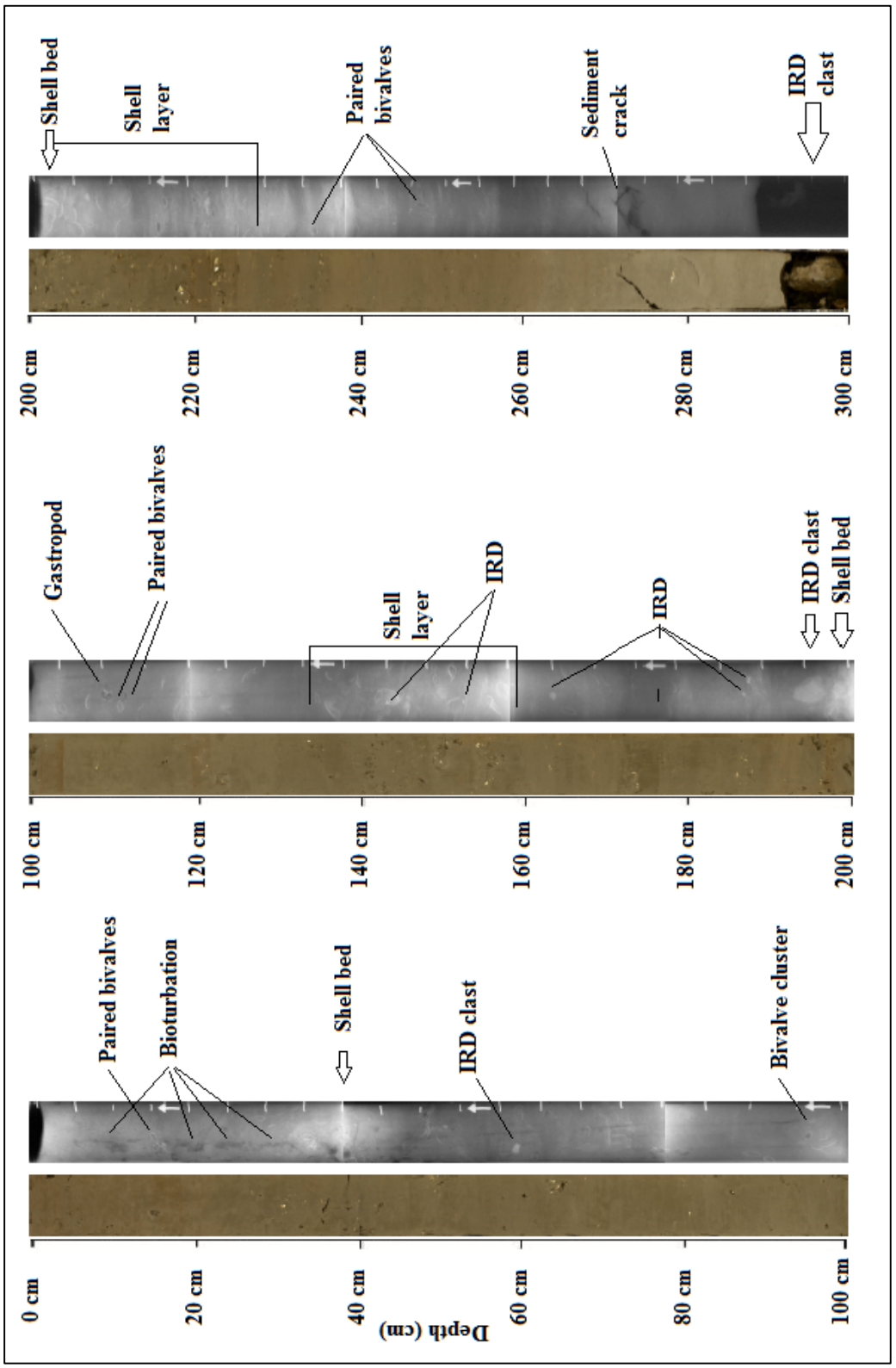


***Figure 5-6 Gravity core JM49 shown by photographs and X-ray images. Major features have been described in the core. Images are plotted against depth.***

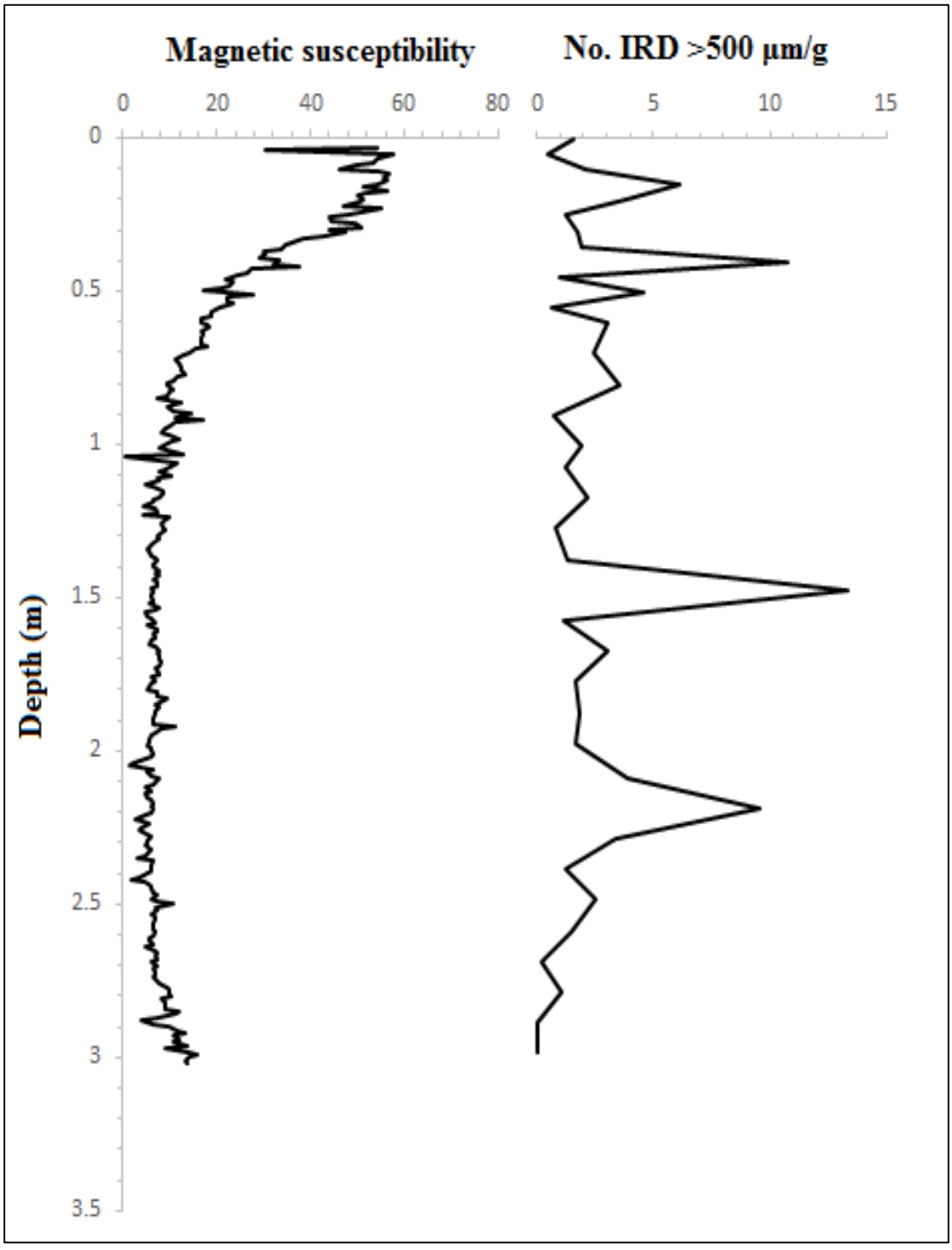


*Figure 5-7 Magnetic susceptibility and IRD concentration plotted against depth for core JM49.*

## 5.6 JM07-049-GC1

Core 49 was retrieved from the outer part of the fjord, at the inner side of the (see Fig. 2.1 in Chapter 2.1). The core length is 304 cm.

### 5.6.1 Unit 1 (304.5 – 202.5 cm)

The unit consists of homogenous silty clay. The colour from the bottom of the core to ~ 270 cm is greyish brown (2.5Y 5/2) turning to olive grey towards the top of the unit. From ~ 242 to 202.5 cm, shell fragments from molluscs are visible. The X-ray image from this unit indicates homogenous sediments from the bottom up to ~ 262, where a clear boundary is observed with few shells. From 250 cm and up to the top of the unit, the sediment is very rich in paired bivalves shells pairs, gastropods and IRD. The interval from 225 cm to 215 shows the shells are oriented horizontally until they reach a sediment boundary at 225 cm. In the interval towards the top, shells and IRD are distributed and laying both laterally and horizontally in the sediment (Fig. 5.6). The magnetic susceptibility is decreasing throughout the unit (Fig 5.7). The concentration of IRD in this unit is the lowest of the entire record, with an average of 2.3 grains/g (Fig. 5.6). In the lower part of the unit, the concentration is low, but it increases up core, towards the top of the unit. The greatest amount of IRD is at 218 cm, with ~ 10 grains/g.

### 5.6.2 Unit 2 (202.5 – 102 cm)

The unit consists of homogenous silty clay of olive grey colour (5Y 4/2) and is very rich in shells from molluscs. Upon first sight, the unit is packed with shell-beds. On closer look through the X-ray images, the unit shows a lot of variability. At the bottom of the core a distinct sedimentary boundary is observed characterised by a change is density from the X-ray pictures. A large clast is found at the boundary. In the interval from 200 cm to ~ 135 cm IRD pebbles are visible, along with a large specimens of molluscs and paired shells. The top part of the interval is rich in paired shells and a gastropod of 2.5 cm height. The magnetic susceptibility is low and very stable throughout the unit (Fig. 5.7). The IRD concentration is slightly higher than in the previous unit, with the average of 2.7 grains/g (Fig. 5.7). A distinct peak in the middle of the unit, at 147 cm, records the greatest amount of IRD in the whole core, with over 13 grains per dry weight sediment.

### 5.6.3 Unit 3 (102 – 0 cm)

Unit 3 consists of homogenous silty-clay and the colour is olive grey (5Y 4/2) from the bottom towards ~ 15 cm, where brown patches are observed. A cluster of mollusc shells is

located from 95 – 100 cm. Above the cluster are 15 cm long bioturbated lines. For the next 55 cm up-core (95 cm – 40 cm) paired shells, bivalve shells and IRD occur. In the interval from 40 cm to 30 cm shells are oriented vertically and clustered. The X-ray images show the top 20 cm of the core are heavily bioturbated. The magnetic susceptibility for this unit is low to begin with, with a gradual increase towards 50 cm. The maximum value of the whole core is 58 (x $10^{-5}$ SI), recorded at 5 cm depth. The top unit records the highest average of the IRD concentration, ~ 2.9 grains per dry weight sediment. At 40 cm and 15 cm, two peaks show IRD concentration of 11 and 6 grains per dry weight sediment, respectively (Fig).

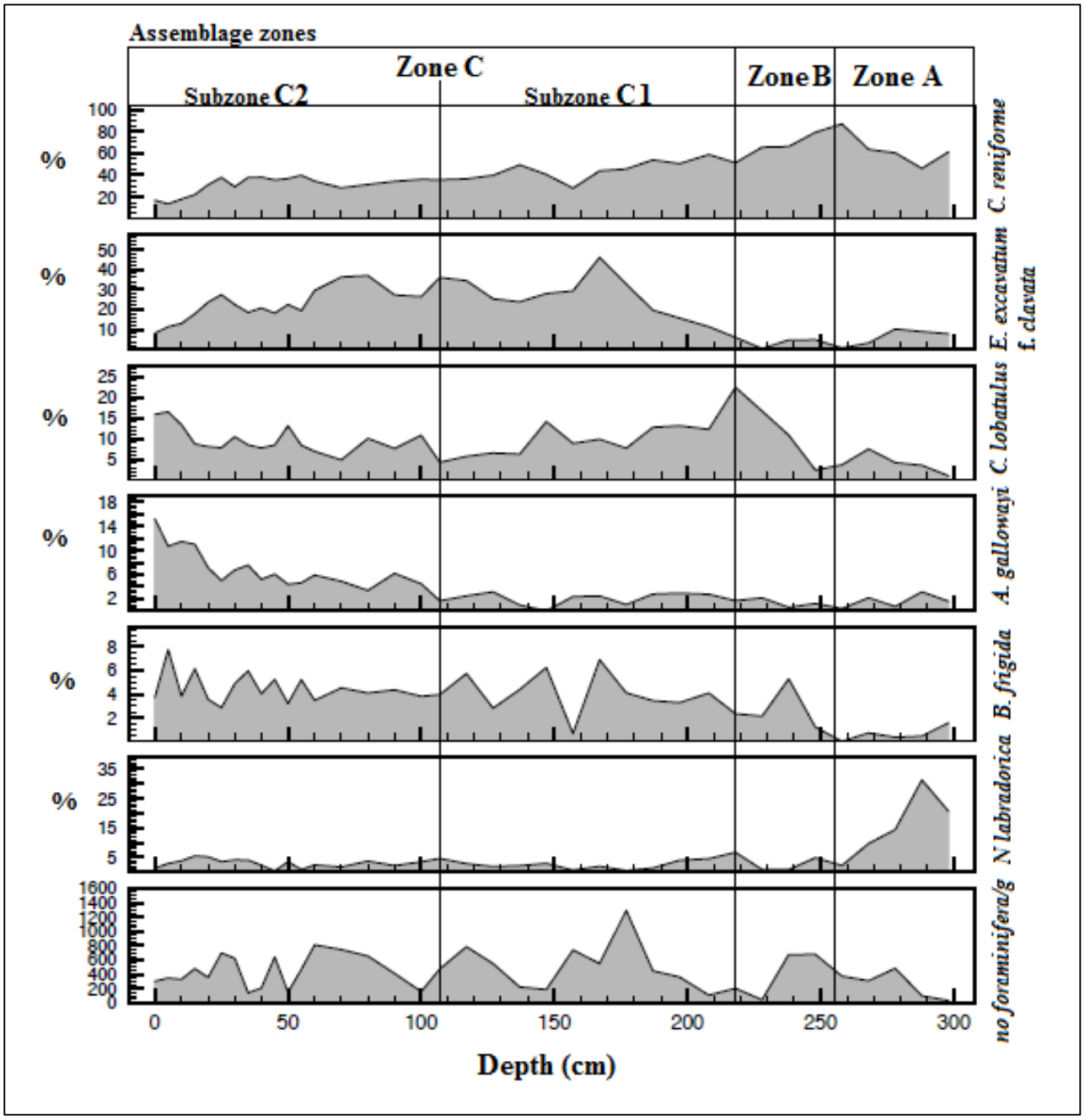


***Figure 5-8 The main calcareous benthic foraminifera calculated as percentages against depth in core JM49. All the benthic foraminifera are compared to the total benthic foraminifera cocentration.***

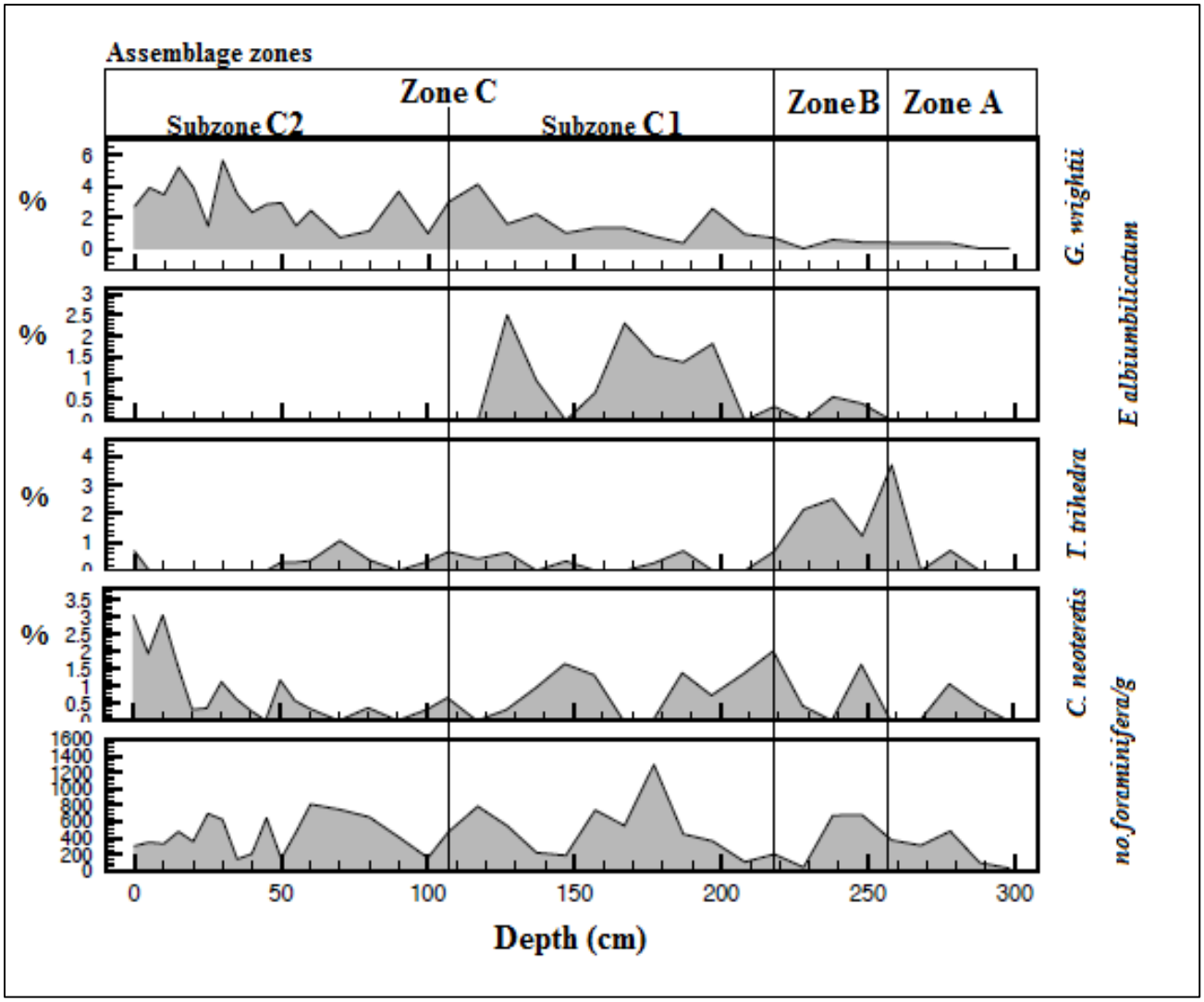


***Figure 5-9 The most common sub species of the benthic foraminifera fauna plottet against depth in core JM49. All the graphs are compared to the total benthic foraminifera concentration.***

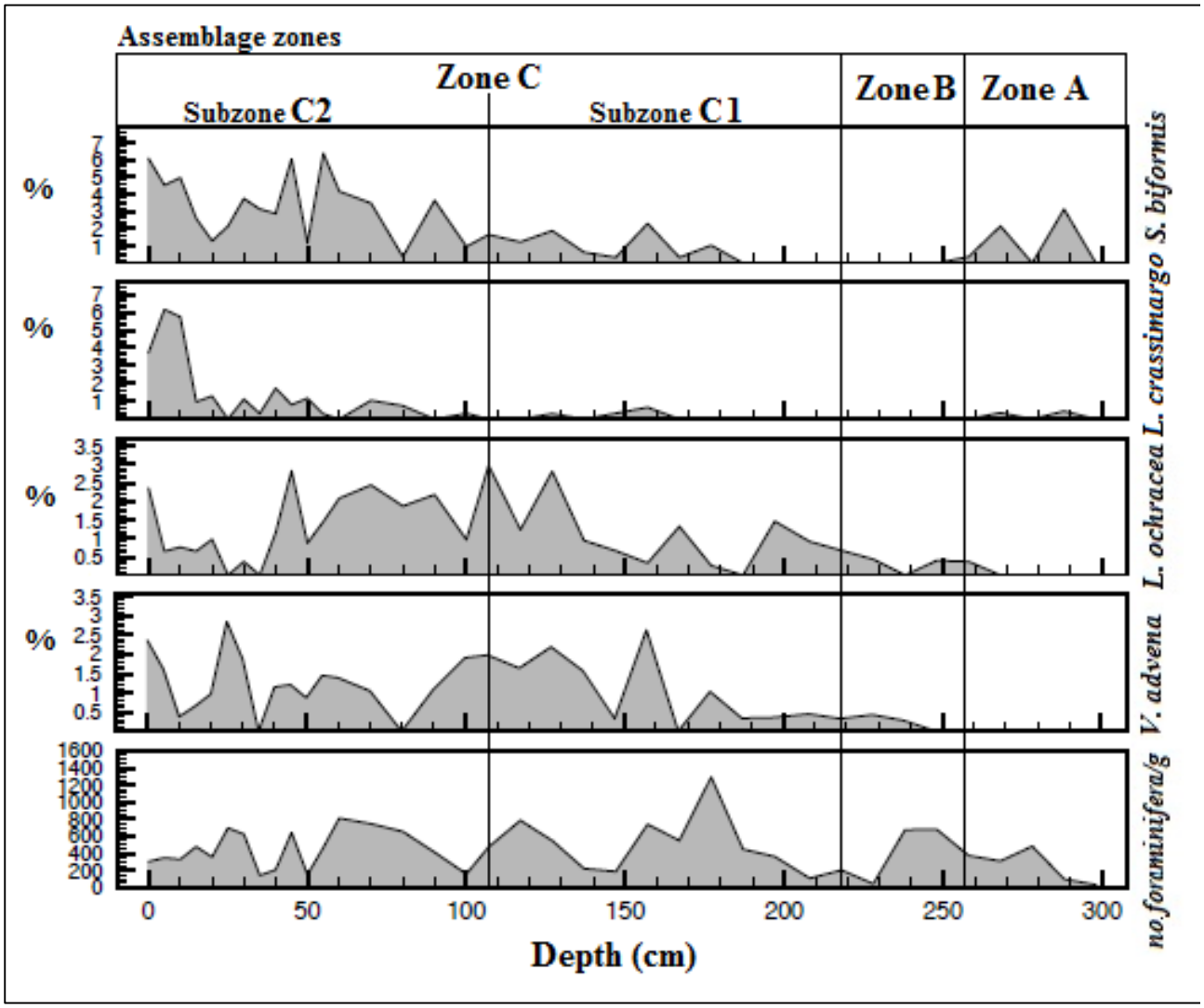


***Figure 5-10 The most common agglutinated species of the benthic foraminifera fauna plotted against depth in core JM49. All the graphs are compared to the total benthic foraminifera concentration.***

## 5.7 Biozones in core JM07-049-GC1

### 5.7.1 Assemblage zone A: *Nonionellina labradorica* (298 – 255 cm)

The name of the zone is given to the primary productivity indicator (Chapter 4.2.4) *Nonionellina labradorica*. It increases in the beginning of the zone, reaching its highest value of 31 % at 288 cm and decreases rapidly gradually towards the upper half of the core. *N. labradorica* has its maximum average of 14 %. The dominating species *Cassidulina reniforme* shows opposite distribution patterns to *Nonionellina labradorica. C. reniforme* decreases in the lower part of the zone down to 46 % at 288 cm, but gradually increases up-core, peaking at 258 cm with values of ~ 87 %. The opportunistic species (Chapter 4.2.3) *Elphidium excavatum* f. *clavata* decreases in relative abundance, together

with the sea-ice indicator (Chapter 4.2.6) *Buccella frigida*. At 258 cm, *B. frigida* is absent and *E. excavatum* f. *clavata* constitutes only 0.7 % of the total fauna. Their average is 6 % and 0.7 %, respectively. *Cibicides lobatulus* increases gradually to a value of 7.5 % at 268 cm, and decreases in the upper half of the zone. Its average of 3.8 % is low (Fig 5.8).

Very few sub-species have considerably high values in this zone. The most dominating subspecies is *Triloculina trihedra*. It reaches its maximum value of 4 % in the upper half of the zone. *Glabratella wrightii* and *Cassidulina neoteretis* are present but both are low in abundance. In the upper half of the zone, *Elphidium albiumbilicatum* is introduced (Fig. 5.9).

The agglutinated species are mostly absent in the zone. The most abundant species is *Spiroplectammina biformis* that has the average of 0.94 %. *Labrospira crassimargo* is present and very low in abundance, and *Lepidodeuterammina ochracea* is introduced at 268 cm (Fig. 5.10).

The abundance has an increasing trend throughout the zone. It increases fast in the lower part and decreases slightly in the middle. In the upper part, it increases again. The abundance average is 328 foraminifera/g.

### 5.7.2 Assemblage zone B: *Cibicides lobatulus* (255 – 219 cm)

This zone is characterised by the rapid increase of *Cibicides lobatulus*. The name of the zone is given due to its relative abundance, and its increase from 2.4 % - 22.4 %, which happens fairly rapidly. Its average of 12.9 % in this zone is the highest. *Cassidulina reniforme* is still the dominating species though its trend is decreasing down to ~ 50 % at 218 cm. *Elphidium excavatum* f. *clavata* is low in the zone, and has its minimum value of 0.4 % at 228 cm. It also has its lowest average value of 5.5 % in this zone. *Buccella frigida* shows a marked increase to about 5.3 % at 238 cm. Its average is 3.3 %. The primary production indicator (Chapter. 4.2.4) *Nonionellina labradorica*, is considerably lower in this zone compared to the previous one. Its average is 3.6 % (Fig. 5.8).

The subspecies *Triloculina trihedra* and *Cassidulina neoteretis* are the most common species in this zone. When *T. trihedra* peaks at 238 cm, *C. neoteretis* is absent. Their average is 1.3 % and 1 %, respectively. *Glabratella wrightii* and *Elphidium*

*albiumbilicatum* are both absent at 228 cm depth. *G. wrightii* has an average of 0.5 % and *E. albiumbilicatum* has an average of 0.3 % (Fig. 5.9).

*Lepidodeuterammina ochracea* and *Verneuilinulla advena* are the only and the most abundant agglutinated species in this zone. *L. ochracea* has an increasing trend from 238 cm and has an average of 0.48 %. *V. advena* is introduced in the lowest part of the zone (248cm) and is present but with low values. Its average is 0.3 % (Fig. 5.10).

The foraminifera abundance has a lowering trend in the zone, decreasing rapidly from 675 foraminifera/g at 238 cm to 41 foraminifera at 228 cm. A short-lived peak is at 218 cm with over 200 foraminifera/g. The abundance average for Zone B is 340 foraminifera per dry weight sediment.

### 5.7.3 Assemblage zone C: *Elphidium excavatum* f. *clavata, Astrononion gallowayi & Cibicides lobatulus* (219 – 0 cm)

*Cassidulina reniforme* is the dominating species in this zone. It has been divided into two subzones (C1 and C2) based on the high-bottom current species (Chapter 4.2.2) *Cibicides lobatulus*. In subzone 1, *C. lobatulus* shows a decreasing trend and in subzone 2, there is a general increasing trend for the species.

#### *5.7.3.1 Subzone C1: Elphidium excavatum f. clavata (219 – 107 cm)*

*Elphidium excavatum* f. *clavata*, a species that indicates unstable environments and high sedimentation rates (Chapter 4.2.3) characterises this zone with its marked increase. It gradually reaches its maximum value of 46 % of the total fauna at 167 cm. At the same depth, *Cassidulina reniforme* is concomitant, decreasing down to ~ 44 %, resulting in the dominance of *E. excavatum* f. *clavata* at 167 cm. *C. reniforme* continues to decrease before it increases again to 49 % at 137 cm. Thereafter the species gradually decreases towards the lower part of the zone. *Cibicides lobatulus* shows a decreasing trend and has the average of ~ 9.2 %. *Buccella frigida* has the same trend as *Elphidium excavatum* f. *clavata*. It increases towards a peak of 6.9 % at 167 cm. *B. frigida*, and decreases down to 0.66 % in the middle part of the zone. It increases again to values of 6.3 % at 147 cm. *Nonionellina labradorica* is relatively low, compared to its values in zone A. Its average is 2.5 % (Fig. 5.8).

*Elphidium albiumbilicatum* increases rapidly in the lower part of the zone and is present throughout the zone. It has a maximum average of 1 %. At 117 cm, the species disappears from the record. *Triloculina trihedra* is present and has very low abundance, but *Glabratella wrightii* is steadily increasing. *Cassidulina neoteretis* is absent from 167 – 177 cm (Fig. 5.9).

The most common agglutinated foraminifera in this zone are *Lepidodeuterammina ochracea, Verneuilinulla advena* and *Spiroplectammina biformis. Labrospira crassimargo* is very low in the zone. The most abundant species *L. ochracea* reaches its maximum value of 3 % in the uppermost part of the zone (107 cm), and has the average of 1.2 %. *Spiroplectammina biformis* shows an increasing trend throughout the zone and has the average of 0.85 %. *V. advena* oscillates throughout the zone and is more abundant in the upper part. It has an average of 1.1% (Fig. 5.10).

The abundance increases rapidly in the lower part of the zone, and reaches its maximum of 1292 foraminifera/g at 177 cm. A second peak with 784 foraminifera/g is recorded at 117 cm. The abundance is oscillating throughout the zone and has a maximum average of 519 foraminifera/g.

#### *5.7.3.2 Sub-zone C2: Astrononion gallowayi & Cibicides lobatulus (107 – 0 cm)*

The zone is characterised by the gradual increase of the high bottom current species (Chapter 4.2.2) *Cibicides lobatulus* and *Astrononion gallowayi*. Both species increase rapidly in the lower part of the sub-zone and reach their maximum value in the upper part. Their average is 9.5 % and 6.7 %, respectively. The values for the dominating *Cassidulina reniforme* are decreasing slowly throughout the zone. Its average of 31 % is 5 % lower than the previous sub-zone. The values for *Elphidium excavatum* f. *clavata* are fluctuating. The species has two distinct peaks, but the general trend is decreasing towards the top of the core. Its average of 23 % is 1 % lower compared to the previous zone. The sea-ice indicator (chapter 3) *Buccella frigida* is relatively stable. A similar trend is with *Nonionellina labradorica,* it is low and stable. Their average is 4.5 % and 3.1 %, respectively (Fig. 5.8).

*Glabratella wrightii* is the most common subspecies in the zone. It is fluctuating and has the average of 2.8 %. *Cassidulina neoteretis* has an increasing trend throughout the sub-

zone. It reaches its maximum value of 3 % at 10 cm and at the sediment surface (0 cm). *Triloculina trihedra* is present in the sub-zone (Fig. 5.9).

The most abundant agglutinated species it this zone is *Spiroplectammina biformis*. It reaches its maximum of 6.4 % at 55 cm and shows an increasing trend in the upper part of the zone. It has an average of 3.3 %. *Lepidodeuterammina ochracea* is more common in the lower part of the zone compared to the upper part. It has an average of 1.36 %. *Verneuilinulla advena* is oscillating throughout the zone and has an average of 1.3 %. *Labrospira crassimargo* is very low in the lower part of the core, but increases rapidly in the upper part. At 15 cm, it increases from 1 % to 6.1 % at 5 cm. Its general trend towards the core top is decreasing. *L. crassimargo* has an average of 1.4 % (Fig. 5.10).

The abundance is high in the lower part of the zone, and shows a decreasing trend in the upper part. It is oscillating with three distinct peaks. The average foraminiferal abundance is 443 foraminifera/g.

## 5.8 CTD description

### 5.8.1 JM06-024-GC3

In the surface water, the salinity is high, about 34.94 ‰ and it gradually decreases down to 34.89 ‰ at the bottom. The temperature is stable in the upper part, around 0.2°C until it crosses 0°C at 70 m depth. After 70 m depth, the temperature continues to decrease in the lower part until it reaches its lowest value of – 0.5°C at the bottom. The density shows three marked changes. The upper 20 m are decreasing until the density starts suddenly to increase. From 20 m to 70 m the density is quite stable. At 70 m is another sudden increase, and the values are gradually increase until at 116 m, when they become stable.

### 5.8.2 JM07-049-GC1

The CTD over core location JM49, has an increasing trend for the salinity and the temperature. Its salinity values are almost 34.86 ‰ in the surface and shows a lowering trend towards 70 m depth, where it reaches its lowest value of 34.844 ‰. Its starts to increase gradually downward, until it reaches the depth of 146 m, with values of 34.86 ‰. A rapid increase follows towards the bottom, and at 162 m depth, the values are 34.89 ‰.

The temperature follows the same trend as the salinity in the upper part, by decreasing. In the surface water, it is -0.9°C, and is stable towards 70 m depth where it is recorded -1°C.

Its lowest value is -1.05 °C. The temperature increases gradually towards the bottom, and rapidly increases at 146 m towards it highest value of -0.64°C. The density follows the same trend from the top of the water mass, down to the bottom.

# 6 Chronology

## 6.1 Radiocarbon dates

The chronology is based upon 11 accelerator mass spectrometry (AMS) radiocarbon dates. Five dates have been obtained from core JM06-024-GC3, (JM24), one from this study and four from Velle‘s study in 2012. Five dates have also been obtained from JM49, four from this study and one from Velle‘s study in 2012. JM24 has previously been interpreted as reworked from 260 cm to the bottom of the core (Velle, 2012), and dates from that interval were discarded. To support this interpretation, nine samples at every 20 cm were taken from the core and investigated. Very few foraminifera were found, and the tests were poorly preserved.

Velle (2012) used the radiocarbon calibration program, CALIB 6.0.1 (Stuvier and Reimer, 1993) and the calibration curve Marine 09 (Reimer et al., 2009), to convert the radiocarbon ages into calibrated ages in cores JM24 and JM49. In this study, all the radiocarbon ages were combined and re-calibrated (Table 6.1), using CALIB 7.0.4 (Stuvier and Reimer, 1993) and the calibration curve Marine 13 (Reimer et al., 2013), and the same regional correction

$\Delta R = 105 \pm 24$ (Mangerud et al., 2009).

***Table 6.1 Combined results from the radiocarbon dating from this study (in bold) and the calibration of Velle's study***

| Lab code | Core | Sampling depth (cm) | $^{14}$C age | Cal.yr BP Calib 7.0.4 1σ range | Cal.yr BP Calib 7.0.4 1 σ mean | Species |
|---|---|---|---|---|---|---|
| | JM06-024-GC3 | 402.5 | 10044 ± 46 | 10806 - 11012 | 10909 | *Nuculana sp.* |
| | JM06-024-GC3 | 303 | 8311 ± 41 | 8600 – 8782 | 8691 | *Yoldiella lenticula* |
| | JM06-024-GC3 | 205 | 6916 ± 44 | 7289 – 7392 | 7341 | *Nuculana pernula* |
| | JM06-024-GC3 | 101 | 4654 ± 31 | 4708 - 4820 | 4764 | *Macoma calcarea* |
| UBA-28387 | JM06-024-GC3 | **47** | **1956 ± 24** | **1336 - 1440** | **1403** | *Cardium sp.* |
| | JM06-024-GC3 | 3 | Modern | - | - | *Cardium sp.* |
| | JM07-049-GC1 | 288 | 8441 ± 40 | 8841 - 8992 | 8917 | *Macoma calcarea* |
| UBA-28391 | JM07-049-GC1 | **208** | **3951 ± 24** | **3745 - 3859** | **3802** | *Macoma calcarea* |
| UBA-28390 | JM07-049-GC1 | **147** | **2186 ± 24** | **1600 – 1703** | **1652** | *Nuculana pernula* |
| UBA-28389 | JM07-049-GC1 | **90** | **1496 ± 22** | **900 - 970** | **935** | *Macoma calcarea* |
| UBA-28388 | JM07-049-GC1 | **50** | **900 ±21** | **414 - 479** | **447** | *Nuculana pernula* |

## 6.2 Age model

The chronology for the age models are established using the calibrated ages with the highest probability within the 1σ range. Ages of samples were acquired assuming uniform sedimentation rate between the dated levels. For core JM24 the oldest dated level is 10,909 cal. yr. BP at the bottom of the core (402.5 cm) (Fig. 6.1). The bottom of the investigated part is at 253 cm. The calculated ages is 8282 cal. yr. BP. For core JM49, the oldest dated level is 8917 cal. yr. BP at the bottom of the core (288 cm). In both cores, the tops are assumed recent.

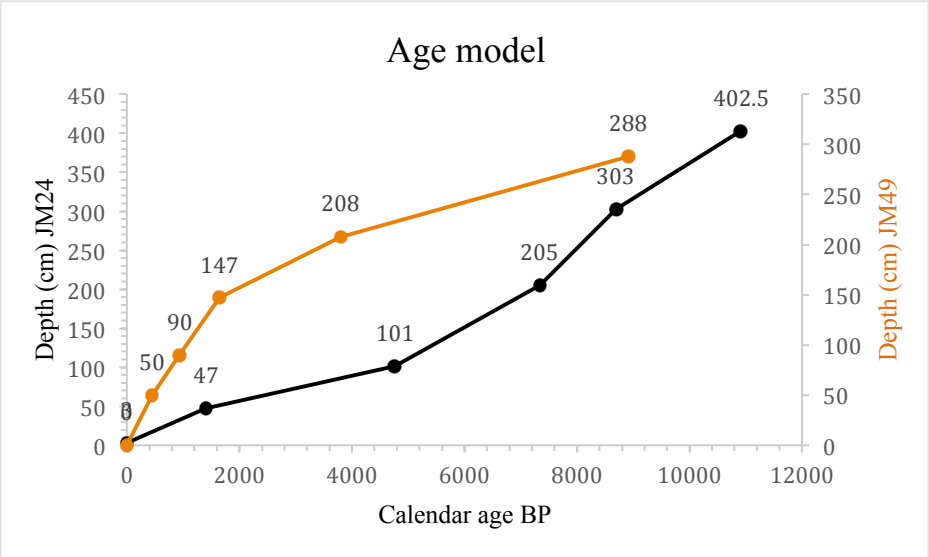


***Figure 6-1 Age-depth plot for the two investigated cores in Smeerenburgfjorden. Black line is an age model for core JM24 and orange line is an age model for core JM49. Numbers above indicate sampling depth of dated material.***

### 6.2.1 Sedimentation rate

In the tables below are the calculated sedimentation rates for cores JM24 and JM49. There is a difference in the sedimentation rate between the two core locations. In front of the fjord sill, (JM24; see Fig. 2.1 in Chapter 2.1), the sedimentation rate is more stable (Fig. 6.1), while the sedimentation rate is relatively higher behind the sill (JM49; see Fig. 2.1 in Chapter 2.1).

***Table 6.2: Sedimentation rate calculated per 1000 years for core JM06-024-GC3***

| Core | Age interval (cm) | Sedimentation rate/1000 yr |
|---|---|---|
| JM06-024-GC3 | 402.4 - 303 | 44.86 |
| JM06-024-GC3 | 303 - 205 | 72.59 |
| JM06-024-GC3 | 205 - 101 | 40.35 |
| JM06-024-GC3 | 101 - 47 | 16.06 |
| JM06-024-GC3 | 47 - 3 | 33.49 |

The sedimentation rate for JM24 is relatively uniform, averaging 37 cm/ka throughout the whole core (Table 6.2). Bivalve samples were collected approximately every 100 cm interval, and each dated bivalve shell in the core marks the boundaries between the units in

the lithological record. In the middle part of the core, the sedimentation rate and the time span between the calibrated ages are different.

In the lower most part of the core (Unit 1; 410 – 303.5 cm, Chapter 5.4) the sedimentation rate is high at 45 cm/ka. The bivalves sampled at 402.5 cm and 303 cm depth (Table 3.2) were dated to 10,909 cal yr. BP and 8691 cal yr. BP. Although the lower part of the core is disturbed, the age span of 2218 years is consistent with the relatively high sedimentation rate.

Unit 2 (303.5 – 203 cm, Chapter 5.4) has the highest sedimentation rate of almost 73 cm/ka but the age span between the sampled intervals is the lowest. The bivalves sampled at 303 cm and 205 cm depth (Table 3.2) were dated at 8691 cal yr. BP and 7341 cal yr. BP. In the middle of Unit 2 (260 cm) is a re-sedimentation boundary (chapter 4), which might disturb the sedimentation rate by giving higher values.

In the lower part of the core, the sedimentation rate is lower compared to the upper part. The lowest recorded sedimentation rate in the core is in the lower part of Unit 4 (101 – 47 cm, Chapter 5.4). The sedimentation rate is 16 cm/ka and the bivalves sampled at 101 cm and 47 cm were dated to 4764 cal yr. BP and 1403 cal yr. BP. The time span between the ages in the lower part of the core is 3361 years, which is the highest recorded in the core.

***Table 6.3 Sedimentation rate calculated per 1000 years for core JM07-049-GC1***

| Core | Age interval (cm) | Sedimentation rate/1000 yr |
|---|---|---|
| JM07-049-GC1 | 288 - 208 | 15.64 |
| JM07-049-GC1 | 208 - 147 | 28.37 |
| JM07-049-GC1 | 147 - 90 | 79.49 |
| JM07-049-GC1 | 90 - 50 | 81.96 |
| JM07-049-GC1 | 50 - 0 | 111.85 |

In the upper part of the core (47 – 3 cm) the sedimentation rate increases again to 33 cm/ka. The time span between the bivalves, sampled at 47 cm (1403 cal yr. BP), and the top of the core (3 cm) is 1403 years, since the dated bivalve at 3 cm is modern.

Sedimentation rate for core JM49 is the lowest in the lowermost part of the core, and gradually increases up-core (Table 6.3). The bivalve shells were collected from different depths of the core and the ages do not represent any lithological boundaries.

The lower most interval in the age model is the longest (288 – 208 cm) and records the lowest sedimentation rate of ~ 16 cm/ka. Bivalve shells dated to 8917 cal yr. BP at 288 cm and 3802 cal yr. BP at 208 cm indicating that 80 cm of sediment from the bottom of the core span 5115 years.

The sedimentation rate increases towards the top and the intervals between the dates samples are shorter. Bivalve shells dated at 208 cm and 147 cm have a time span from 3802 cal yr. BP to 1652 cal yr. BP, respectively. The calculated sedimentation rate is 28 cm/ka.

The interval between 147 cm, dated to 1652 cal yr. BP and 90 cm, dated to 935 cal yr. BP is 57 cm long. 717 years indicate a sedimentation rate of 79 cm/ka, which is relatively higher compared to previous intervals. Bivalve shells samples at 90 cm and at 50 cm were dated to 935 cal yr. BP and 447 cal yr. BP, respectively. The sediment interval of 40 cm indicates sedimentation rate of nearly 82 cm/ka. The upper most part of the core has the highest sedimentation rate. The youngest bivalve shell, dated to 447 cal yr. BP is the lowest dated interval in the core and the top of the core is assumed to represent modern time. This interval indicates a sedimentation rate of nearly 112 cm/ka for the last 447 years.

# 7 Interpretation

Based on the age model and the results of the distribution pattern of IRD, relative abundance of benthic calcareous/agglutinated foraminiferal species and the magnetic susceptibility curves, the records have been plotted versus the calibrated $^{14}C$ ages (Fig. 71). Furthermore, the records have been divided into the following time intervals: 10,000 – 6800 $^{14}C$ yr BP (early Holocene); 6800 – 4500 $^{14}C$ yr BP (middle Holocene) and 4500 $^{14}C$ yr BP to present (late Holocene) (Fig. 7.2; 7.3; 7.4)). The calibrated $^{14}C$ ages have been plotted versus the foraminiferal data and the magnetic susceptibility, and are used for further interpretation of the lithology and the biozones.

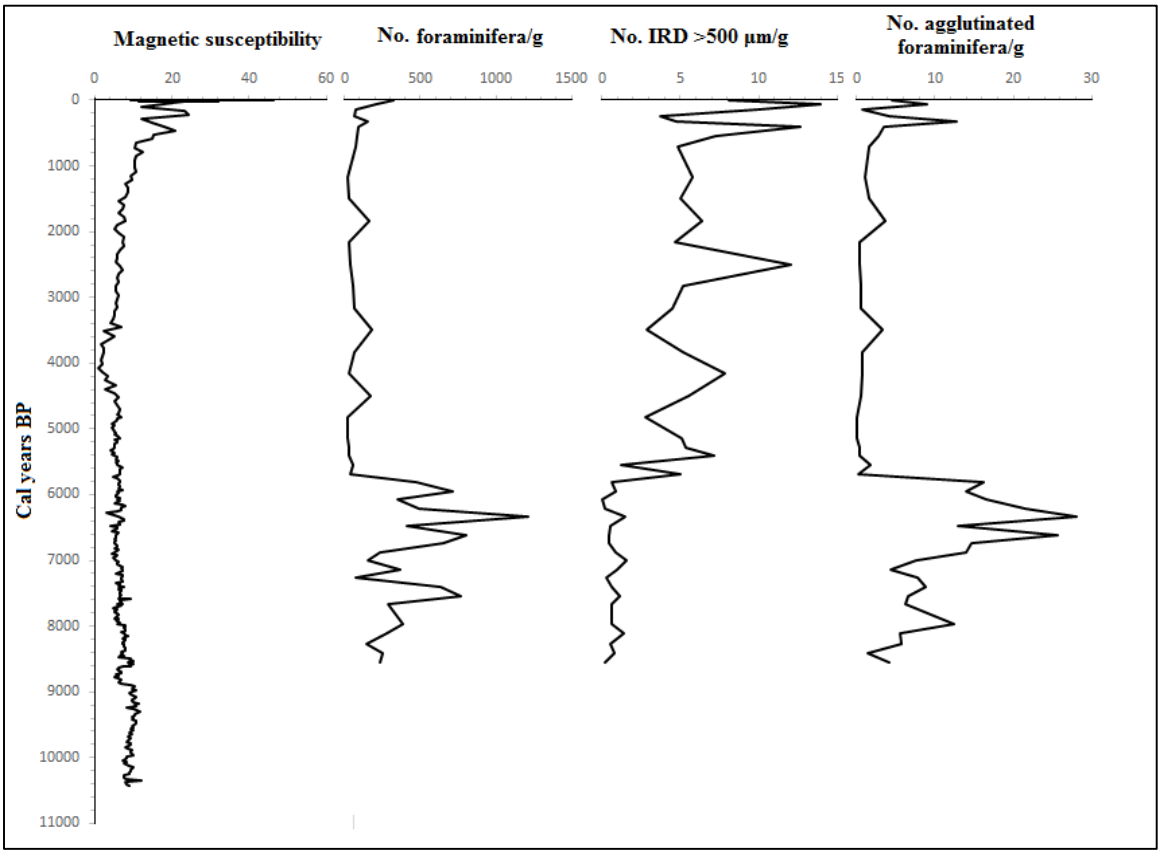


***Figure 7-1 Proxy data from JM24 plotted against depth.***

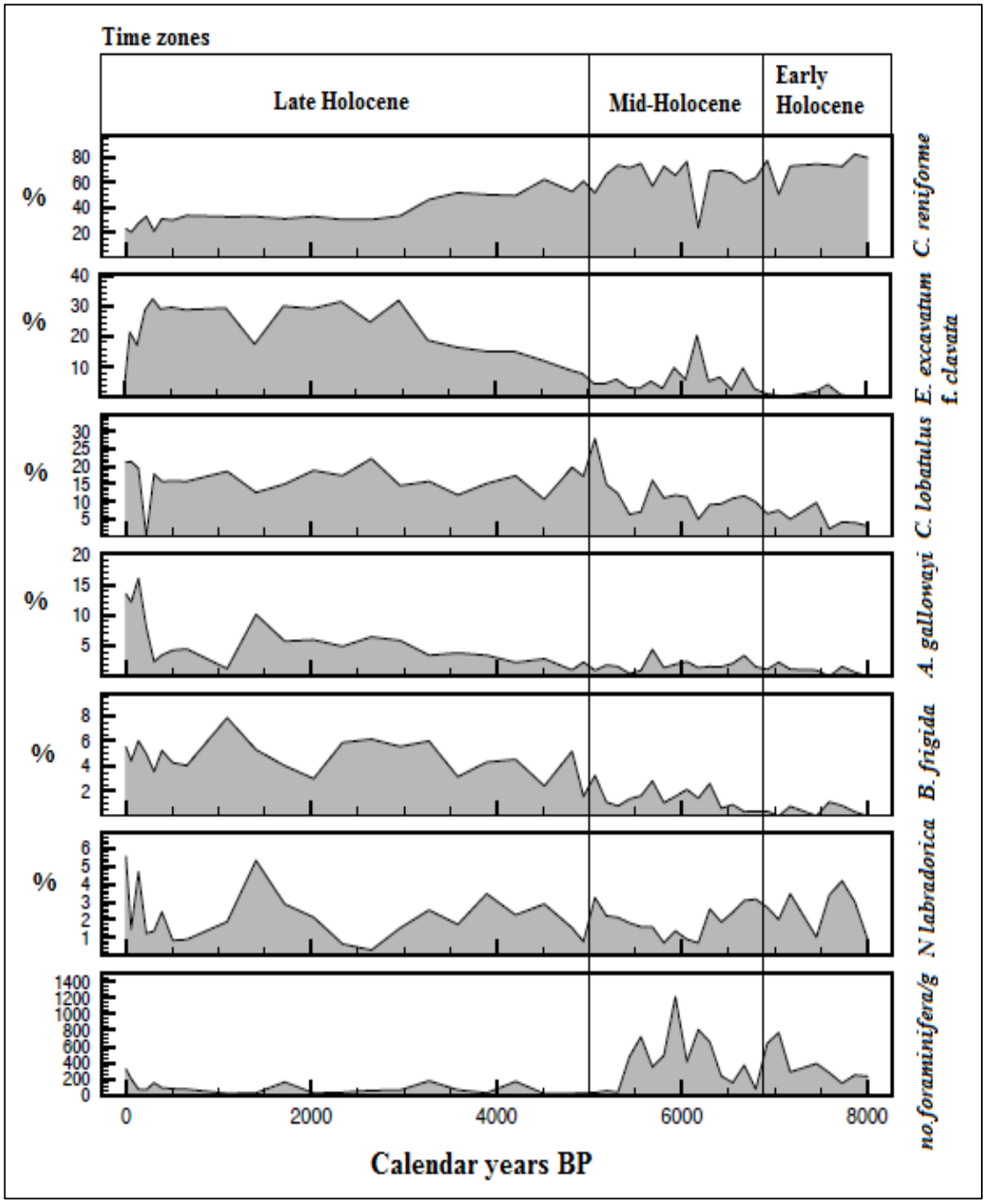


*Figure 7-2 Main calcareous benthic foraminifera species plotted against age for core JM24. The time zones represent Holocene intervals*

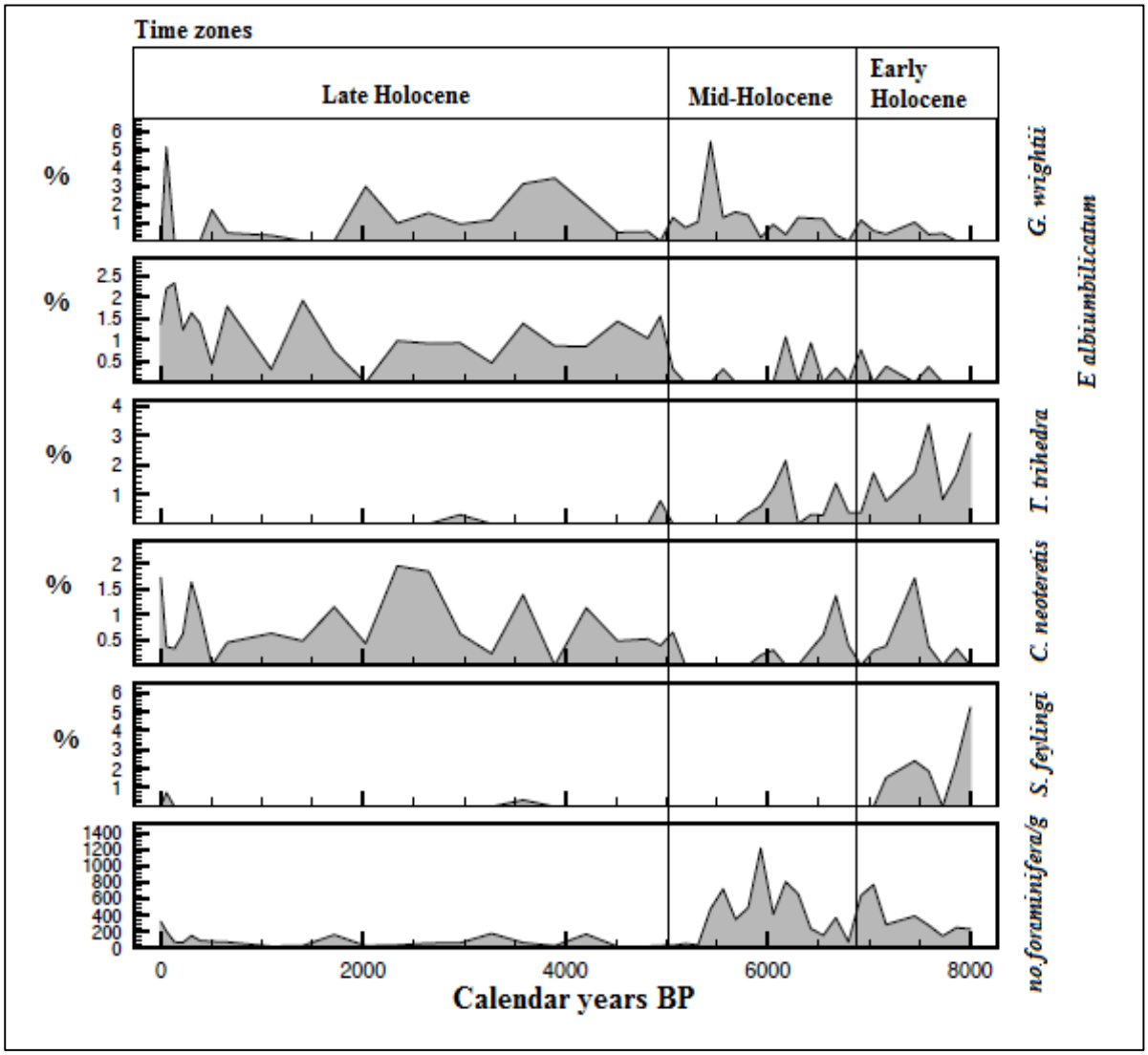


*Figure 7-3 Sub calcarcareous benthic foraminifera species plotted against age for core JM24. The time zones represent Holocene intervals*

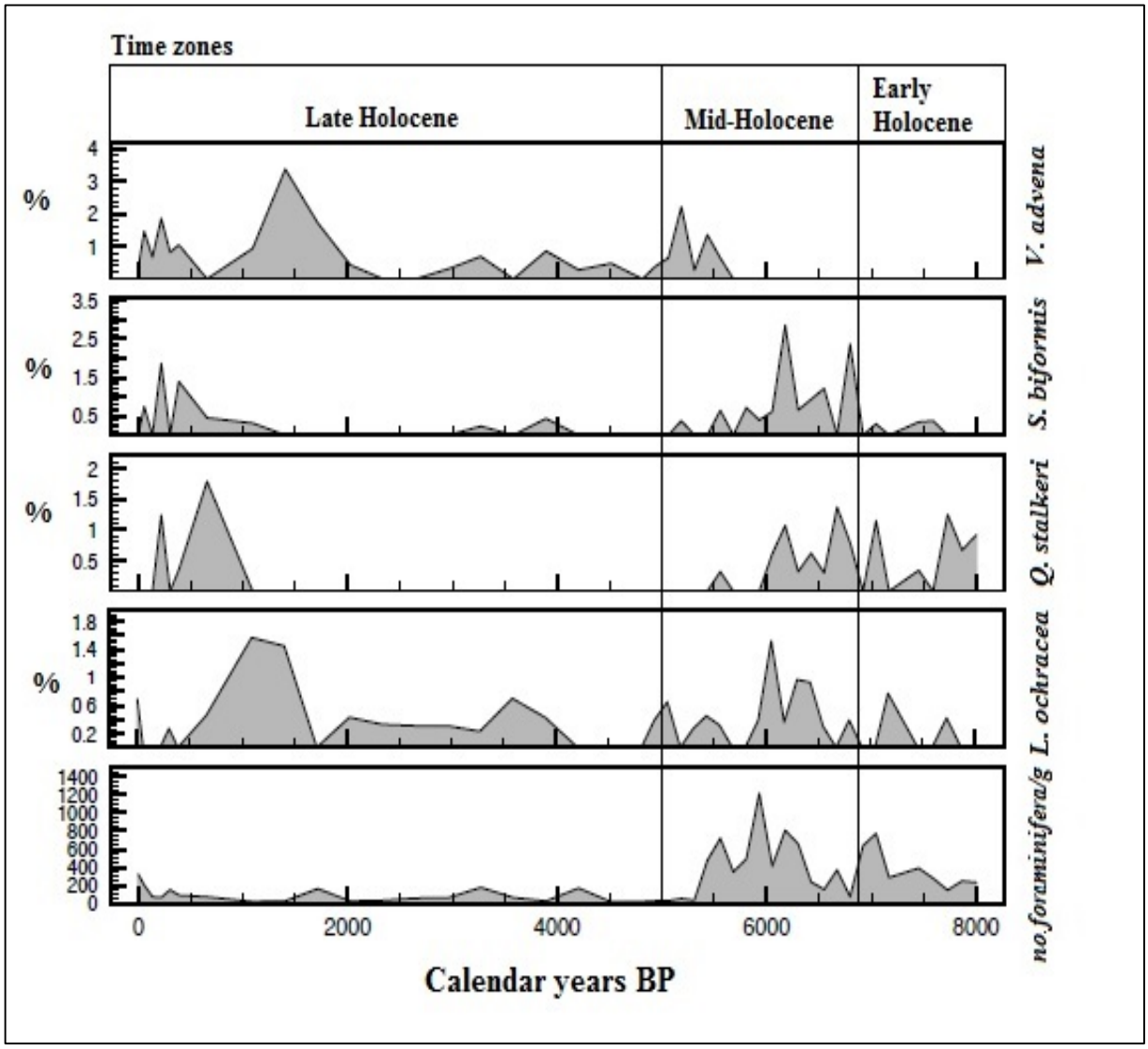


***Figure 7-4 Most common agglutinated benthic foraminifera species plotted against age in core JM24. The time zones represent Holocene intervals***

## 7.1 JM06-024-GC3

### 7.1.1 Time interval 10,000 – 6800 $^{14}$C yr BP (early Holocene).

The time interval of 10,909 cal yr. BP to 6796 cal yr. BP corresponds to the depth from 402.5 cm to 183 cm, respectively. X-ray images reveal that the lowest part of the core terminates in sediments containing clasts, which may indicate that the core represents a glaciomarine environment. The magnetic susceptibility is stable in the lowermost part but at 8912 cal yr BP (313 cm depth) is a sharp decrease from 10 (SI x $10^{-5}$) to 7 (SI x $10^{-5}$). This sharp increase in the magnetic susceptibility data indicates increased supply of magnetic material (Fig 7.1). Molluscs observed in this time interval are few and scattered

and no distinct shell-bed is observed (Fig 5.1). The concentration of IRD is very low throughout the period (Fig. 7.1), indicating restricted ice rafting.

The re-sedimentation previously interpreted to occur at 260 cm depth (Fig. 5.1), which corresponds to 8099 cal yr BP, shows no changes in the magnetic susceptibility curve. In Velle's study (2012), two mollusc shells were dated to 8691 cal yr. BP at 303 cm depth and 7341 cal yr. BP at 205 cm depth (Table 61). The ages indicate that the sediments are undisturbed, but to support Velle's interpretation of disturbed sediments, samples were collected at 20 cm intervals (see Chapter 3). The samples had very few foraminifera and the tests were poorly preserved. Rasmussen and Thomsen (2014) mention that high sedimentation rate preserves calcareous benthic foraminifera better and low sedimentation rate preserves agglutinated foraminifera better. The disturbed interval has the highest sedimentation rate in the core (see Age model), but it is nearly barren of foraminifera and the few that are present, are poorly preserved. The low concentration indicates re-sedimentation that caused poor preservation of the foraminifera throughout the disturbed interval.

The foraminifera in the lowermost studied part of the core (253 cm) indicates an age of 8002 cal yr. BP. The time interval after 8000 cal yr BP represents periods with influence of warmer waters. The calcareous foraminiferal species *Cassidulina reniforme* indicates a glaciomarine environment (Chapter 4.2.1) and its high abundance is connected to the influx of Atlantic Water to the area (Hald et al., 2004; Ślubowska et al., 2005; Ślubowska-Woldengen et al., 2007). The low values of the opportunistic species *Elphidium excavatum* f. *clavata*, a tidewater glacier proximal species indicates a glacier was located near the core location since it prefers low salinity and sea-ice cover (Chapter 4.2.3). The absence of *E. excavatum* f. *clavata* supports the interpretation of warmer bottom waters. *Nonionellina labradorica* shows relatively high percentages and with a decreasing trend in this interval. It has been linked to organic matter associated with Atlantic water (Schafer and Cole, 1986; Hunt and Corliss, 1993; Steinsund, 1994; Hald and Korsun, 1997; Jennings et al., 2004) and the Polar front (Jennings et al., 2004). The interaction between the Atlantic Water and the Polar Water produces strong hydrological fronts (Hald and Steinsund, 1996) and the presence of *N. labradorica* indicates that the environment is under the influence of warmer Atlantic Water.

The agglutinated foraminifera show an increasing trend early in the interval and a decreasing trend in the lower part (Fig. 7.4). The highest abundance of agglutinated foraminifera is found in areas affected by Arctic Water (Rasmussen and Thomsen, 2014), and the increasing trend of agglutinated foraminifera suggest that the environment is affected by oscillations between Atlantic Water and Arctic Water. The end of the early Holocene is at 6796 cal yr. BP (183 cm depth).

### 7.1.2 Time interval 6800 – 4500 $^{14}$C yr BP (mid - Holocene).

The time interval of 6796 cal yr. BP to 4515 cal yr. BP corresponds to the depth from 183 cm to 97 cm, respectively. The magnetic susceptibility shows a lowering trend, indicating a reduction in magnetic material transported to the core location. The X-ray images show a large clast between 178 cm (6672 cal yr. BP) and 173 cm (6548 cal yr. BP). This indicates the onset of IRD sedimentation, possibly related to regrowth of tidewater glaciers in the vicinity. The IRD graph (Fig. 7.1) shows a sudden increase at 5433 cal yr. BP, which corresponds to 128 cm depth, indicating increased ice rafting. Hald et al. (2004) mentions that increased rafting in Van Mijenfjord during the mid-Holocene may be a response to a reduction of the equilibrium line altitude, causing increased tidewater glaciation. The increased IRD activity in Smeerenburgfjorden could indicate similar processes. An increasing trend in the amount of paired shells and bivalve shells up-core indicates favourable conditions for mollusc growth in the late mid-Holocene.

A sudden drop in *Cassidulina reniforme* concomitant to a sudden increase in *Elphidium excavatum* f. *clavata* indicates a rapid cooling around 6200 cal yr BP (Fig. 7.2). This could indicate a fluctuation between warmer and colder water masses as a response to the regrowth of tidewater glaciers. At 5309 cal yr. BP, *C. reniforme* starts to decrease. The species can tolerate relatively low salinity (Holtedahl and Bjerkeli, 1982; Steinsund et al., 1994; Polyak et al., 2002). The decrease is interpreted to represent temperature change rather than salinity change. At 5061 cal yr. BP the opportunistic species *E. excavatum* f. *clavata* starts to increase, indicating a colder environment and water of high turbidity (Fig. 7.2). The high bottom-current indicator *Cibicides lobatulus*, records its maximum value at 5061 cal yr. BP, suggesting high current activity. The amount of *C. lobatulus* lowers in the late mid-Holocene. It prefers salinities higher than 32 ‰ (Steinsund et al., 1994) and the lowering trend might indicate the stronger dominance of low salinity Arctic Water.

In faunas around Svalbard and the Barents Sea, the agglutinated foraminifera are most common in Arctic Waters (Steinsund et al., 1994; Korsun and Hald, 1998; Rasmussen and Thomsen, 2014). The concentration of agglutinated foraminifera in this time interval increases rapidly at 6672 cal yr. BP and their maximum abundance reach 28 agglutinated foraminifera/g at 5929 cal yr BP. The high amount of agglutinated foraminifera in the earlier part of the mid-Holocene indicates good preservation of the foraminifera. In late mid-Holocene, the concentration of agglutinated foraminifera is very low and almost barren at 4515 cal yr. BP (Fig. 7.4).

Areas influenced by Polar water tends to have poor preservation of calcium carbonate (Steinsund and Hald, 1994; Hald and Steinsund, 1996;), and the relatively low values of benthic foraminifera/g in late mid-Holocene, together with higher relative abundance of *E. excavatum* f. *clavata* is an indicator of an influence of cold Polar water in the area.

### 7.1.3 Time interval 4500 $^{14}$C yr BP – present (late Holocene)

The time interval of 4515 cal yr. BP corresponds to core depth of 97 cm. 0 cm is assumed to represent present time. Early in late Holocene, the magnetic susceptibility decreases to its lowest value of 1.1 x $10^{-5}$ SI indicating very limited amount of magnetic material in the sediment. For the last 4000 years, an increase in the magnetic susceptibility curve indicates a rapid increase of magnetic material in the core. The maximum average values in the upper 96 cm is 12 x $10^{-5}$ indicating an increase of magnetic material. This increase could be interpreted as a change in source material from the glaciers over to the core location. The IRD graph (Fig. 7.1) indicates enhanced iceberg rafting and possibly sea ice cover. The material transported by icebergs from the glaciers and deposited along the fjord, could be the reason for the increase in the magnetic susceptibility values (e.g. Velle, 2012).

X-ray images show increased IRD deposition towards present time and there is an increase in layers of shell-beds (Fig. 5.6). The sediment intervals between are mostly barren of bivalve shells and paired shells. The barren intervals are interpreted as times of unfavourable conditions for shell growth, compared to short intervals of favourable conditions, where shell-beds can form. The bivalve shells and paired shells are smaller in late Holocene compared to the shells in the mid-Holocene, indicating that the mid-Holocene is more favourable for shell growth (Fig. 5.6). This also indicates different water

mass dominance in the area. In the mid-Holocene there might be more influence of the Atlantic Water, while in the late Holocene, the cold Arctic/Polar Water is more dominant.

The foraminifera indicate colder bottom water conditions, by the relative dominance of *Elphidium excavatum* f. *clavata*. The low concentration of benthic foraminifera indicates presence of cold Arctic/Polar Water, compared to the early Holocene and the early mid-Holocene (Fig. 7.2). The higher relative abundance of *Nonionellina labradorica* indicates high amount of fresh organic rich detritus in the area 1404 cal yr. BP. At the same time, the sea-ice indicator (Chapter 4.2.6) *Buccella frigida* increases to its maximum percentage, indicating the presence of sea ice. Jennings et al. (2004) mentions that *N. labradorica* correlates positively to the environment of the Polar Front, with high organic content of the sediment. Therefore, the interval from 2648 cal yr BP. to 1092 cal yr. BP (Fig. 7.2) is interpreted to represent enhanced organic material in the area, and the presence of the Polar Front.

The concentration of benthic foraminifera is relatively low throughout the Holocene (Fig. 7.2). The sedimentation rate in the late Holocene is the lowest recorded from 4515 cal yr. BP to 1403 cal yr. BP (97 – 47 cm). The low concentration together with low sedimentation rate, could be the cause of the poor preservation of the calcareous foraminifera. The sedimentation rate increases the last 1403 years (47 – 0 cm), which is reflected in increased preservation of calcareous species. The agglutinated abundance is relatively low throughout late Holocene, but increases the last 500 cal yr. BP (Fig. 7.4). In general, agglutinated foraminifera increase in the upper sediment layers because they have not disintegrated yet (refs in Rasmussen 2014). The calcareous benthic foraminifera shows a similar increase for the last 135 cal yr. BP, which could indicate reappearance of warmer Atlantic Water, better preservation or both. The oscillations in concentrations of the agglutinated foraminifera in the last 500 cal yr. BP may indicate fluctuations between the cold Polar/Arctic Water and Atlantic Water.

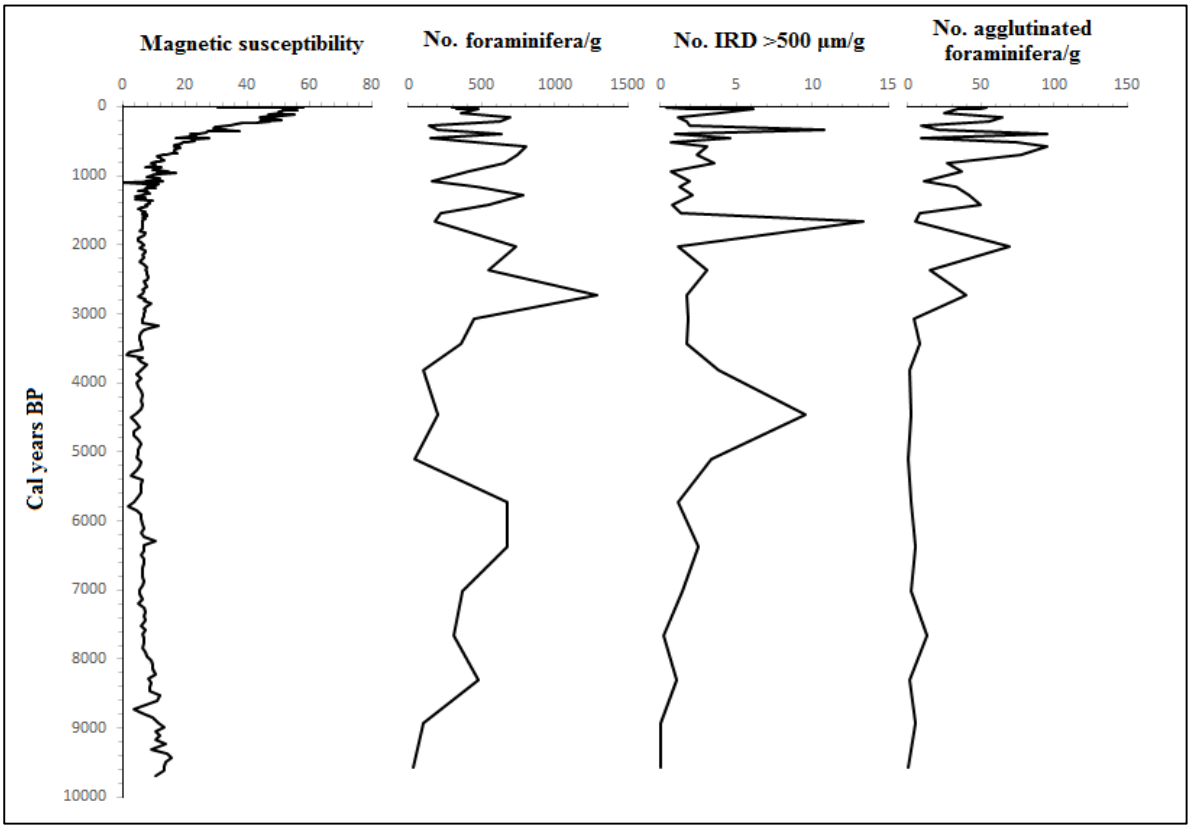


*Figure 7-5 Proxy data from JM49 plotted against depth.*

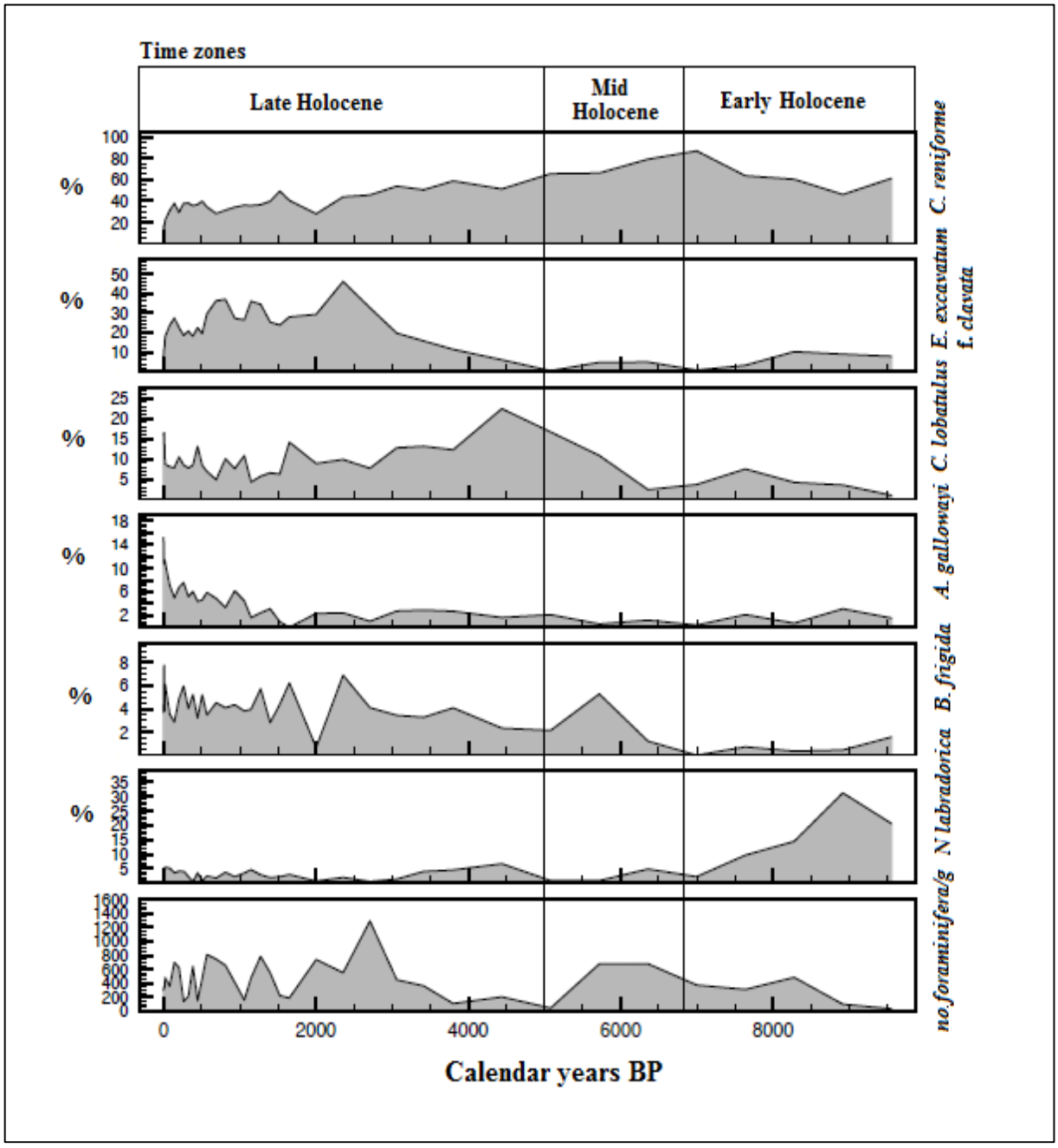


***Figure 7-6 Main calcareous benthic foraminifera species plotted against age for core JM49. The time zones represent Holocene intervals.***

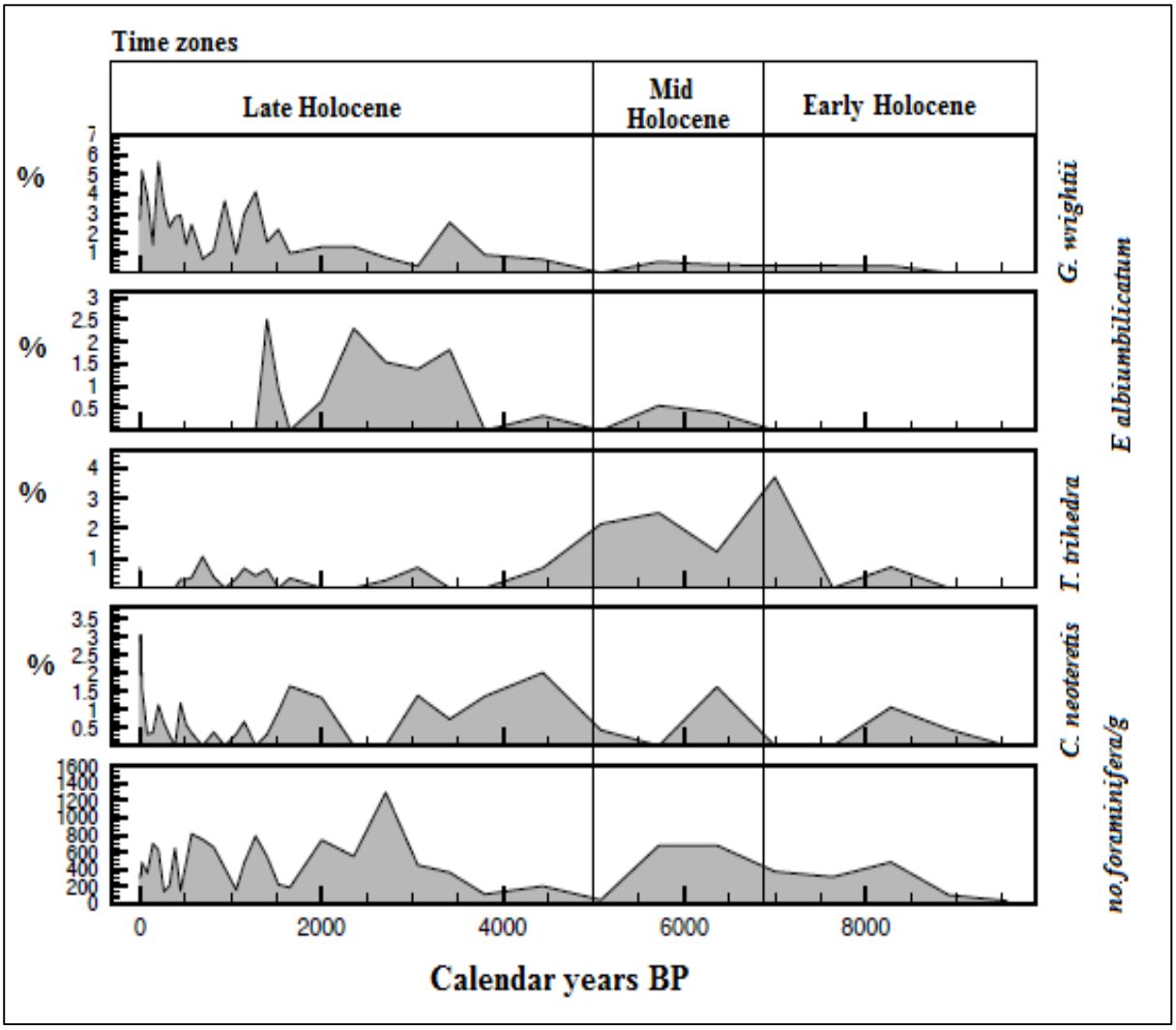


*Figure 7-7 Sub calcarcareous benthic foraminifera species plotted against age for core JM49. The time zones represent Holocene intervals.*

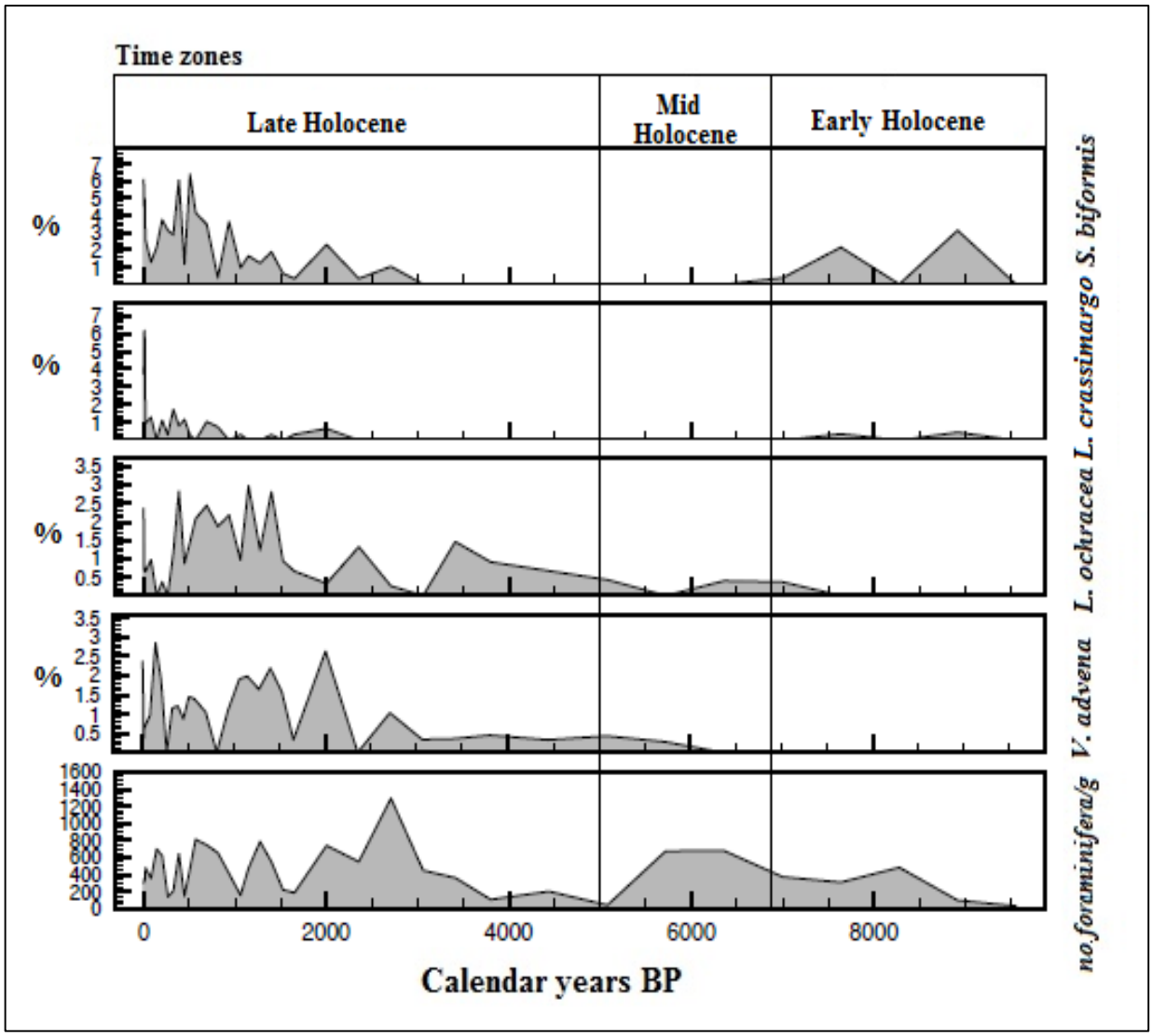


***Figure 7-8 Most common agglutinated benthic foraminifera species plotted against age in core JM49. The time zones represent Holocene intervals.***

## 7.2 JM07-049-GC1

### 7.2.1 Time interval 10,000 – 6800 $^{14}$C yr BP (early Holocene).

The time interval of 9812 cal yr. BP to 6807 cal yr. BP corresponds to the depth of 303 cm to 255 cm. During the earliest part of the early Holocene, the magnetic susceptibility curve has a relatively rapid decrease from 13.4 x $10^{-5}$ SI at 8981 cal yr. BP to 3.8 x $10^{-5}$ SI at 8725 cal yr. BP (Fig. 7.5). This decrease is interpreted as decrease in supply of magnetic material to the sediment. Throughout the remaining part of the early Holocene, the magnetic susceptibility values are relatively stable, indicating stable and continuous

amount of magnetic material in the sediments. The IRD graph indicates low iceberg rafting in the early Holocene as a response to the retreat of the glaciers during the last glaciation.

The X-ray images show that the lowermost part of the core, indicating a time from 9812 cal yr BP at 302 cm to 7574 cal yr. BP at 267 cm, is barren of IRD, bivalve shells and paired shells. The environment is unfavourable for mollusc growth and indicates the last stages of the deglaciation. At the end of the early Holocene, the first bivalve shells are observed in the X-ray images, indicating the onset of the mid-Holocene. The time after 7574 cal yr. BP, represents the introduction of Atlantic Water to the area, with increased amount of bivalve shells in the core.

*Nonionellina labradorica* prefers salinities of 33 – 34 ‰ and temperatures lower than 1°C (Steinsund et al., 1994). At 8917 cal yr. BP, which corresponds to 288 cm depth, *N. labradorica* has its highest percentage in the core. It represents the interaction between Atlantic Water and Polar Water, indicating the Polar Front. The species decreases gradually until it reaches only 2% of the total fauna 7000 cal yr BP. This gradual reduction indicates the retreat of the Polar Front and. The temperate water indicator (Chapter 4.2.1), *Cassidulina reniforme* reaches its highest value at 7000 cal yr. BP, indicating a maximum influx of warmer water, probably Atlantic Water, to the area. The foraminifera in the early Holocene indicate oscillations between cold Polar/Arctic Water and warmer Atlantic Water.

The foraminiferal abundance shows an increasing trend throughout early Holocene (Fig. 7.6; 7.7; 7.8). The abundance increases from 30 foraminifera/g in the beginning of early Holocene to 372 foraminifera/g in the end of the early Holocene. As mentioned above (JM06-024-GC3; mid-Holocene) cold Polar/Arctic Water affects the preservation of calcareous foraminifera, resulting in lower abundance early in this time interval. The influx of relatively warmer Atlantic Water and good mixing promotes the increase in numbers of foraminifera, resulting in increased concentration late in the interval. The low sedimentation rate of 16 cm/ka calculated from the beginning of the early Holocene (8917 cal yr. BP at 288 cm) to early late Holocene (3802 cal yr BP at 208 cm), indicates the flux may have been lower. This low sedimentation rate indicates reduced amount of material deposited over the core location from early Holocene to early late Holocene.

### 7.2.2 Time interval 6800 – 4500 $^{14}$C yr BP (mid - Holocene).

The time interval from 6807 cal yr. to BP 4505 cal yr. BP corresponds to core depth of 255 cm to 219 cm. The magnetic susceptibility curve shows that the sediment has similar amount of magnetic material, indicating no major change in the sedimentary environment.

The X-ray images show increased amount of bivalve shells and shell pairs towards the end of the mid Holocene. The increasing size of bivalves (Fig. 5.6) suggests that conditions for mollusc growth became more favourable towards the end of the time interval. No clasts are visible in the X-ray images. From 5720 cal yr. BP the IRD graph (Fig. 7.5) shows an increasing trend in deposition of IRD throughout mid-Holocene, indicating the onset of glacier regrowth (see JM06-024-GC3; mid-Holocene), probably due to reappearance of cold Polar/Arctic water to the area.

The sedimentation rate for the interval is the same as for early Holocene, 16 cm/ka. In early mid-Holocene, the benthic foraminiferal abundance is high. At 5720 cal yr. BP, it decreases rapidly towards the end of the interval. This rapid decrease correspond to the increase in IRD (Fig. 7.5) indicating a deteriorating environment. *Elphidium excavatum* f. *clavata* starts to increase at 5081 cal yr BP, marking the onset of cold Polar/Arctic Water inflow to the area, together with the gradual decrease of *Cassidulina reniforme* (Fig. 7.6). *Cibicides lobatulus* increases gradually from 6360 cal yr BP towards the end of the time interval, indicating increased bottom water currents in the area (Fig. 7.6).

The agglutinated foraminiferal concentration is still low throughout the time interval, indicating poor preservation of the foraminifera in the sediment since the sedimentation rate is slow.

### 7.2.3 Time interval 4500 $^{14}$C yr BP – present (late Holocene)

This time interval from 4505 cal yr. BP corresponds to 219 cm depth. 0 cm is assumed to represent present time. The magnetic susceptibility is stable until it increases rapidly from c. 1000 cal yr. BP. The resolution of the curve is high (Fig x), because the sedimentation rate is the highest in this interval (see Age model). This increase in magnetic material is interpreted to be the same as in core JM24 (see above), enhanced iceberg rafting and seasonal sea ice cover carrying great amount of sediment and fine material, with enhanced magnetic material towards the present. The X-ray images indicate increased shell occurrence early in the late Holocene. At 195 cm depth (corresponds to 3379 cal yr BP) in

the X-ray image (Fig. 5.6) is a large clast that is interpreted as IRD. The X-ray images show evenly distributed and well preserved mollusc shells and paired shells, together with IRD pebbles that increase towards the present. The high sedimentation calculated from the age model (see Age model) preserves the calcium carbonate from the beginning of the time interval towards the present.

The benthic foraminiferal abundance is the highest at 2709 cal yr BP, with 1291 foraminifera recorded per gram. After this maximum, the abundance oscillates towards the present.

This is the interval where the agglutinated foraminifera are around 30 % of the total fauna (Fig. 7.8). The high sedimentation rate of this interval (see Age model) preserves calcareous foraminifera better and demotes the preservation of agglutinated foraminifera (Rasmussen and Thomsen, 2014). In this time interval, the agglutinated foraminifera are well preserved apart from the sedimentation rate. Alve (1996) suggests the possibility that the typical agglutinated shelf foraminifera may have higher preservation potential that the deep-sea taxa as a general adaption to more stressed environments. The high concentration of agglutinated foraminifera in this interval might be related to the preservation of agglutinated species in the upper part of the cores. Generally the agglutinated foraminifera have a poor preservation potential resulting in disintegration soon after death (e.g. Schröder, 1988; Denne and Sen Gupta, 1989; Wollenberg and Kuhnt, 2000; Murray and Alve, 2011; Rasmussen and Thomsen, 2014). The benthic foraminiferal species are abundant in the time close to present, and the lowering trend of *Elphidium excavatum* f. *clavata* indicates the return of warmer water. *Cassidulina reniforme* is also decreasing, which might indicate the mixing of the water masses over the core location.

# 8 Discussion and correlation

## 8.1 Environment and climate

Holocene marine records show a mid – late Holocene cooling period following an early-mid Holocene Climatic Optimum c. 10,000 – 8000 years BP. Marine records show that the cooling is stepwise and that it follows the declining summer insolation trend (Ślubowska et al., 2005; Rasmussen et al., 2012). Climatic and oceanographic developments from the North Atlantic Ocean and the Nordic Seas indicate a long term and uninterrupted cooling trend from 10,000 – 0 years BP (Marchal et al., 2002). In the Arctic Ocean, records from around Svalbard and in the Barents Sea show the same cooling of the Atlantic Water, indicating a climate deterioration (e.g. Kaufman et al., 2004; McBean et al., 2005; Miller et al., 2010; Rasmussen et al., 2012). The general cooling record in the Arctic Ocean is interrupted by a warming period centred around 9000 years BP ( 2004; Ślubowska et al., 2005; Ślubowska-Woldengen et al., 2007; Skirbekk, 2010), and the results from this study indicate an early Holocene warming around 9000 cal yr. BP (Fig. 7.6; 7.7; 7.8).

Atmospheric general circulation models (AGCMs) can be used to study the spatial pattern of atmospheric response to orbital parameter changes in order to understand the mechanisms of solar radiation to produce large climate changes. In the study of Kutzbach and Guetter (1986) fourteen AGCM experiments are performed, showing a "snapshot" view of the general circulation for specified orbital parameters. The changes in latitudinal and seasonal distribution of solar radiation is assumed to associate with the orbital parameter changes. During the last phase of the LGM 18,000 years ago, the average surface temperature (land and ocean) was about 4 K lower in the Northern Hemisphere in July and January. The northern land temperature was 7 K higher 9000 years ago than during the last phase of the (LGM). The global average temperature increased to modern values 9000 years ago where northern land surface temperature was about 1 K warmer in July and about 0.5 K colder in January (Kutzbach & Guetter, 1986).

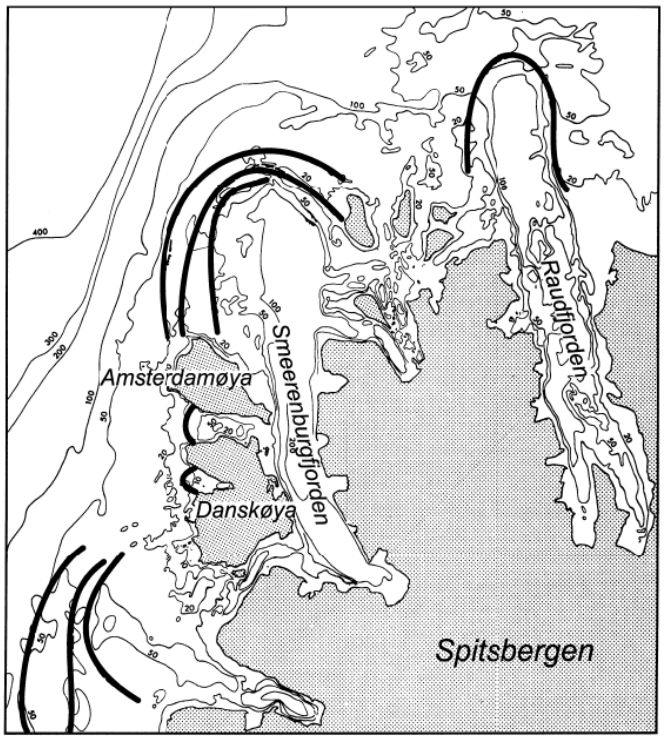


***Figure 8-1 Figure showing the moraines that mark the maximum extent of the Late Weichselian ice sheet. The image is modified from Liestøl 1972.***

The initial deglaciation of the LGM ice sheet started around 13,000 $^{14}$C BP on the west coast of Spitsbergen (Mangerud and Svendsen, 1990; Svendsen et al., 1992; Landevik et al., 1992; Lloyd et al., 1996; Landvik et al., 1998; Koç et al., 2002). Submarine moraines on the northwestern corner of Spitsbergen (Fig. 8.1) have terrestrial parts that have been dated by mollusc shells that indicate an age of the Late Weichselian 18,000 – 20,000 years ago. Along Smeerenburgfjorden, the glacier front withdrew 20 km during the last deglaciation, from the fjord mouth to the inner most part of the fjord (Salvigsen, 1979).

The initial warming of the high-latitude North Atlantic Ocean may be the trigger of the rapid deglaciation of western Spitsbergen around 12,500 years BP (Mangerud, 1977; Svendsen and Mangerud, 1992), Solar radiation began to increase from 20,000 years and was high around 12,000 years ago and it is also considered to be one of the reason that the deglaciation started. The solar radiation in the Northern Hemisphere reached extremes in the early Holocene (9000 years BP). The radiation was 37 $m^{-2}$ (8%) greater in July compared to today, and the temperature was 2.5 °C warmer over land north of 70°N (Kutzbach & Guetter, 1986).

Immediately after the deglaciation, there are evidences of seasonal open conditions in the near-shore Svalbard, shown by the prominent raised marine beach terraces on the west coast of Svalbard. Between 10,500 and 9,000 years the sea level fell rapidly, depositing raised beaches parallel to the shoreline (Forman, 1990). Fjord glaciers on western Spitsbergen retreated rapidly (Forman, 1989) and according to Forman (1990), the northwestern Spitsbergen was peripheral to glacial loading and was deglaciated early. Svendsen and Mangerud (1992) suggest that the glacier recession from the shelf did not stop at the coast, but continued inland, well above the marine limit. This recession may be due to warmer climate rather than rising eustatic sea level, although it may be a factor to consider in the beginning.

Evidence for the Late Weichselian and Holocene glacial history of Svalbard is found in a continuous stratigraphic record from Lake Linné (Linnévatnet) on the west coast, one of the largest lakes on Svalbard. This geomorphological and sedimentological evidence indicate that the glacier Linnébreen melted away completely during the early Holocene, before redeveloping in the mid-Holocene (Mangerud and Svendsen, 1990).

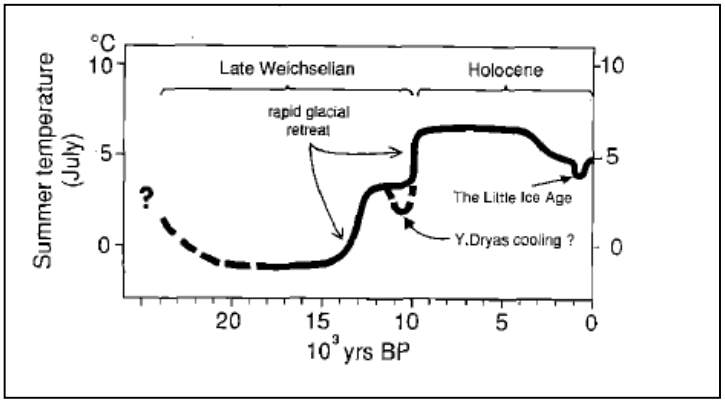


***Figure 8-2 Estimated July temperatures for the last 20,000 years for the west coast of Spitsbergen. Figure from Svendsen and Mangerud, 1992.***

Birks (1991) studied the plant macro flora around Skardtjørna, a small lake in front of Linnévatnet on the west coast of Svalbard, and concluded that the climate 8000 – 4000 years BP resembled that of the inland area today, with a mean temperature of at least 1.5°C higher. Occurrence of fossil floras in the lower most zone, which is only found inland today, indicate a denser and more luxurious vegetation in the early Holocene compared to today. This implies a time of maximum warmth in this profile.

Distribution patterns of the warm water fauna *Mytilus edulis* indicate that the species was abundant along the west coast of Svalbard during warm intervals during the Holocene (Salvigsen, 1992; Salvigsen, 2002; Berge et al., 2004). The species had been absent from Svalbard fjords for 1000 years, when it reappeared in 2004, but had not been found in great abundance for the last 7000 years. One of the reasons for its reappearance is the increased northward mass transport of Atlantic Water by the West Spitsbergen Current (Berge et al., 2004).

## 8.2 Paleoceanographic implications: development during the Holocene and comparison to west and north Svalbard

The results from cores JM06-024-GC3 and JM07-049-GC1 are discussed and are mainly compared to cores JM02-440 from Bellsund Trough (Ślubowska-Woldengen, 2007) and NP94-51 from Hinlopen Trough at the northern Svalbard margin (Koç et al., 2002; Ślubowska et al., 2005). The distribution patterns of the benthic foraminifera for all records are very similar. Close correlation between the records suggest similar timing of changes.

### 8.2.1 Early Holocene

Since the record does not reach further than 9900 cal yr. BP for the cores in this study, the evidence of earlier activity from Bellsund and Hinlopen Trough are used as an estimate for Smeerenburgfjorden. In Hinlopen Trough, the surface and bottom waters remained in a glacial distal environment after 10,800 cal yr, BP with seasonal ice cover, low ice rafting and proximity to the Polar Front, while the Arctic Coastal Front remained close to the western site during the early Holocene. The inflow of Atlantic water to Hinlopen resulted in low temperature changes, apart from the climatic optimum with 4 – 5°C warmer waters in the Nordic Seas (Koç et al., 1993). Ślubowska et al. (2005) mention that there is no distinct evidence for the Holocene Climatic Optimum close to the core site in Hinlopen Trough, apart from the change in seasonal productivity of benthic and planktonic foraminifera. In core JM24, which is located in front of the sill (Fig. 3.1), it is possible to see an increased productivity in the lower most part of the core (from 8100 cal yr. BP to 7100 cal yr. BP), where the abundance is relatively high. At 7400 cal yr. BP (148 cm depth), the abundance maximum value is 1200 foraminifera/g (Fig. 7.2) and the sedimentation rate of 73 cm/ka in early Holocene (Table 6.2) is the highest in the core. The benthic abundance in core JM49 is lower during the Holocene compared to JM24 (Fig. 7.2;

7.6). At 8300 cal yr. BP in core JM49, the abundance is around 480 foraminifera/g, and the sedimentation rate of 16 cm/ka prevails for 5115 years, from (288 – 208 cm) (Fig. 7.6; see Age model) . The high sedimentation rate preserves the calcareous benthic foraminifera better, opposite to the low sedimentation rate, which preserves agglutinated foraminifera better (Rasmussen and Thomsen, 2014). The difference in the location of the cores is the primary reason for this, since the warm Atlantic Water may have passed over the core location on the shelf, in front of the sill, but not over the core site of the inner part.

Salvigsen (1992) described the distribution of the thermophilous mollusc *Mytilus edulis* during early Holocene. This warm waters mollusc reached from Hornsund in south Svalbard to Blomstrandhalvøya in Kongsfjorden on the west coast. The species is also found in Hinlopen Through and even further east. This species indicates the Holocene Thermal Maximum in coastal waters west and north of Svalbard at c. 8700 – 7700 cal yr BP. This species has however not been found at the north-western corner of Svalbard, since there have been no positive shoreline displacements after 9500 BP. *Mytilus edulis* can only be expected to be found in submarine deposits along the shore.

### 8.2.2 Middle Holocene

The most prominent event during middle Holocene is the retreat of the Atlantic Water and cooling of the area. The shift from high relative abundance of *Cassidulina reniforme* towards relatively high relative abundance of *Elphidium excavatum* f. *clavata* in all cores is recorded during the mid-Holocene and suggests a change in the bottom water conditions. The glaciomarine environment indicator species (Chapter 4.2.1) *C. reniforme* prefers higher salinity whereas the opportunistic species *E. excavatum* f. *clavata* can tolerate low salinity. This lowering of salinity suggests reduced inflow of Atlantic Water to the core sites. This change is recorded in both cores in the period from 6800 to 4500 cal yr BP (Fig. 7.2; 7.6). For core JM24 the foraminiferal shift occurs at c. 6100 cal yr BP, but for JM49 the shift occurs later at c. 5600 cal yr BP. This time difference between the cores may be related to the sill, which may have protected the fjord from change from the outside. The reason for this time difference might be related to the flow strength of the Atlantic Water in this time interval. The presence of Atlantic Water might have affected the area in front of the sill for a longer time, than in the area behind the sill. The error in the radiocarbon ages must also be considered. Mangerud and Gulliksen (1975) discuss the circulation of carbon and draw attention to the stable surface layer of the Arctic Ocean, preventing exchange of

carbon from the atmosphere to the deeper water masses. They also indicate that permanent pack ice cover of the Arctic Ocean probably delays the atmospheric and the surface water exchange of carbon, compared with ice cover free oceans. Spitsbergen is situated on the boundary between the Atlantic Water and Arctic Water, which may have caused delayed influences of Atlantic Water during the Late Holocene. During the mid-Holocene the water along the west Spitsbergen is known to have been warmer (Ślubowska-Woldengen, et al., 2007; Skirbekk et al., 2010; Rasmussen et al., 2012; Rasmussen et al., 2014). This may have caused slightly lower apparent ages.

Elverhøi et al. (1980) studied the diversity foraminiferal fauna in the innermost part of Kongsfjorden (northwest Svalbard). The sampling area lies just outside the front of the grounded glacier Kongsvegen and has a water depth of 50 m. The foraminiferal assemblage here is strongly dominated by *C. reniforme* followed by *E. excavatum*. The bottom salinity in the fjord is 33‰, and is considerably high, and is the main reason for the dominance of *C. reniforme*. Higher frequency of *E. excavatum* is expected under more brackish conditions.

### 8.2.3 Late Holocene

Around 3800 cal yr BP, the relative abundance of *E. excavatum* f. *clavata* in core JM24 is stable and high. The values for both *C. reniforme* and *E. excavatum* f. *clavata* in core JM49 oscillate more throughout the late Holocene and it is more unclear, when the shift is complete. In Hinlopen Trough, the foraminifera shift occurred much sooner, around 4500 cal yr BP. The reason for this earlier shift is that core NP94-51 is retrieved from the deeper part of the shelf further north, while cores JM24 and JM49 are from the inner shelf and a fjord and are more affected by terrestrial climate and glaciers. The location of JM49 from inside the sill may not have this clear change, since there could be continuous influx cold water from the local glaciers that could affect the bottom water conditions more than in the outer part of the sill.

In the core from the western Bellsund Trough are warm water species present. In Hinlopen Trough, there is few warmer water species, which may indicate that the inflow of the Atlantic Water was not strong enough to the area, or that the warming in the Nordic Seas (Koç et al., 1993) was only due to increased solar insolation. In Smeerenburgfjorden, the

complete faunal diversity is strongly dominated by Arctic species and almost no warm water species were present indicating cold conditions.

### 8.2.4 CTD

The CTD retrieved at the core locations in April (Fig. 2.3), gives evidence of the difference between the cores that could have prevailed during the late Holocene. It shows that for core JM24, the salinity lowers gradually from the sea surface towards the sediment surface. The upper water mass is above 0°C and the salinity is above 34.91 ‰. The lower part shows colder water masses of below 0°C and salinity under 34.91 ‰. When these values are compared to core JM49 it is clear that there is difference between the water masses over each core locations. The upper water mass in JM49 shows lower temperature and salinity with temperatures falling below -1°C and salinity around 34.85 ‰. In the lower water mass the temperature increases slightly to around -0.9°C and the salinity gradually increases to 34.86 ‰. The sill located in between the core sites mainly causes the salinity and temperature difference. Core location JM49 is closer to nearby glaciers (Fig introduction), and the lower temperature and salinity indicate water masses that are considerably colder and fresher. The slightly warmer water masses in front of the sill (JM24) are not present in the surface water or the bottom water behind the sill. However, it is also possible that the sill is preventing this colder and fresher water to reach core location JM24. In the study from Ślubowska-Woldengen et al. (2007), the CTD profile collected in August reveals that the warm Atlantic water (7.3°C and 35.2 ‰) is confined to the shelf area of the continental margin. On the shelf, the water is a mixture of Arctic Surface Water (7.1 °C and 34.9 ‰) and Polar Water (6.4°C and 34.4 ‰) (Fig. 8.3).

The CTD data collected in August represent water masses during the summer time, while the CTD in April are water masses from late winter. In August, the shelf area has higher temperatures and salinity compared to the conditions in late winter. Although the salinity is quite similar, the major difference is the temperature. The salinity difference between the continental slope and the shelf may be caused by the fresh water influx from the glaciers in Smeerenburgfjorden, which does not pass the continental sill, but stay confined to the fjord (Fig. 2.2; 3.1). The salinity from core the core location of JM24 indicates that the most prominent water mass is the ASW since the PW has lower salinity than recorded over the core location. However the temperature and salinity given in Ślubowska-Woldengen et al. (2007) is an average, and to be more accurate on what water masses are located over or

near the core location, more precise information is needed. To get more precise information about the salinity and temperature difference in Smeerenburgfjorden I would suggest a CTD collection in August.

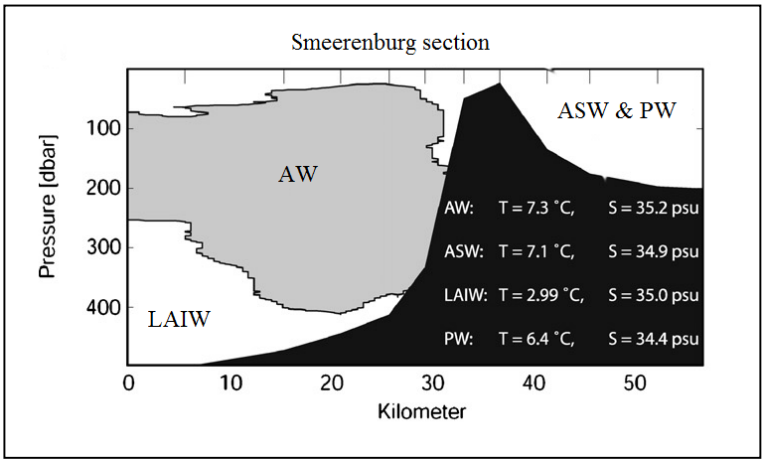


***Figure 8-3 Water mass distribution across the shelf and slope from Smeerenburg section. The maximum temperature and salinity from CTD stations is given. Atlantic Water (AW) is grey, Lower Arctic Intermediate Water (LAIW) - Arctic Surface Water (ASW) - and Polar Water (PW) are white. (Ślubowska-Woldengen, 2007)***

## 8.3 Application of benthic foraminifera stable isotopes

Stable oxygen and carbon isotope analysis on the benthic foraminifera (see Method chapter) is a widely used in paleoceanographic and paleoclimatic studies (Shackleton, 1974).

### 8.3.1 Oxygen Isotopes

The shelf area west of Spitsbergen represents the dynamic exchange and mix between Atlantic, Arctic and glacial waters (Saloranta and Svendsen, 2001; Nilsen et al., 2008) which can happen within an annual cycle. The sudden shift from the dominance of fresh and cold Arctic Water during the winter to a warm saline water during the summer indicates high seasonal of temperature variations (Svendsen et al., 2002; Cottier et al., 2005; Nilsen et al., 2008). The flow of Atlantic water in the WSC (see Introduction chapter) is normally along the bottom, below the Arctic water of ESC (Fig. 1.2), but in the study of Tverberg and Nost, (2009), the Atlantic water was also present at the surface. This resulted in an increased temperature of the whole water column (Cottier et al., 2007; Jernas et al., 2010). Tverberg and Nøst (2009) interpreted this Atlantic inflow to be changes in the density gradient between the Atlantic water of the WPC and the Arctic Water of ESC.

The study of Zajączkowski et al. (2010) shows that the application of stable oxygen and carbon isotopes of benthic foraminifera is partly limited by the species-specific vital effects. As mentioned earlier, *Cibicides lobatulus* prefers to live in coarser sediment, with strong bottom water currents, while *Cassidulina reniforme* and *Nonionellina labradorica* are more typical sediment dwelling forms. Therefore, *C. lobatulus* is more likely to record the bottom water conditions while *C. reniforme* and *N. labradorica* record the pore water conditions. The composition of living and dead stable isotopes ($\delta^{18}O$ and $\delta^{13}C$) were plotted uncorrected for vital effects (Fig) and a distinct offset is noticed in *C. lobatulus*.

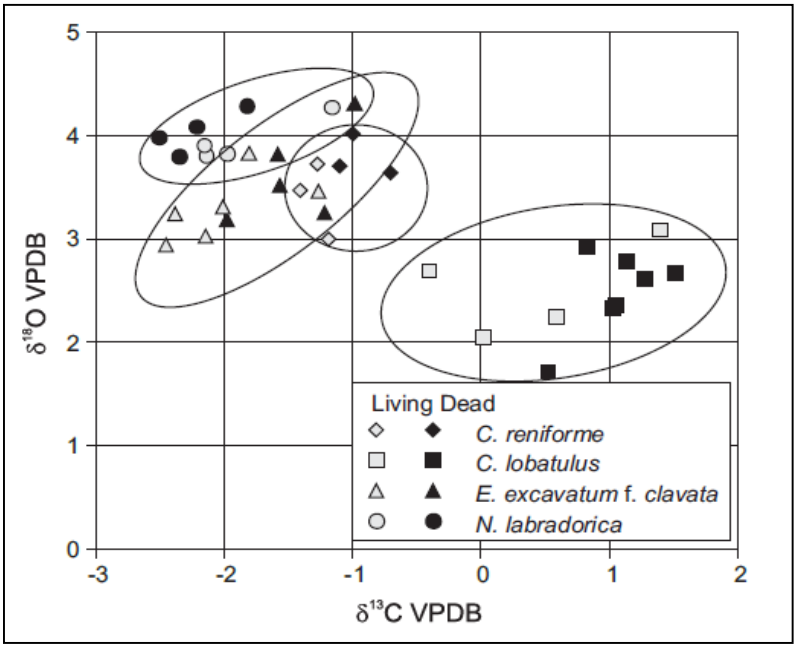


***Figure 8-4 Oxygen and carbon records from four live and dead foraminiferal species in the study of Zajączkowski et al., 2010. The species shows the difference in the values of the epibenthic foraminifera, Cibicides lobatulus, compared to the endobenthic species Cassidulina reniforme, N. labradorica and Elphidium excavatum f. clavata.***

The benthic $\delta^{18}O$ values for each species from this study show a different trend. The epibenthic species *Cibicides lobatulus* is the only species that shows no distinct trend towards the present (Fig. 8.5). Its values in the early Holocene is oscillating, with jumps between 0.5 ‰ and 0.74 in the period from 8000 cal yr. BP to 5000 cal yr BP. The oscillations are high during early Holocene and early in the mid-Holocene in core JM24 (see Chronology; Age model). The oscillations indicate a temperature variation of 2 – 3°C (assuming constant salinity values) (Fig. 8.5). The $\delta^{18}O$ values are low in the early Holocene with a relatively stable trend towards the mid-Holocene. From 5000 cal yr. BP towards the present, the values indicate a temperature oscillations of 1 °C (0.27 ‰),

indicating temperature fluctuations between a cooling (high values) and warming (low values) (Fig. 8.5). At 300 cal yr. BP, the values increase suddenly to 4.04 ‰ from 3.62 ‰ at 650 cal yr BP, indicating a cooling of 1.7°C.

*N. labradorica* is an endobenthic species that thrives in the spring bloom characterized by fresh food supply (Korsun and Hald, 1998, 2000; Polyak et al., 2002; Rasmussen et al., 2012). The $\delta^{18}O$ values for this species is recorded from ~9600 cal yr. BP and are increasing towards 7000 cal yr. BP, indicating a cooling trend (Fig. 8.5). The values increase gradually from 3.86 ‰ at the bottom of the core to 4.66 ‰ at 7000 cal yr. BP, showing that the pore-water temperature in the fjord (JM49) decreased over 3°C. From 7000 cal yr. BP to 2700 cal yr BP, the values are however decreasing slowly (Fig 8.5). The values decrease from 4.41 ‰ to 4.58 ‰ indicating a temperature increase of 0.7°C until the values suddenly increase at 2300 cal yr BP to a value of 4.58 ‰. This increase corresponds to a temperature cooling of 0.7°C. The general trend is decreasing towards the present indicating a warming, but the values are oscillating

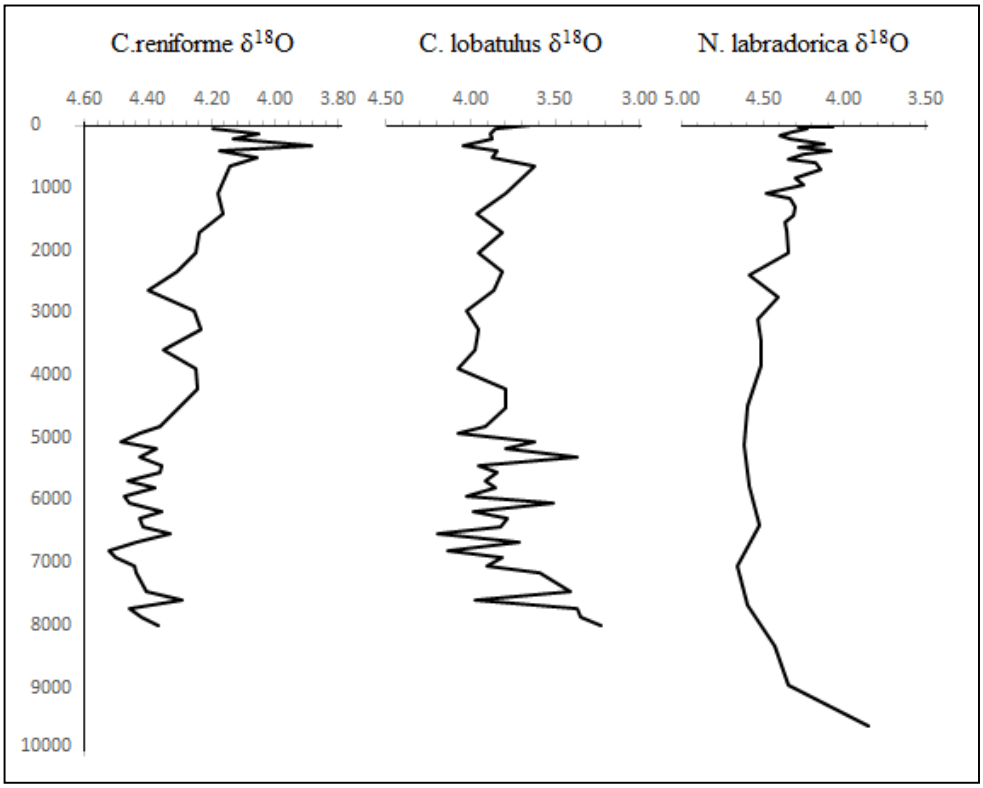


***Figure 8-5 Oxygen isotope records from three benthic foraminifera from Smeerenburgfjorden. C. reniforme and C. lobatulus represent core JM24 while N. labradorica represents core JM49.***

The infaunal species *C. reniforme* shows a relatively stable trend throughout the Holocene. The largest oscillations is in the end of early Holocene, from 7600 cal yr BP with values of 4.29, increasing to 4.52 ‰ at 6800 cal yr. BP. This increase indicates a cooling of 1 °C (0.24‰ change in $\delta^{18}O$ values). The mid-Holocene shows minor oscillations, indicating a stable temperature throughout the time interval. From 4800 cal yr. BP the values start to decrease, indicating a warming in the early late Holocene. The warming is interrupted at 3600 cal yr. BP, by an increase of 0.25°C (0.1 ‰ change in $\delta^{18}O$ values). The trend increases after the sudden cooling for a short time, before the temperature become cold again 2650 cal yr. BP. The general trend from 2650 cal yr BP is warming. The values decrease significantly (0.5 ‰ change in $\delta^{18}O$ values) indicating a temperature increase of 2°C towards the present.

*C. reniforme* and *N. labradorica* show a similar warming trend towards the present. As mentioned earlier, these species are infaunal (Chapter 4.2.1; 4.2.4) representing the pore water temperature change. The species vary during the last 5000 cal yr. BP, as *C. reniforme* shows a more obvious warming towards the present. This difference might be related to the vital effects, since *N. labradorica* has been corrected for -0.2 ‰ (see Methods), but *C. reniforme* has not. Austin and Kroon (1996) indicate that *C. reniforme* precipitates its shell in disequilibrium with an offset of 0.13 ‰ $\delta^{18}O$.

*C. lobatulus* is an epibenthic species (Chapter 4.2.2) and as mentioned earlier it reflects the $\delta^{18}O$ of the bottom water. The stable values of the species might indicate that it calcifies in stable seasonality. In Hornsund fjord in southwestern Svalbard, the *C. lobatulus* calcifies during the summer time while *N. labradorica* calcifies in cold spring situations (Zajączkowski et al., 2010). The seasonality of the calcification between the species might be a reason for the $\delta^{18}O$ difference (Fig. 8.6). The similarity between *N. labradorica* and *C. reniforme* might indicate that the latter species calcifies in spring situations, a little later than *N, labradorica*. When the species are plotted in the same graph (Fig. 8.6) the spring calcifying species (*N. labradorica* and *C. reniforme*) have generally higher values than the summer calcifying one (*C. lobatulus*).

When the species calcify 8000 yr. BP, the values differ significantly. *C. lobatulus* has the lowest values, and *N. labradorica* has the highest values. This difference is also observed in the study of Rasmussen et al. (2012) in Isfjorden, although it is observed prior to 8200 cal yr. BP. This offset in $\delta^{18}O$ values is interpreted as increased seasonal contrast in bottom

water temperature, with inflow of warmer Atlantic Water along the bottom of the fjord during the summer and mixing with cold water during the winter. The contrast is slightly lower after 5000 cal yr. BP

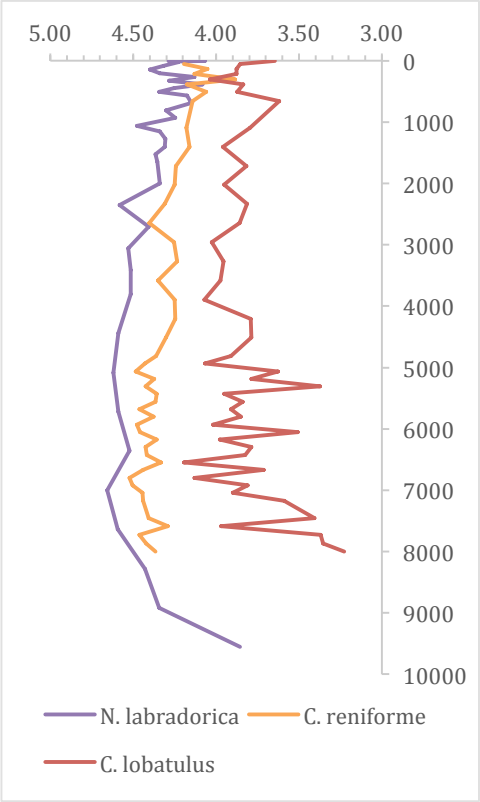


***Figure 8-6 Oxygen isotope records from cores JM24 and JM49 combined.***

### 8.3.2 Carbon isotopes

The $\delta^{13}C$ values of the summer calcifying species *Cibicides lobatulus* are generally higher, compared to the spring calcifying, infaunal species *Nonionellina labradorica* and *Cibicides reniforme* (Fig. 8.7). High $\delta^{13}C$ values indicate a good ventilation of the bottom water, and the values of *C. lobatulus* throughout the Holocene are generally increasing. The same increasing trend is shown in the epifaunal species *N. labradorica and C. reniforme*, although their values are significantly lower. The average $\delta^{13}C$ values of *C. reniforme* is -1.5 ‰ while the average $\delta^{13}C$ values of *N. labradorica* is centred around -2 ‰.

*C. lobatulus* reflects the $\delta^{13}C$ values of the fjord bottom water, since it is epifaunal, while the infaunal species represent the $\delta^{13}C$ values of the pore water (Ivanova et al., 2008). The records seem to be more stable before 5000 cal yr. BP for *C. reniforme* and *C. lobatulus*,

located in front of the fjord mouth sill, while *N. labradorica* is more unstable after 4000 cal yr. BP, located behind the sill (Fig. 2.2; 3.1).

Foraminiferal concentration shows a general increasing trend from the beginning of the record towards 5000 cal yr. BP in core JM24 (Fig. 8.7), and from 5000 cal yr. BP the concentration is decreasing. The same pattern is shown in the foraminiferal concentration for core JM49, it starts to decrease after 4000 cal yr. BP (Fig. 8.7). This productivity decrease in the foraminiferal concentration for both species might be the cause in the increasing trend of the $\delta^{13}C$ values for all of the stable isotopes (Fig. 8.7).

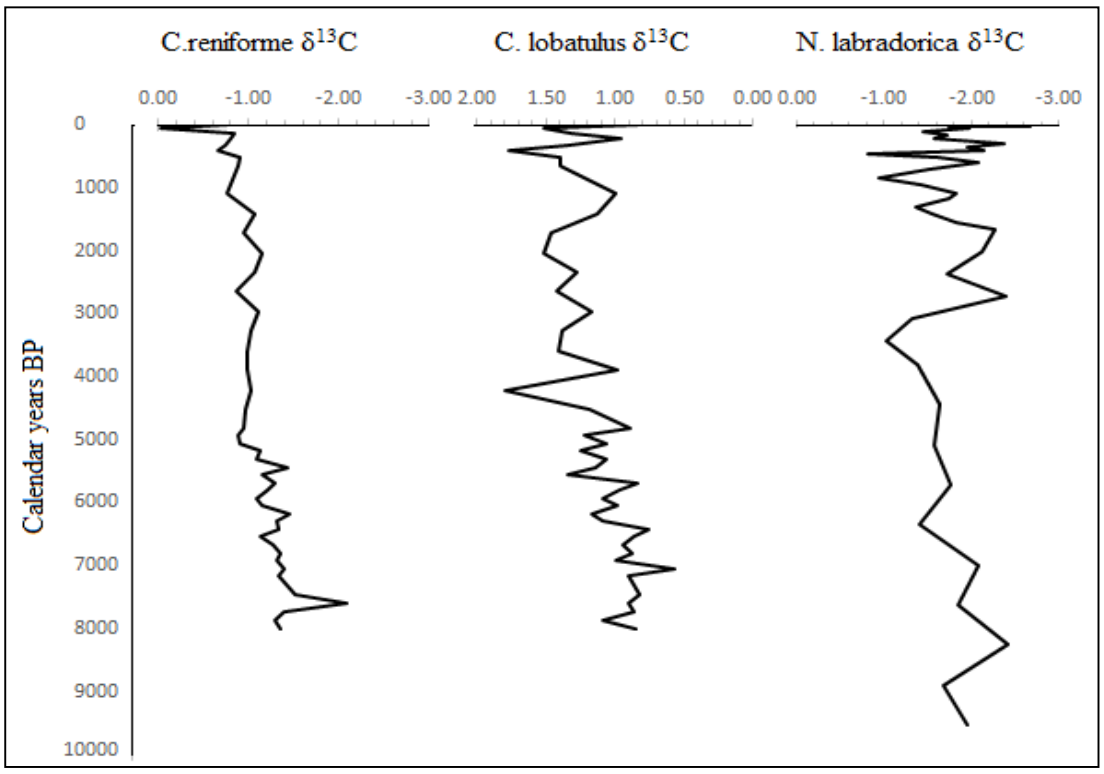


***Figure 8-7 Carbon isotope records from three benthic foraminifera from Smeerenburgfjorden.*** **C. reniforme** ***and*** **C. lobatulus** ***represent core JM24 and*** **N. labradorica** ***represents core JM49.***

## 8.4 IRD from Smeerenburgfjorden compared to Sea Surface Temperature in Svalbard and in the Barents Sea

In Hald et al., (2004) it is inferred that IRD is a more reliable indicator presence and activity of tidewater glaciers than records of sedimentation rates. The source of IRD is mainly by iceberg rafting and sea-ice, and the amount of IRD recorded in cores JM24 and JM49 is worth considering as a proxy indicator. The IRD record from Smeerenburgfjorden

is compared to a high-resolution SST (Sea Surface Temperature) record from the Western Barents Sea (Sarnthein et al., 2003) and the western Svalbard margin (Hald et al., 2004) and to the summer insolation at 78°N (Berger and Loutre, 1991). The SST records are reconstructed by applying the modern technique, termed transfer functions, to planktonic foraminiferal faunal data. The records are interpreted to reflect latitudinal temperature gradients of AW in the Spitsbergen Current during the Holocene (Hald et al., 2004). In the study of Sarnthein et al. (2003) the size fraction used for foraminifera analysis was 150 µm compared to 100 µm in the study of Hald et al. (2003). This difference might indicate higher absolute temperatures estimates for the Svalbard margin, since it includes more of smaller sub-polar species that indicates higher SST.

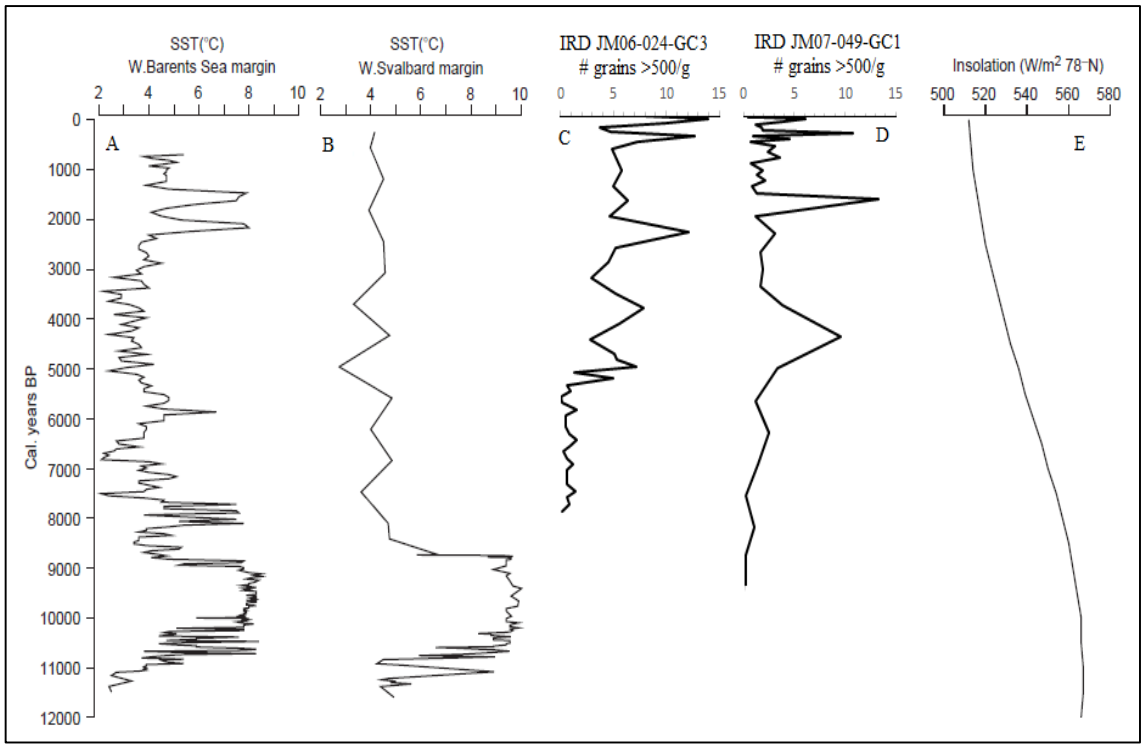


***Figure 8-8 correlation between SST records from A – Western Barents Sea (Sarnthein et al., 2003), B – Western Svalbard margin (Hald et al., 2004), C – IRD record from JM06-024-GC3 (present study), D – IRD records from JM07-049-GC1 (present study) and E – insolation at 78°N (Berger and Loutre, 1991).***

As mentioned earlier in the chapter, the early Holocene seems to represent the Holocene Climatic Optimum, as can be seen in the SST records from the Barents Sea and the Svalbard margin (Fig. 8.8). The IRD records from Smeerenburgfjorden are too young to show indications of the climatic optimum, and the values are low around 9000 cal years BP. The summer insolation is strong during early Holocene. In Smeerenburgfjorden,

sedimentation rates are higher during the early Holocene in core JM24 while for core JM49 the sedimentation rate is higher during the late Holocene.

The IRD oscillations from core JM49 during the early Holocene correlate with the increased SST in the Western Barents Sea. Sarnthein et al., (2003) speculates that the warming around 2200 and 1700 – 1800 cal years BP might be a late Holocene warming termed the Roman Climatic Optimum. This event is also noted in the NGRIP ice core record (Johnsen et al., 2001) and in the foraminiferal record from Marchal et al., (2001). Sarnthein et al. (2003) interprets this warming to increased inflow of Atlantic Water to the area. Core JM24 lacks oscillations in late Holocene probably due to the lower time resolution here but has similarly high values that as JM49.

Hald et al. (2004) note that small abrupt cooling/warming episodes can be linked to changes in the water masses, such as the displacements of the Arctic front system separating cool Arctic Water from the warmer Atlantic Water. This explanation applies well to the IRD data from Smeerenburgfjorden. The more stable conditions in core JM24 may represent more influence from the warmer Atlantic water in the area, whereas the oscillations of the JM49 record might be the change in influence of Arctic Water versus Atlantic Water. However, since the location of JM49 is further inside the fjord, it is also possible that the cold water originates from the local glaciers instead of the Arctic water.

## 8.5 Paleoenvironmental reconstruction in Smeerenburgfjorden using proxy records in cores JM06-024-GC3 and JM07-049-GC1

The proxy data for relative abundance of the foraminiferal species, *Elphidium excavatum* f. *clavata*, *Cassidulina reniforme*, isotopes and IRD are presented in Fig. 8.9 for core JM06-024-GC3 and in Fig. 8.10 for JM07-049-GC1.

### 8.5.1 Proxy variations

The seawater $\delta^{18}O$ variations reflect salinity changes and it is a result of three factors: melting of ice, changes in the hydrological cycle and changes in rate of advection and mixing of water masses (Duplessy et al., 2001). The oxygen isotopic record from Smeerenburgfjorden corrected for ice volume changes shows an increasing trend throughout the Holocene (Fig. 8.7, See Isotope chapter). Both cores from Smeerenburgfjorden show oxygen isotopic optimum conditions during early-middle

Holocene. When there is a 0.25 ‰ increase in the isotopic record measured in foraminifera, it indicates a 1°C lowering of the temperature (Shackleton, 1974) if salinity stays constant.

The IRD records from Smeerenburgfjorden show that it is present throughout the cores, and gives evidence that the northwest corner of Svalbard never fully deglaciated during the Holocene.

Foraminiferal data is the main source used in this thesis and the reconstruction is based on data available from the foraminiferal records in cores JM24 and JM49. The habitat preferences and the source of nutrition both in the fjord mouth and behind the fjord sill is the main basis for the reconstruction in Smeerenburgfjorden.

### 8.5.2 Data from JM06-024-GC3

Below is proxy data from core JM24 (Fig. 8.9), which is located in front of the sill (Fig. 2.2; 3.1)

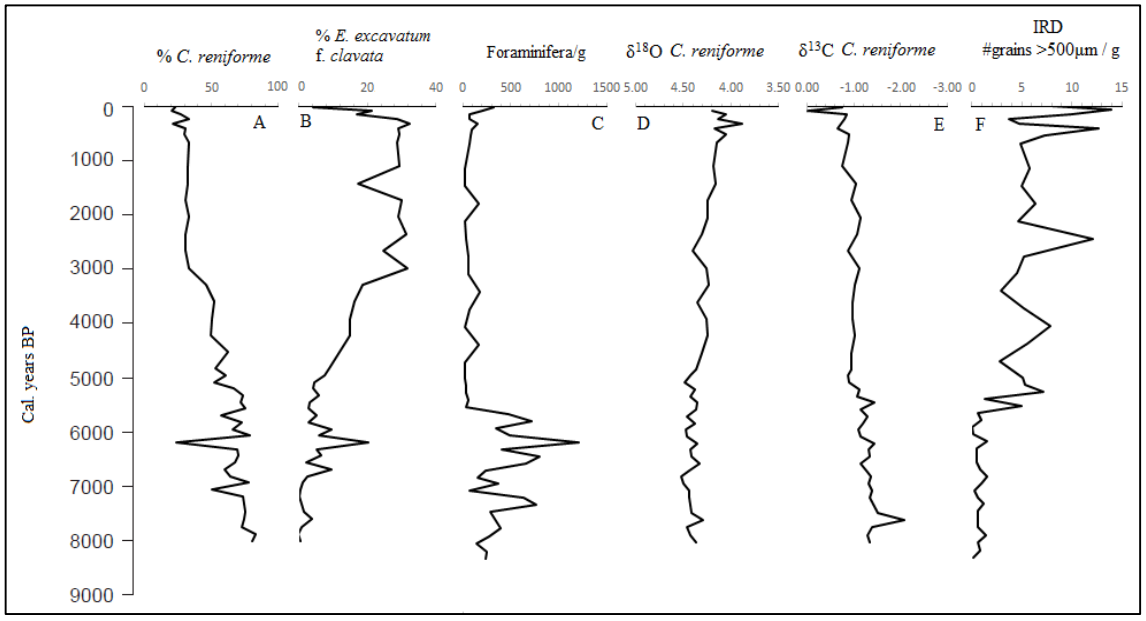


***Figure 8-9 Proxy records for sediment core JM06-024-GC3, Smeerenburgfjorden, northwest Spitsbergen: A - % Cassidulina reniforme; B - % Elphidium excavatum f. clavata; C – Foraminiferal abundance per gram dry weight sediment; D – $\delta^{18}O$ measured on the benthic foraminifera C. reniforme corrected for ice volume changes; E - $\delta^{13}C$ measured on the benthic foraminifera C. reniforme; F – ice rafted debris (IRD) per gram dry weight sediment.***

The $\delta^{18}O$ values have an increasing trend from the early Holocene towards the late Holocene of 0.49 ‰, indicating a cooling of nearly 2°C for the last 7500 cal yr. BP (Fig 8.9D). The $\delta^{13}C$ values in early Holocene show a rapid increase after a peak of -2‰, at

8040 cal yr BP (Fig. 8.9 E). This low value corresponds to decreased $\delta^{18}O$ values at 8040 cal yr. BP, indicating the last stages of the deglaciation and the transition from an area characterized by glaciers, towards an area characterized by tidewater glaciers. Soon after the $\delta^{13}C$ peak, the values slightly vary reflecting the optimum warming of the early Holocene (10,000 – 6800 cal yr. BP) (Fig. 8.9D; 8.9E).

The IRD data corresponds well to the optimum warming, with low values in the early Holocene (Fig. 8.9F). The benthic foraminiferal concentration and the IRD concentration show opposite trend (Fig. 8.9C). The reason could be that the bottom water conditions become better in the early Holocene, due to the inflow of warmer and saline Atlantic Water. To support this, the opportunistic species *Elphidium excavatum* f. *clavata,* which prefers cold polar water is relatively low from 7600 – 7500 cal years BP, while the glaciomarine environment indicator *Cassidulina reniforme,* which prefers warmer Atlantic Water, is relatively high, but shows a decreasing trend (Fig. 8.9A). The sudden shift in the percentage values between *E. excavatum* f. *clavata* and *C. reniforme* is a distinct indicator of a bottom water change. As mentioned earlier in conclusions (see Paleoceanographic implications), the shift between these two species may indicate a sudden bottom cooling during the Optimum Warming (Fig. 8.9A; 8.9B). That indicates the depletion of the warmer Atlantic Water and the intrusion of colder Polar/Arctic water to the area.

The general trend for the mid Holocene (6800 – 4500 cal years BP), is the transition from warmer water towards cooler water. This change of water masses may support the transition from moderate to low tidewater glaciers towards increased glaciation. *E. excavatum* f. *clavata* and *C. reniforme* have completely shifted at 4500 cal years BP, indicating gradual shifts in the bottom water during the mid-Holocene (Fig. 8.9A; 8.9B). Values of the high bottom current indicator *Cibicides lobatulus* are high during the mid-Holocene (Fig. 8.7) The high values indicates increased cold-water influx to the area, which represents rapidly shifting bottom currents (Chapter 4.2.2). During the mid-Holocene, the abundance peaks at 5200 cal years BP (Fig. 8.9C). The decreasing values of the dominating *C. reniforme* indicates decreased uptake of carbon, giving way for other benthic foraminiferal species to increase for a relatively short time, since the habitat is not very favourable. The $\delta^{18}O$ values are low the mid-Holocene, representing warmer waters. The IRD values oscillate but show a gradual increase (Fig. 8.9F). This data supports the interpretation that the environment is warmer compared to early Holocene. The $\delta^{13}C$ values

are stable, with a general increasing trend towards the late Holocene (Fig. 8.9E). As mentioned earlier, the increase might be a result of low benthic foraminiferal concentration in the mid-Holocene.

Late Holocene proxy records, indicate a transition from warmer waters to colder polar/arctic waters. The $\delta^{18}O$ rapidly deplete concomitant the increasing values of the IRD (Fig. 8.9D; 8.9F). The foraminiferal fauna is dominated by the opportunistic species *Elphidium excavatum* f. *clavata,* and the benthic foraminiferal concentration is very low (Fig. 8.9B; 8.9C). Elverhøi and Bomstad, (1980) interpret that the strong dominance of this species gives evidence of restricted living conditions for the foraminifera and Polyak et al., (2002) argue that it may be due to its high nutritional and habitat versatility. Values for *Cibicides lobatulus* are high and more stable during the late Holocene compared to early Holocene, indicating high-energy bottom currents (Fig. 8.7).

### 8.5.3 Data from JM07-049-GC1

Below is the proxy data from core JM49 (Fig. 8.10), which is located behind the sill (Fig. 2.2; 3.1).

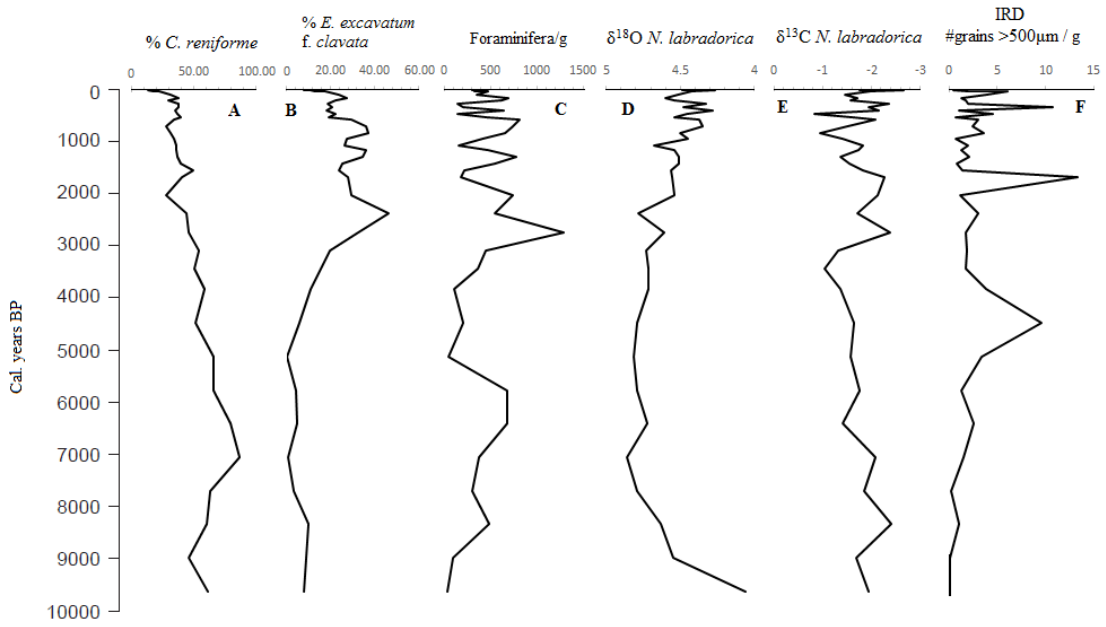


***Figure 8-10 Proxy record for sediment core JM07-049-GC1, Smeerenburgfjorden, northwest Spitsbergen: A - %* Cassidulina reniforme*; B - %* Elphidium excavatum *f.* clavata*; C – Foraminiferal abundance per gram dry weight sediment; D – $\delta^{18}O$ measured on the benthic foraminifera* N. labradorica*; E - $\delta^{13}C$ measured on the benthic foraminifera* N. labradorica*; F – ice rafted debris (IRD)***

The $\delta^{18}O$ values increase rapidly in the early Holocene (10,000 – 6800 cal yr. BP.). The increase of 0.59 ‰ from the lowest part of the record towards 7000 cal. yr. BP, indicate a cooling of 2.36 °C in the inner part of the fjord (Fig. 8.10D). Values for *Cassidulina reniforme* are the highest at the same time as the $\delta^{18}O$ values are the lowest (Fig. 8.10A; 8.10D). This indicates that *C. reniforme* thrives well in relatively warmer waters and that the environment represents tidewater glaciated area. The values for *Elphidium excavatum* f. *clavata* are low in the early Holocene, the opposite of *C. reniforme*, since it thrives better in sea-ice covered areas and close to tidewater glaciers (Fig. 8.10A; 8.10B). *E. excavatum* f. *clavata* starts to increase at the boundary of the mid to late Holocene (4500 cal yr. BP) indicating a change in the bottom environment (Fig. 8.10B). The benthic foraminiferal concentration is generally high during early Holocene while the IRD concentration is relatively low (Fig. 8.10C; 8.10F).

The benthic foraminiferal concentration shows a decreasing trend during the late mid-Holocene (6800 – 4500 cal yr. BP) (Fig. 8.10C). The trend of the $\delta^{13}C$ follows the same trend as the benthic foraminiferal concentration (Fig. 8.10E). When the concentration decreases, the $\delta^{13}C$ increases, indicating higher carbon concentration in the sediments. The IRD concentration increases when the benthic foraminiferal concentration decreases (Fig. 8.10C; 8.10F), indicating a more deteriorating bottom water environment in the mid-Holocene. The benthic foraminiferal species *Cassidulina reniforme* has generally decreasing values throughout the mid-Holocene while *Elphidium excavatum* f. *clavata* shows an indication of an increase (Fig. 8.10A; 8.10B).

During the late Holocene (4500 cal yr. BP - present), the IRD value are relatively oscillating. The peaks indicate climate deterioration opposite to the values of the benthic foraminiferal concentration, which shows a decreasing trend (Fig. 8.10C; 8.10F). The benthic foraminiferal concentration and the $\delta^{13}C$ values show the same trend. Decreased concentration correlates to the increased carbon values (Fig. 8.10C; 8.10E). The glaciers start to enhance periodically with frequent shifts in the bottom water conditions, and increased calving. The increased foraminifera abundance is usually high when the IRD record is low (e.g. Hald et al., 2004; Hald & Korsun, 2008) which is the trend throughout the Holocene in Smeerenburgfjorden. This could indicate an oscillating oceanic front between the retreating Atlantic Water and the cold-water flux from growing glaciers in the fjord. *E. excavatum* f. *clavata* and *C. reniforme* indicate the dominance of colder water in

the fjord during the late Holocene, with their shift in dominance (Fig. 8.10A; 8.10B). The high bottom current species (Chapter 4.2.1) *Cibicides lobatulus* (see Foraminifera graphs Chapter 5) has high values during the late Holocene, indicating high-energy bottom water currents, which may have been a result of the oscillation between the Atlantic Water and the cold Arctic Water and the growing glaciers in the area.

# 9 Conclusions and summary

The studies of the benthic foraminifera, benthic isotopes and the sediment lithology from cores JM06-024-GC3 and JM07-049-GC1 show the evolution of the paleoceanography in Smeerenburgfjorden on the northwestern corner of Svalbard for the last 9000 – 10,000 years.

- The lithology indicates an unfavourable environment in the early Holocene, with limited mollusc shells present in the sediment. X-ray photos show that after c. 5000 cal yr. BP, IRD clasts become more abundant towards the present.
- The benthic foraminiferal fauna records change in the bottom water. *Cassidulina reniforme* dominates the early Holocene, indicating a glaciomarine environment. Mid-Holocene represents the transition from warmer towards colder period, with foraminifera dominance shift. The late Holocene represents colder periods with the high values of *Elphidium excavatum* f. *clavata*.
- The benthic isotope record indicate an improvement of the climate from the last stages of the LGM and throughout the early Holocene. The isotopic record indicates temperature oscillations during the early Holocene of up to 3°C. Oxygen isotope values after 5000 cal yr BP indicate a warming towards the present, indicated by decreased benthic concentration values. The correlation between the isotopically analysed species shows the different calcifying period of early spring to summer.
- The carbon isotope records indicate a good ventilation of the water mass in the sediment. The decreasing trend of the benthic foraminiferal concentration might be the reason for increased carbon values towards the present.
- The IRD record from core JM24 indicate a stable presence of Atlantic Water for the mid – late Holocene. The IRD record from both cores (JM24 and JM49) start to increase after 5000 cal yr. BP indicating a significant change in the water mass, triggering increased ice rafting.
- In late Holocene, the agglutinated species show a significant increase in core JM49, which might be connected to the increased sedimentation rate during that interval. In core JM24, the agglutinated species are significantly higher during the early Holocene. The agglutinated species thrive in colder waters, indicating a cooling with its high concentration.

The Holocene reconstruction in Smeerenburgfjorden indicates local changes that can be correlated further to proxy data from the regional area of west Svalbard margin.

# 10 References


Aagaard K. and Greisman, P. (1975). Toward New Mass and Heat Budgets for the Arctic Ocean. *Journal of Geophysical Research, 80*(27) 3821 – 3827.

Aagaard, K., Swift, J.H. and Carmack, E.C. (1985). Thermohaline Circulation in the Arctic Mediterranean Seas. *Journal of Geophysical Research 90(C3),* 4833 – 4846.

Aksu, A.E. and Mudie, P.J. (1985). Late Quaternary stratigraphy and paleoecology of Northwest Labrador Sea. *Marine Micropaleontology 9*(6), 537 – 557.

Alve, E. (1996). Benthic foraminiferal evidence of environmental change in the Skagerrak over the past six decades. *Norske geologiske undersøkelser. Bulletin 430*, 85 – 93.

Austin, W.E.N. and Kroon, D. (1996). Late glacial sedimentology, foraminifera and stable isotope stratigraphy of the Hedbridea Continental Shelf, northwest Scotland. *Geological Society, Londin, 11*, 187 – 213

Berge, J., Johansen, G., Nilsen, F., Gulliksen, B. and Slagstad, D. (2005). Ocean temperature oscillations enable reappearance of blue mussel *Mydilus edulis* in Svalbard after a 1000 year absence. *Marine ecology progress series, 303*, 167 – 175.

Berger, A. and Loutrem M.F. (1991). Insolation values for the climate of the last 10 million years. *Quaternary Science Reviews, 10*, 297 – 317.

Birks, H.H. (1991). Holocene vegetational history and climatic change in west Spitsbergen – plant macrofossils from Skardtjørna, an Arctic lake. *Holocene 1*(3), 209 – 218.

Blais-Stevens, A. and Patterson, T. (1998). Environmental indicator potential of foraminifera from Saanich inlet, Vancouver Island, British Columbia, Canada. *Journal of Foraminiferal Research, 28*(3), 201 – 219.

Bodevik, S., Mangerud, J., Birks, H.H., Gulliksen, S. and Reimer, P. (2006). Radiocarbon Reservoir Ages During the Allerød and Younger Dryas. *Science, 312*, 1514 – 1516.

Boulton, G.S. (1979). Glacial history of the Spitsbergen archipelago and the problem of a Barnets Shelf ice sheet. *Boreas, 8*, 31 - 57.

Bowman, S. (1990). Radiocarbon dating.*Univeristy of California*. 64 p.

Broecker, W.S. (1991). The Great conveyor. Oceanography, 4: 79-89.

Broecker, W.S. (1997). Thermohaline Circulation, the Achilles Heel of Our Climate System: Will Man-Made CO2 Upset the Current Balance? Science, 278(5343): 1582-1588

Coplen, T. (1996). New guidelines for reporting stable hydrogen, carbon and oxygen-ratio data. *Geochemica et Cosmochimica Acta, 60*(17), 3359 – 3360.

Cottier, F., Tvergberg, V., Inall, M., Svendsen, H., Nilsen, F. and Griffiths, C. (2005). Water mass modification in an Arctic fjord through cross-shelf exchange: The seasonal hydrography of Kongsfjorden, Svalbard. *Journal of Geophysical Research 110*, 1 – 18.

Cottier, F. R., Nilsen, F., Inall, M.E., Gerland, S., Tverberg, V. and Svendsen, H. (2007). Wintertime warming of an Arctic shelf in response to large-scale atmospheric circulation. *Geophysical Research Letters, 34,* L10607.

Denne, R.A and Sen Gupta, B.K. (1989). Effects of Taphonomy and Habitat on the Record of Benthic foraminifera in Modern Sediments. *Palaios, 4*, 414 – 423.

Denton, G.H. and Hughes, T.J. (1981) The last great ice sheets. *Wiley*.

Dowdeswell, J.A. and Dowdeswell, E.K. (1989). Debris in icebergs and rates of glaci-marine sedimentation: observations from Spitsbergen and a simple model. *The Journal of Geology, 97*(2), 221 – 231.

Duplessy, J.C., Ivanova, W., Murdmaa, I., Paterne, M and Labeyrie, L. (2001). Holocene paleoceanography of the Barents Sea and variations of the northward heat transport by the Atlantic Ocean. *Boreas, 30*, 2 – 16.

Duplessy, J.C., Cortjio, E., Ivanova, E., Khusid, T., Labeyrie, L., Levitan, M., Murdmaa, I. and Paterne, M. (2005). Paleoceanography of the Barents Sea during the Holocene. *Paleoceanography, 20*(6), 13p.

Elverhøi, A. and Bomstad, K. (1980). Late Weichselian glacial and glaciomarine sedimentation in the western, central Barents Sea. *Norsk Polarinstitutt*.

Elverhøi, A., Liestøl, O. and Nagy, J. (1980). Glacial erosion, sedimentation and microfauna in the inner part of Kongsfjorden, Spitsbergen. *Norsk Polarinstitutt 172*, 33 – 62.

Feyling-Hanssen, R. W. (1964). Foraminifera in Late Quaternary deposits in the Oslofjord area: *Norges Geologiske Undersøkelse, 225*, 383 pp.

Forman, S.L. (1989). A 17,000 year glacio-eustatic sea-level record: Influence of glacial melting on the Younger Dryas event and deep-ocean circulation. *Nature, 342*, 637 – 642.

Forman, S.L. (1990). Post-glacial relative sea-level history of northwestern Spitsbergen, Svalbard.*Gological Society of America Bulletin, 102,* 1580 – 1590.

Forwick, M. and Vorren, T.O. (2006). Holocene mass-transport activity and climate in outer Isfjorden, Spitsbergen: marine and subsurface evidence. *The Holocene, 17*(6), 707 – 716.

Gammelsrød, T. and Rudels, B. (1983). Hydrographic and current measurements in the Fram Strait, August 1981. *Polar Research 1*, 115 – 126.

Gilbert, R. (1990). Rafting in glacimarine environments. *Geological Society Special Publication, 53*, 105 – 120.

Grosswald, M.G. (1980). Late Weichselian ice sheet of Northern Eurasia. *Quaternary Research, 13(1)*, 1 – 32.

Hald, M. and Korsun, S. (1997). Distribution of modern benthic foraminifera from fjords of Svalbard, European Arctic. *Journal of Foraminiferal Research, 27*(2), 101 – 122.

Hald, M. and Korsun, S. (2008). The 8200 cal. yr BP event reflected in the Arctic fjord, Van Mijenfjorden, Svalbard. *The Holocene, 18*(6), 981 – 990.

Hald, M. and Korsun, S. (1997). Distribution of modern benthic foraminifera from fjords of Svalbard, European arctic. *Journal of Foraminiferal Research 27*(2), 101 – 122.

Hald, M. and Steinsund, P.I. (1992). Distribution of surface sediment benthic foraminifera in the southwestern Barents Sea. *Journal of Foraminiferal Research 22*(4), 347 – 362.

Hald, M., Steinsund, P.I., Dokken, T., Korsun, S., Polyak, L. and Aspeli, R. (1994). Recent and Late Quaternary distribution of *Elphidium excavatun* f. *clavatum* in arctic seas.*Cushman Foundation Special Publication, 32*. 142 – 153.

Hald, M., and Steinsund, P.I. (1996). Benthic foraminifera and carbonat dissolution in the surface sediments of the Barents and Kara Seas. *Berichte zur Polaraforschung, 212,* 285 – 307.

Hald, M. and Vorren, T. (1987). Foraminiferal stratigraphy and environment of Late Weichselian deposits on the continental shelf off Troms, Northern Norway. *Marine Micropaleontology 12*, 129 – 160.

Hald, M., Ebbesen, H., Forwick, M., Godtliebsen, F., Khomenko, L., Korsun, S., Olsen, L.R. and Vorren, T.O. (2004). Holocene Pleoceanography and glacial history of the West Spitsbergen area, Euro-Arctic margin. *Quaternary Science Reviews, 23,* 2075 – 2088.

Hansen, A. and Knudsen, K.L. (1995). Recent foraminiferal distribution in Freemansundet and Early Holocene stratigraphy on Edgeøya, Svalbard. *Polar Research 14*(2), 215 – 238.

Hisdal, V. (1998). Svalbard nature and history. *Polarhåndbok No. 12.* Norsk Polarinstitutt. 118 p.

Holtedahl, H. and Bjerkli, K. (1982). Late Quaternary sediments and stratigraphy on the continental shelf off Møre-Trøndelag, W. Norway. *Marine Geology 45*, 179 – 226.

Hopkins, T.S. (1991). The GIN Sea – A synthesis of its physical oceanography and literature review 1972 – 1985. *Earth-Science Reviews 30,* 175 – 318.

Huddart, D. and Peacock, J.D. (1990). Early Holocene morainal bank sedimentology and marine ecology, Skjoldungebrae gorge, North Scoresby Land, East Greenland. *Geological Society of London, 53*(1), 289 – 305.

Hunt, A.S. and Corliss, B.H. (1993). Distribution and microhabitats of living (stained) benthic foraminifera from the Canadian Arctic Archipelago. *Marine Micropaleontology 20*(3 – 4), 321 – 345.

Husum K. and Hald, M. (2004). Modern foraminiferal distribution in the subarctic Malangen Fjord and adjoining shelf, northern Norway. *Journal of Foraminiferal Research 34*(1), 34 – 48.

Isaksson, E., Hemanson, M., Hicks, S., Igarashi, M., Kamyama, K., Moore, J., Motoyama, H., Muir, D., Pohjola, V., Vaikmae, R., van de Wal, R.S.W. and Watanabe, O. (2003). Ice cores from Svalbard – useful archives of past climate and pollution history. *Physics and Chemistry of the Earth, 28*. 1217 – 1228.

Ivanova, E. V., Ovsepyan, E. A., Risebrobakken, B. And Vetrov, A. A. (2008). Downcore distribution of living calcareous foraminifera and stable isotopes in the western Barents Sea. *Journal of Foraminiferal Research, 38*(4), 337 – 356.

Jennings, A.E. and Helgadóttir, G. (1994). Foraminiferal assemblages from the fjords and shelf of Eastern Greenland. *Journal of Foraminiferal Research, 24*(2), 123 – 144.

Jennings, A.E., Weiner, N.J., Helgadottir, G. and Adrews, J.T. (2004). Modern foraminifera faunas of the southwestern to northern Iceland Shelf: oceanographic and environmental controls. *Journal of Foraminiferal Research 34*(3) 180 – 207.

Jernas, P., Klitgaard-Krisensen, D., Koç, N. and Tverberg, V. (2010). Response of recent benthic foraminifera inflow of Atlantic Water; evidence from annual sampling in a glacial fjord, Svalbard.

Johnsen, S.J., Dahl-Jensen, D., Gundestrup, N., Steffensen, J.P., Clausen, H. B., Miller, H., Masson-Delmotte, V., Sveinbjörnsdóttir, A.E. and White, J. (2001). Oxygen isotope and palaeotemteratures records from six Greenland ice-core stations: Camp Century, Dye-3, GRIP, GISP, Renland and NorthGRIP. *Journal of Quaternary Science, 16*(4), 299 – 307.

Kaufman, D.S., Ager, T.A., Anderson, N.J., Andrews, P.M., Bartlein, P.J, Brubaker, L.B., Coats, L.L., Cwynar, L.C., Duvall, M.I., Dyke, A.S, Edwards, M.E., Eisner, W.R., Gajewski, K., Geirsdóttir, A., Hu, F.S., Jennings, A.E., Kaplan, M.R., Kerwin, M.W., Loxhkin, A.V., MacDonald, G.M., Miller, G.H., Mock, C.J., Oswald, W.W:, Otto-Bliesner, B.L. Porinchu, D.F., Rhuland, K., Smol, J.P., Steig, E.J. and Wolfe, B.B. (2004). Holocene thermal maximum in the western Arctic (0 – 180°W). *Quaternary Science Reviews, 23*, 529 – 560.

Kiær, H., (1899). Talamophora: The Norwegian North-Atlantic Expedition 1876 – 1878: *Christiania*, *7*, 1–13.

Korsun, S. and Hald, M. (1998). Modern Benthic foraminifera off Novaya Zemlya Tidewater Glaciers, Russian Arctic. *Arctic and Alpine Research, 30*(1), 61 – 77.

Korsun, S., Hald. M., Panteleeva, N. and Tarasov, G. (1998). Biomass of foraminifera in the St. Anna Trough, Russian arctic continental margin. *Sarsia, 83*, 419 – 431.

Korsun, S., and Hald, M. (2000). Seasonal dynamics of benthic foraminifera in a glacially fed fjord of Svalbard, European Arctic. *Journal of Foraminiferal Research, 30* (4), 251 – 271.

Koç, N., Jansen, E. and Haflidason, H. (1993). Paleoceanographic reconstructions of surface ocean conditions in the Greenland, Iceland and Norwegian Seas through the last 14 ka based on diatoms. *Quaternary Science Reviews, 12*, 115 – 140.

Koç, N., Klitgaard-Kristensen, D., Hasle, K., Forsberg, C.F. and Solheim, A. (2002). Late glacial palaeoceanography of Hinlopen Strait, northern Svalbard. *Polar Research, 21*(2), 307 – 314.

Kubischta, F., Knudsen, K.L., Ojala, A.E.K. and Salonen, V.P. (2011). Holocene benthic foraminiferal record from a high-arctic fjord, Nordaustlandet, Svalbard. *Geografiska Annaler, 93*(4), 227 – 242.

Kutzbach, J.E. and Guetter, P.J. (1986). The influence of chancing orbital parameters and surface boundary conditions on climate simulations for the past 18 000 years. *Journal of Atmospheric Sciences, 43*(10), 1726 – 1759.

Landvik, J.Y., Bolstad, M., Lycke, A.K., Mangerud, J. and Sejrup, H.P. (1992). Weichselian stratigraphy and paleoenvironment at Bellsund, Western Svalbard. *Boreas, 21*, 335 – 358.

Landvik, J.Y., Bondevik, S., Elverhøi, A., Fjeldskaar, W., Mangerud, J., Salvigsen, O., Siegert, M.J., Svendsen, J.I. and Vorren, T.O. (1998). The last glacial maximum of Svalbard and the Barents Sea Area: Ice sheet extent and configuration. *Quaternary Science Reviews, 17*, 43 – 75.

Lloyd, J., Kroon, D., Laban, C. and Boulton, G. (1996). Deglaciation history and palaeoceanography of the western Spitsbergen margin since the last glacial maximum. *Late Quaternary Paleoceanography of the Northern Atlantic Margins 111,* 289 – 301.

Loeng, H. (1991). Features of the physical oceanographic conditions of the Barents Sea. *Polar Research 10(1),* 5 – 18.

Mangerud, J. (1977). Late Weichselian Marine Sediments containing shells, foraminifera, and pollen, at Ågotnes, western Norway. *Norsk Geologisk Tidsskrift, 57*, 23 – 54.

Mangerud, J., and Svendsen, J.I. (1990). Deglaciation chronology inferred from marine sediments in a proglacial lake basin, western Spitsbergen, Svalbard. *Boreas, 19*(2), 49 – 72.

Mangerud, J., Bolstad, M., Elgersma, A., Helliksen, D., Landvik, J.Y., Lønne, I., Lycke, A.K., Salvigsem O., Sandahl, T. and Svendesn, J.I. (1992). The Last Glacial Maximum on Spitsbergen, Svalbard. *Quaternary Research, 38*, 1 – 31.

Mangerud, J., Bondivik, S., Gulliksen, S., Hufthammer, A.K. and Høisæter, T. (2006). Marine $^{14}C$ reservoir ages for 19th century whales and molluscs from the North Atlantic. *Quaternary Science Reviews, 25*, 3228 – 3245.

Mangerud, J., and Gulliksen, S. (1975). Apparent radiocarbon ages of recent marine shells from Norway, Spitsbergen and Arctic Canada. *Quaternary Research, 5*, 263 – 273.

Mangerud, J., Gulliksen, S. and Larsen, E. (2009). $^{14}C$-dated fluctuations of the western flank of teh Scakndinavian ice sheet 45 – 25 kyr BP compared with Bølling – Younger Dryas fluctuations and Dansgaard-Oeschger events in Greenland. *Boreas 39,* (2), 382 – 342.

Mangerud, J., Landvik, J.Y., Salvigsen, O., and Miller, G.H. (1985) Lake Linnévatnet, Svalbard, a possible 40,000 years continuous record of lacustrine and marine sedimentation. *Abstr 14th Arctic Workshop, Arctic Land-Sea Interactions*. 82 – 85.

Manley, T.O. (1995). Branching of Atlantic Water within the Greenland-Spitsbergen Passage: An estimate of recirculation. Journal of Geophysical Research, 100(C10): 20 627-20 634

Marchal, O., Cacho, I., Stocker, T.F., Grimalt, J.O., Calvo, E., Martrat, B., Shackleton, N., Vautravers, M., Gortijo, E., van Kreveld, S., Andersson, C., Koç, N., Chapman, M., Sbaffi, L., Duplessy, J.C., Sarnthein, M., Turon, J.L., Duprat, J. and Jansen, E.

(2002). Apparent long –term cooling of the sea surface in the northeast Atlantic and Mediterranean during the Holocene. *Quaternary Science Reviews, 21*, 455 – 483.

McBean, G., Alekseev, G., Chen, D., Forland, E., Fyfe, J., Groisman, P.Y., King, R., Melling, H., Vose, R. and Whitfield, P.H. (2005). Arctic climate: past and present. *Acia Scientific Report. Cambridge University Press,* Cambridge, UK, 21 – 60.

McCabe, A.M., Haynes, J.R. and MacMillan, N.F. (1986). Late-Pleistocene tidewater glaciers and glaciomarine sequences from north County Mayo, Republic of Ireland. *Journal of Quaternary Science, 1*(1), 73 – 84.

Miller, A.A.L. (1991). Quaternary foraminiferal biostratigraphy of three shallow geotechnical boreholes, Balmoral, Cohasset and Panuke well sites, Western Sable Island Bank. *Geological Exploration and Offshore Services, 6*, 87 pp.

Miller, G.H. Allay, R.B., Brigham-Grette, J., Fitzpatrick, J.J., Polyak, L., Setteze, M.C. and White, J.W.C. (2010). Arctic amplification: can the past predict the future? *Quaternary Science Reviews, 29*, 1679 – 1715.

Munsell, R. (1973). Soil colour charts. *Macbeth division of Kollmorgen Corporation*. New York, 19 p.

Murray, J.W. (1991). Ecology and Paleoecology of Benthic Foraminifera.

Murray, J.W. (2001). The niche of benthic foraminifera, critical thresholds and proxies. *Marine Micropaleontology 41*, 1 – 7.

Murray, J.W. and Alve, E., (2011). The distribution of agglutinated foraminifera in NW European seas: Baseline data for the interpretation of fossil assemblages. *Palaeontologia Electronica, 14*(2), 14A:41p.

Nagy, J. (1965). Foraminifera in some bottom samples from shallow waters in West Spitsbergen: Norsk Polarinstitutt Årbok 1963, 109 – 125.

Nilsen, F., Cottier, F., Skogseth, R. and Mattsson, S. (2008). Fjord-shelf exchanges controlled by ice and brine production: the interannual variation of Atlantic Water in Isfjorden, Svalbard. *Continental Shelf Research 28,* 1838 – 1853.

Ostermann, D.R. and Curry, W.B. (2000). Calibration of stable isotopic data: An enriched $\delta^{18}O$ standard used for source gas mixing detection and correction. *Paleoceanography, 15*(3), 535 – 360.

Ottesen D., Dowdeswell, J.A., Landvik, J.Y and Mertiner, J. (1998). Dynamics of the Late Weichselian ice sheet on Svalbard inferred from high-resolution sea-floor morphology. *Boreas, 36*(3), 286 – 306.

Ottesen, D., Dowdeswell, J.A., Landvik, J.Y. & Mienert, J., **(**2007). Dynamics of the Late Weichselian ice sheet on Svalbard inferred from high-resolution sea-floor morphology. *Boreas*, *36,* 286 – 306.

Ottesen, D. and Dowdeswell, J.A. (2009). An inter-ice-stream glaciated margin: Submarine landforms and a geomorphic model based on marine-geophysical data from Svalbard. *Geological Society of America Bulletin,* 1647 – 1665.

Ó Cofaigh, C., and Dowdeswell, J.A. (2001). Laminated sediments in glacimarine environments: diagnostic criteria for their interpretation. *Quaternary Science Reviews, 20*, 1411 – 1436.

Phleger, F.B. (1960). Ecology and distribution of recent foraminifera. *The Johns Hopkins Press*. Baltimore, 297 p.

Polyak, L., Korsun, S., Febo, L.A., Stanovoy, V., Khusid, T., Hald, M., Paulsen, B.E. and Lubinski, D. (2002). Benthic foraminifera assemblages from the southern Kara Sea, a river-influenced arctic marine environment. *Journal of Foraminiferal Research 32*(3), 252 – 273.

Quinn, R., Bull, J.M. and Dix, J.K. (1998). Optimal Processing of Marine High-Resolution Seismic Reflection (CHIRP) Data. *Marine Geophysical Researches 20,* 13 – 20.

Rasmussen, T.L Thomsen, E., Śubowska, M.A. Jessen, S., Solheim, A. and Koç, N. (2007). Paleoceanographic evolution of the SW Svalbard margin (76°N) since 20,000 $^{14}$C yr BP. *Quaternary Research, 67,* 100 – 114.

Rasmussen, T.L., Forwick, M. and Mackensen, A. (2012). Reconstruction of inflow of Atlantic Water to Isfjorden, Svalbard during the Holocene: Correlation to climate and seasonality. *Marine Micropaleontology, 94 – 95*, 80 – 90.

Rasmussen, T.L., and Thomsen, E. (2014). Brine formation in relation to climate changes and ice retreat during the last 25,000 years in Storfjorden, Svalbard, 76 – 78°N. *Paleoceanography, 29*, 911 – 929.

Rasmussen, T.L., Thomsen, E., Skirbekk, K., Ślubowska-Woldengen, M., Kristensen, D. K. and Koç, N. (2014) Spatial and temporal distribution of Holocene temperature maxima in the northern Nordic Seas: interplay of Atlantic, Arctic and polar water masses. *Quaternary Science Reviews, 92,* 280 – 291.

Reimer, P. J., Baillie, M. G. L., Bard, E., Bayliss, A., Beck, J. W., Blackwell, P. G., Ramsey, C. B., Buck, C. E., Burr, G. S., Edwards, R. L., Friedrich, M., Grootes, P. M.,Guilderson, T. P., Hajdas, I., Heaton, T. J., Hogg, A. G., Hughen, K. A., Kaiser., K. F., Kromer, B., McCormac, F. G., Manning, S. W., Reimer, R. W., Richards, D. A., Southon, J. R., Talamo, S., Turney, C. S. M., van der Plicht, J. and Weyhenmeyer, C. E.,(2009). *Radiocarbon, 51,* 1111 – 1150.

Reimer,P.J., Bard, E., Bayliss,A., Beck, J.W., Blackwell, P.G., Ramsey, C.B., Buck, C. E., Cheng, H., Edwards, R.L., Friedrich, M., Grootes, P.M., Guilderson, T.P., Haflidason, H., Hajdas, I., Hatté, C., Heaton, T.J., Hoffmann, D.L., Hogg, A.G., Hughen, K. A., Kaiser, K.F., Kromer, B., Manning, S.W., Niu, M., Reimer, R.W., Richards, D.A., Scott, E.M., Southon. J.R., Staff, R.A., Turney, C.S.M and van de Plicht, J. (2013). Intcal 13 marine 13 radiocarbon age calibration curves 0 – 50,000 years cal BP. *Radiocarbon, 44*(4), 1869 – 1887.

Rosoff, D.B. and Corliss, B.H. (1992). An analysis of recent deep-sea benthic foraminiferal morphotypes form the Norwegian and Greenland seas. *Palaeogeography,Palaeoclimatology, Palaeoecology 91*, 13 – 20.

Rudels, B. On the mass balance of the Polar Ocean with special emphasis on the Fram Strait. (1987). *Norsk Polarinstitutt*, 188. 52p.

Saidova, Kh.M. (2009). Asseblages of Benthic foraminifers in the White Sea. *Oceanology, 49*(4), 499 – 504.

Saher, M., Klitgaard-Kristensen, D., Hald, M., Korsun, S. and Jørgensen, L.L. (2009). Benthic foraminifera assemblages in the Central Barents Sea: an evaluation of the effect of combining live and total fauna studies in tracking environmental change. *Norwegian Journal of Geology,89,*149 – 161.

Saloranta, T.M., Svendsen, H. (2001). Across the Arctic front west of Spitsbergen: high-resolution CTD sections from 1998 – 2000. *Polar Research 20(2),* 177 – 184.

Salvigsen, O. (1979). The last deglaciation of Svalbard. *Boreas 8*, 229 – 231.

Salvigsen, O., Forman, S.L. and Miller, G.H. (1992). Thermophilous molluscs on Svalbard during the Holocene and their paleoclimatic implications. *Polar research 11*(1), 1-10.

Salvigsen, O., (2002). Radiocarbon-dated *Mytilus edulis* and *Modiolus modiolus* from northern Svalbard: climatic implications. *Norsk Geografisk Tidsskrift, 56*, 56 – 61.

Sarnthein, M., Van Kreveld, S., Erlenkreuser, H., Grootes, P.M., Kucera. M., Plaufman, U. and Scholz, M. (2003). Centennial-to-millennial-scale periodicities of Holocene climate and sediment injections off the western Barents shelf, 75°. *Boreas, 32*, 447 – 461.

Schafer, C.T. and Cole, F.E. (1986). Reconnaissance Survey of Benthonic Foraminifera from Baffin Island Fjord Environments. *Geological Survey of Canada 39*(3) 232 – 239.

Schafer, C.T. and Cole, F.E. (1988). Environmental associations of Baffin Island fjord agglutinated foraminifera. *Atlantic Geoscience Centre 41*, 307 – 323.

Schröder-Adams, C.J. and McNeil, D.H. (1990). Biostratigraphic distribution of agglutinated foraminifera in Oligocene and Miocene shallow to deep-water facies of the Beaufort-Mackenzie Basin. *Geological Survey of Canada, Open File 2306*, 2 – 12.

Setoyama, E., Kaminski, M.A. and Tyszka, J. (2011). Campanian agglutinated foraminifera from the Lomonosov Ridge, IODP Expedition 302, ACEX, in the paleogeographic context for the Arctic Ocean. *Micropaleontology, 57*(6), 507 – 530.

Shackleton, N.J. (1974). Attainment of isotopic equilibrium between ocean water and the benthonic foraminifera genus *Uvigerina* : isotopic changes in the ocean during the Last Glacial. *Les methods quantitatives d´étude des vatiations du climat au cours du Pléistocéne, Colloques Inernationaux du C.N.R.S., 219*, 203 – 209.

Skarðhamar, J. and Svendsen, H., (2010) Short-term hydrographic variability in a stratified Arctic fjord. *Institute of marine research,* 18p.

Skirbekk, K. (2007). Rekonstruksjon av paeomiljø i Kongsfjordrenna, vest for Svalbard, de siste ~11 800 år, basert på bentiske foraminiferer og sedimentologiske undrsøkelser. *Universitetet i Tromsø*, Tromsø, 92 p.

Skirbekk, K., Klitgaard Kristiansen, D., Rasmussen, T., Koç, N and Forwick, M. (2010). Holocene climate variations at the entrance to a warm Arctic fjord: evidence from Kongsfjorden through, Svalbard. *Geological Society of London* 291 – 206.

Ślubowska, M. A., Koç, N., Rasmussen, T.L. and Klitgaard-Kristiansen, D. (2005). Changes in the flow of Atlantic water into the Arctic Ocean since the last deglaciation: Evidence from the northern Svalbard continental margin, 80°N. *Paleoceanography, 20* (PA4014).

Ślubowska-Woldengen, M., Rasmussen, T.L., Koç, N., Klitgaard-Krisensen, D., Nilsen, F. and Solheim, A. (2007). Advection of Atlantic Water to the western and northern Svalbard shelf since 17,500 cal yr BP. *Quaternary Science Reviews, 26,*463 – 478.

Stein, R., Fahl, K., Ivanov, G.I., Levitan, M.A. and Tarasov, G. (1999). Modern and late quaternary depositional environment of the St. Anna Trough Area, Northern Kara Sea. *Berichte zur Polarforschung, 342*, 245 pp.

Steinsund, P.I. (1994). Benthic foraminifera in surface sediments of the Barents and Kara Seas; modern and late Quaternary applications. *University in Tromsø*, Tromsø.

Steinsund, P.I. and Hald, M. (1994). Recent calcium carbonate dissolution in the Barents Sea: Paleoceanographic applications. *Marine Geology, 117*(1 – 4), 303 – 316.

Stuvier, M. and Reimer P.J. (1993). *Radiocarbon, 35*, 215 – 230.

Stuvier, M., Pearson, G.W. and Braziunas, T. (1986). Radiocarbon Age Calibration of Marine Samples back to 9000 cal yr BP. *Radiocarbon, 28*(2B), 980 – 1021.

Sun, M.Y., Carroll, M.L., Ambrose Jr, W.G., Clough, L.M., Zou, L. and Lopez, G.R. (2007). Rapid consumption of phytoplankton and ice algae by Arctic soft-sediment benthic communities: Evidence using natural and $^{13}$C-labeled food materials. *Journals of Marine Research, 65;* 561 – 588.

Svendsen, H., Beszczynzka-Møller, A., Hagen, J.O., Lefauconnier, B., Tverberg, V., Gerland, S., Ørbæk, J.B., Bischof, K., Papucci, C., Zajaczkowski, M., Azzolini, R., Brulund, O., Wiencke, C., Winther, J.G. and Dallmann, W. (2002). The physical environment of Kongsfjorden-Krossfjorden, an arctic fjord system in Svalbard. *Polar Research 21(1),* 133 – 166.

Svendsen, J.I., and Mangerud, J. (1992). Paleoclimatic inferences from glacial fluctuations on Svalbard during the last 20 000 years. *Climate Dynamics, 6*, 213 – 220.

Svendsen, J.I., and Mangerud, J. (1997). Holocene glacial and climatic variations on Spitsbergen, Svalbard. *The Holocene, 7*(1), 45 – 57.

Tverberg, V. and Nøst, O.A. (2009). Eddy overturning across a shelf edge front: Kongsfjorden, west Spitsbergen. *Journal of Geophysical Research, 144* C04024.

Velle, J.H. (2012) Holocene sedimentary environments in Smeerenburgfjorden, Spitsbergen. *University in Tromsø.* Tromsø, 128 p.

Vorren, T.O., Hald, M. and Thomsen, E. (1984). Quaternary sediments and environments on the continental shelf off northern Norway. *Marine Geology 57*, 229 – 257.

Wang, P. and Chappell, J. (2001). Foraminifera as Holocene environmental indicators in the South Alligator River, Northern Australia. *Quaternary International 83 – 85,* 47 – 62.

Wollenburg, J.E. and Mackensen, A. (1998). Living benthic foraminifers from the central Arctic Ocean: faunal composition, standing stock and diversity. *Marine Micropaleontology 34*, 153 – 185.

Zajączkowski, M., Szczuziński, W., Plessen B. and Jernas, P. (2010). Benthic foraminifera in Hornsund, Svalbard: Implications for paleoenvironmental reconstructions. *Polish Polar Research 31*(4), 349 – 375.